THE UNIVERSITY
of EDINBURGH

Synthesis of Optical Probes for the Visualization of Human Neutrophil Elastase

Vikki Evans

THE UNIVERSITY *of* EDINBURGH

Doctorate of Philosophy

The University of Edinburgh

2018

Abstract

Optical medical imaging is a new technology that uses light to improve clinical processes such as disease diagnosis and tumour margin delineation. It has the potential to produce high-resolution images in real-time, with continuously generated images on or in biological tissues at a molecular level. Imaging inside the lung can be accomplished via the use of microendoscopy, and this has been used to detect and analyse several pulmonary diseases, which traditionally have been hard to unequivocally define.

Several pulmonary diseases have been linked with overactive leukocytes within the lung. A class of leukocytes, neutrophils, are used by the body to aggressively destroy potential pathogens with an arsenal of proteases including human neutrophil elastase (HNE) at its disposal. However, overexpression of unregulated HNE has been implicated in a number of pulmonary diseases, such as fibrosis, COPD and acute lung injury with irreversible damage caused to lung tissue through protein degradation. Currently in the clinic, it is difficult to identify and quantify unregulated HNE *in vivo* using traditional methods of diagnosis. Thus, the ability to quantify and evaluate numbers of neutrophils and levels of HNE using an *in vivo* technique would be very valuable.

Within this work, a library of optical probes to selectively detect HNE at a molecular level were designed and evaluated. The probes consist of two parts: an inhibitor warhead designed to irreversibly bind to HNE, and a fluorophore. Two different classes of warheads have been synthesised and conjugated to a variety of fluorophores that emit over a range of wavelengths. Having optical probes over the span of several wavelength ranges is beneficial as it allows

multiplex imaging so several diseases can be screened simultaneously, as well as removing the probes from possible tissue autofluorescence wavelengths.

The probes were evaluated for their binding efficacy with HNE, toxicity against erythrocytes and then, subsequently used to detect and image the presence and localisation of HNE within neutrophils. It is envisioned that the use of optical probes to detect HNE overexpression will lead to quicker diagnoses for patients with debilitating pulmonary diseases.

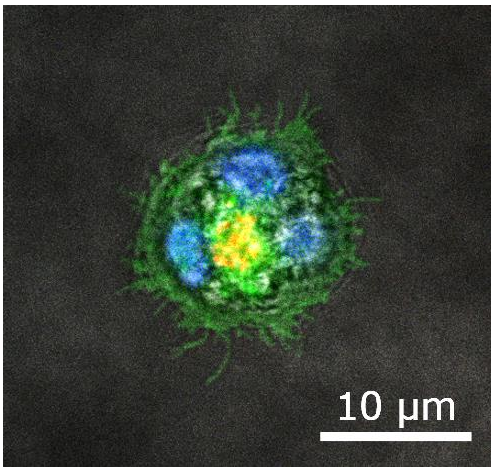

Dying neutrophil labelled with DAPI (blue), CellTracker green (green) and optical probe **52** (red).

Lay Summary

Human neutrophil elastase (HNE) is an enzyme found in neutrophils that is used to digest proteins and degrade pathogens. This maintains the body in a healthy manner and prevents infections spreading further throughout the body. In some diseases, the neutrophil's response is not switched off, or is accidentally switched on, even if no microbe present and so the neutrophil starts to digest healthy tissue instead. The damage is irreversible and symptomatic of lung diseases such as emphysema, fibrosis and chronic obstructive pulmonary disease (COPD).

In this thesis, several targeting molecules were synthesised to bind to HNE and label the enzyme with a fluorescent dye to detect areas with high levels of neutrophil activity. The aim of this was to speed up diagnosis of lung diseases, as the current gold standard in clinics can be time consuming and uncomfortable for the patient. After the synthesis of the optical probes, they were tested using purified enzyme and imaged in activated neutrophils to stimulate a patient's disease.

Contents

Declaration of Authorship

The research detailed within this thesis has been accumulated by the author in the duration of her PhD studentship between the dates of October 2015 and October 2018 under the supervision of Professor Mark Bradley, School of Chemistry, University of Edinburgh. The work, data, and interpretation presented here are those of the author unless there was significant collaborative contribution made, in which case it has been clearly recognised. Where published work has been consulted or quotations made, the source has been clearly cited.

This work has not been submitted for any other degrees or professional qualifications.

Signed Vikki Evans

Vikki Evans

Date 14 October 2019

Acknowledgements

Firstly, and most importantly, I would like to thank my supervisor Professor Mark Bradley for the opportunity to work within his research group for my PhD. It was an excellent experience working in such a large and diverse group, and I was fortunate to have such an interesting and stimulating research project.

My thanks also go to Professor Kev Dhaliwal and Dr Annamaria Lilienkampf for their supervisory support and tutelage. There are many unsung heroes in the chemistry department who keep the research going smoothly. In particular, I would like to thank Dr L Murray and Mr J Bella in the NMR department for all of my stereochemical nightmares, Dr L McKay and Mr A Taylor in the mass spectrometry lab, Dr G Nichols for his crystallography expertise and Mr T Calder and Mr M Forrest for their efforts in keeping research constantly moving.

The nature of an interdisciplinary project means there are numerous people who are vital for each part. Proteus has a vast number of people who need thanking: Thane, Katjana, Jo, Philip, Dominic, Duncan, Beth, Emma, and Dr Anne Moore to name but a few.

I would also like to thank my fellow Bradlonians, both past and present, for their friendship and guidance throughout the past three years. In particular, Dr Sarah Walker, Dr Kevin Neumann and (almost Dr) Gavin Birch for their help in all synthesis issues, Dr Jess Clavadetscher for her expertise in biological experiments, and to Antonio and Paul for their friendship; always there to lend an ear when things got frustrating, or a beer to celebrate.

Lastly, I would like to thank my parents and brothers, for their guidance, support (emotionally, sometimes financially) and love throughout my PhD. I

am beyond thankful for them putting up with me and my emotions during the ups and downs of my academic career. I swear this is the last degree!

Abbreviations

ALI	**Acute lung injury**
AMC	Aminomethyl coumarin
ARDS	Acute respiratory distress syndrome
AU	Arbitrary units
BAL	Bronchoalveolar lavage
Boc	*tert*-Butyloxycarbonyl group
BODIPY	Boron-dipyrromethene
CatG	Cathepsin G
Cbz	Carboxybenzyl group
COPD	Chronic obstructive pulmonary disease
CT	Computed tomography
Cy	Cyanine
DCC	*N*,*N*'-Dicyclohexylcarbodiimide
DIC	*N*,*N*'-Diisopropylcarbodiimide
DIPEA	*N*,*N*'-Diisopropylethylamine
DMF	Dimethylformamide
DMSO	Dimethylsulfoxide
ELSD	Evaporative light scattering detector

ESI	Electrospray ionisation
EtOH	Ethanol
FA	Formic acid
FITC	Fluorescein isothiocyanate
Fmoc	Fluorenylmethoxycarbonyl
FRET	Forster resonance energy transfer
HEPES	4-(2-hydroxyethyl)-1-piperazineethanesulfonic acid
HFIP	Hexafluoro isopropanol
HNE	Human neutrophil elastase
HOBt	Hydroxybenzotriazole
HPLC	High performance liquid chromatography
HSPyU	Dipyrrolidino(*N*-succinimidyloxy)carbeniumhexa fluorophosphate
IC_{50}	Half maximal inhibitory concentration
K_i	Inhibitory constant
LC-MS	Liquid chromatography mass spectrometry
MALDI-ToF	Matrix-assisted laser desorption/ionization- time of flight
MeOH	Methanol
MTT	3-(4,5-dimethylthiazol-2-yl)-2,5-diphenyl tetrazolium bromide
NHS	*N*-Hydroxysuccinimide

NIR	Near infrared
NMR	Nuclear magnetic resonance
Oxyma	Ethyl (hydroxyimino)cyanoacetate
PBS	Phosphate-buffered saline
PEG	Polyethylene glycol
PET	Positron emission tomography
PI	Propidium iodide
^{i}PrOH	*iso*-Propanol
PyBrOP	Bromo-tris-pyrrolidino-phosphonium hexafluorophosphate
RP-HPLC	Reverse-phase high-performance liquid chromatography
RFU	Relative fluorescence units
SDS-PAGE	Sodium dodecyl sulfate–polyacrylamide gel electrophoresis
SPECT	Single photon emission computed tomography
rt	Room temperature
THF	Tetrahydrofuran
TLC	Thin layer chromatography
TMS	Trimethylsilane
TSTU	*N*,*N*,*N*′,*N*′-Tetramethyl-*O*-(*N*-succinimidyl)uronium tetrafluoroborate
UV-Vis	UV- visible spectroscopy

Chapter 1 Introduction

1.1 Optical medical imaging

Medical imaging has been instrumental in disease diagnosis since X-ray imaging was first discovered by Röntgen in 1895. The power of imaging being demonstrated by the rapid growth of X-ray technologies, and by the start of the First World War, most hospitals in the UK had X-ray units within their walls.[1] Since the 1960's, several new imaging techniques have come to the forefront, such as computed tomography (CT), magnetic resonance imaging (MRI), positron emission tomography (PET) and single photon emission computed tomography (SPECT) that have radically changed how doctors diagnose and monitor patients. X-ray, CT and MRI imaging are mostly focussed on determining the topography, whereas PET and SPECT were some of the first techniques to incorporate radioactive contrast agents for functional imaging.[2] PET imaging has been instrumental in improving cancer patient survival by elucidation of the location of small tumours before the surgery, as well as allowing the clinician a method of monitoring the effectiveness the radiotherapy treatment is over time. One of the most widely used imaging agents is fluorodeoxyglucose, (^{18}FDG, **1** Figure 1.1), an ^{18}F labelled glucose that is used to determine the location of cancerous cells and tumours, due to enhanced cancerous cell uptake of ^{18}F-glucose (followed by the phosphorylation that leads to 'trapping' inside cells), giving hotspots of tumours on the PET scan.[3]

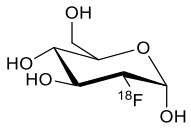

1

Figure 1.1. Structure of ^{18}F deoxyglucose, one of the most popular PET imaging agents.

CT imagery is one of the most popular techniques for hard tissues, due to the speed of acquisition and no requirement of a radiotracer. However, it lacks the resolution needed for soft tissue unless contrast agents are used.[4] Iopromide (**2**, Figure 1.2) is an iodinated contrast agent commonly used to visualise soft tissue at higher resolutions, though this requires millimolar concentrations which can lead to toxicological issues.[2,5]

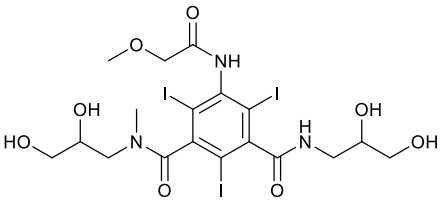

2

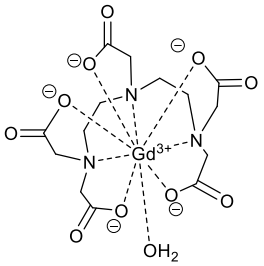

3

Figure 1.2. The CT contrast agent Iopromide (**2**, Ultravist), and the MRI contrast agent Gd-DTPA, **3**.

MRI uses electromagnetic radiation to investigate the anatomy of the patient and give more detailed outline of the morphological changes in the structure of tissue in both health and disease. The strong magnetic radiation is absorbed by hydrogen present in saturated fats and water, and then emitted at a radiofrequency that is detected and compiled into an image. Due to the high water content in soft tissue ionising radiation is not required, however, 30% of MRI procedures in the US use a contrast agent.[6] Gd-DTPA (**3**, Figure 1.2) is an FDA approved gadolinium-based contrast agent used in diagnosis of CNS diseases by monitoring how fast the enhancement dissipates. Gd enhancement

is fleeting in healthy tissue, but the enhancement lingers in the presence of lymphatic damage and lesions.[6,7] MRI gives higher resolution images than PET, but is ineffective in emergency medicine due to the length of time required for an image.

Single photon emission computed tomography is the incorporation of radiotracers into CT scan. SPECT utilises radiotracers that emit gamma rays, unlike PET which uses positron emitting substances.[8] The blood flow of the patient is monitored by the presence or absence of radiation, for example in the treatment of stroke victims, cranial flow can be monitored to detect damaged areas of the brain. SPECT offers the advantage of being cheaper and more readily available than PET, due to radiotracers used having longer half-lives (^{99m}Tc $t_{1/2}$ = 6 h, ^{18}F $t_{1/2}$ = 109 min).[9]

There can be pitfalls in using these methodologies, such as cost, limited specificity but one of the most significant is the radioactive dose delivered to the patient, whether it is through the agent (PET, SPECT) or collecting the image itself (X-ray/CT). Additionally, when using PET and SPECT, the radiotracer must be synthesised which requires highly specialised equipment along with rapid delivery and imaging.[10]

The technique of optical medical imaging (OMI) is being rapidly developed for diagnostic imaging. With OMI, contrast can be achieved using endogenous fluorophores, autofluorescence or specifically developed imaging agents containing a fluorophore.[11] Using fluorescence offers advantages over other imaging modalities, as it requires no radiation and the equipment has the potential to be more compact, affordable and mobile.[12] Additionally, using imaging agents that fluoresce in different spectral ranges allows multiplexing, giving the ability to screen multiple targets simultaneously. Optical imaging is highly sensitive and can achieve high resolution images, giving in depth knowledge at the site of interest at a molecular level in real time.[2]

Optical endomicroscopy uses optical fibres to focus on an accessible area, e.g. lungs, gastrointestinal tract, reproductive tract, etc. It can be specifically aimed to areas of interest in order to direct biopsy or detect disease.[4] However, drawbacks for optical endomicroscopy include the limited field of view and the need for an optical fibre.[4] Reduction of signal can occur through repeated excitation of the imaging agent, through photobleaching and the destruction of the fluorophore, reducing the ability to monitor the target over a long period of time.[13]

1.1.1 Fluorescence

OMI can be achieved *in vivo* using imaging agents and fluorescence. Fluorescence is one mechanism that allows the emission of light from a compound after the absorption of photons. It can be visualised simply through a Jablonski diagram (Figure 1.3).[14]

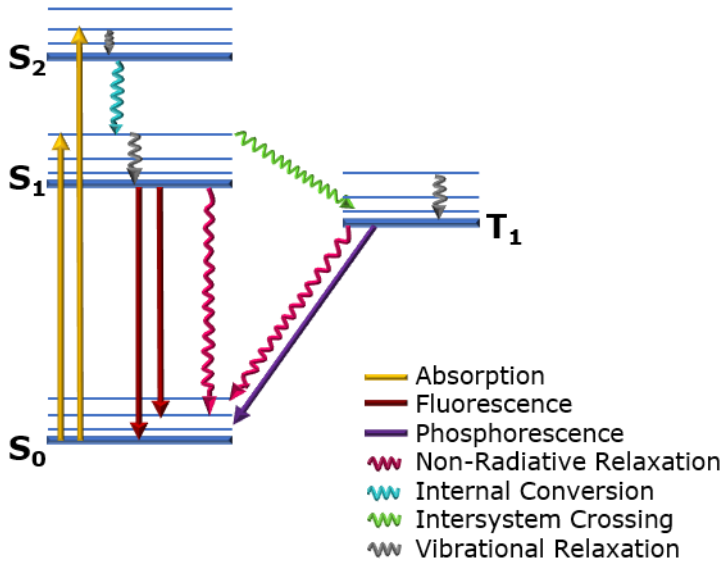

Figure 1.3. A Jablonski diagram indicating the absorption of photons to excite molecules and their subsequent relaxation to generate fluorescence. The straight arrows indicate the photon absorption and emission routes, while the wavy arrows indicate methods of relaxation.

The molecular ground state is excited by the absorption of a photon, inducing its movement to an excited energy level (S_1, Figure 1.3) but can reside at any number of vibrational energy states, according to Frank-Condon rules. The molecule vibrationally relaxes to the closest semi-stable energy level, before undergoing internal conversion to move from one excited level to the lowest, as Kasha's rule states that fluorescence will only occur from the lowest excited level (S_1). Upon reaching it, a photon will be emitted as the electron returns to the ground state (fluorescence), or if there is non-radiative relaxation, then simply transition to the ground state without emission.

The molecule can also move to an excited triplet state (T_1), in a process known as intersystem crossing (ISC, Figure 1.3). ISC is forbidden, as it requires changing the spin state of the electron. The electron relaxes from T_1, to induce phosphorescence (or again, non-radiative relaxation).

The photons emitted are lower in energy than the photon absorbed therefore the emission is at a longer wavelength than the excitation. The difference between the excitation and emission maxima is known as the Stokes shift. This is indicative of the journey travelled by the photon, as a large Stokes shift implies significant energy loss due to excited state transitions. A small Stokes shift is suggestive of energy loss simply through changes in vibrational energy states. The efficiency of fluorescence can be determined through its so-called quantum yield; the percentage of photons emitted divided by the total number of photons absorbed. The quantum yield, in addition to the extinction coefficient of the fluorophore, can be used to define the 'brightness' of the fluorophore.

A fluorophore selected for biological imaging should ideally be chosen to avoid intrinsic autofluorescence of physiologically prevalent molecules such as haemoglobin, while also avoiding excitation wavelengths capable of absorbance by water, etc. (Figure 1.4). This has led to the concept of an ideal *in vivo* imaging window, between 650–900 nm.

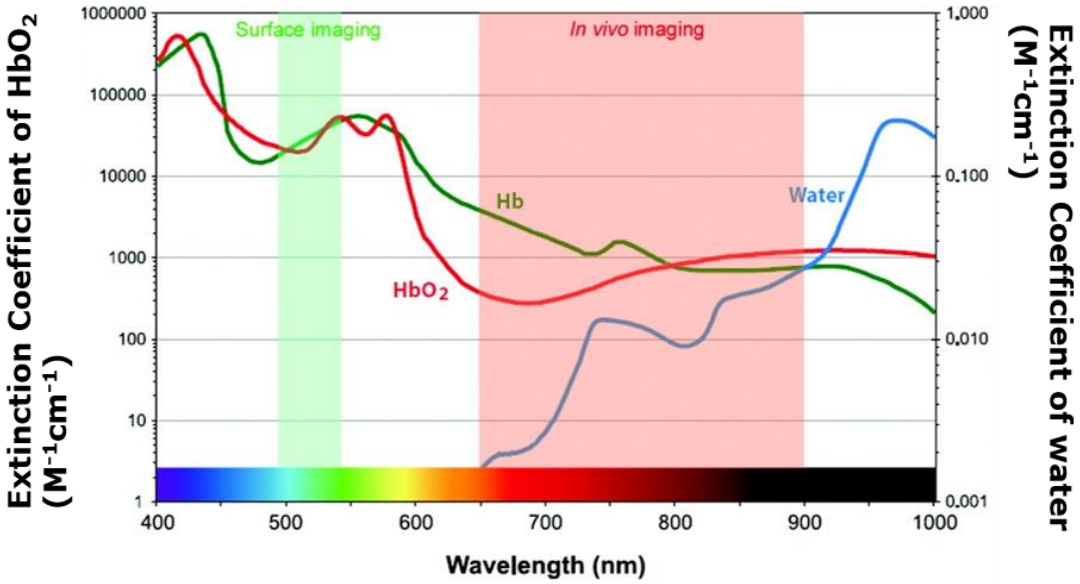

Figure 1.4. A graph plotting wavelength versus the extinction coefficients of several physiological relevant molecules. Reprinted with permission from Chem. Rev. 2010 May 12; 110(5): 2620–2640. Copyright 2009 American Chemical Society.[15]

1.1.2 *In vivo* optical imaging agents

When using optical medical imaging the choice of fluorophore can be vital, mostly determined by the excitation and emission wavelengths, quantum yield, and lifetime. Currently, there are three compounds approved by the FDA as imaging agents: the dyes indocyanine green (ICG, **4**) and fluorescein (**5**) and 5-aminolevulinic acid.[16] ICG (Figure 1.5) is a heptamethine dye that has been used in intraoperational angiography for over fifty years, and is frequently used to monitor the vascular structure during operations of the heart, eye, etc.[15,17,18] with far red excitation and emission wavelengths ($\lambda_{Ex/Em}$ = 785/800 nm) and a high extinction coefficient (ε_{782} = 194 000 $cm^{-1}M^{-1}$ in EtOH).[19] However, its quantum yield is low (Φ = 0.08 in EtOH/H_2O, 7:3), but this can be overcome by the lack of background fluorescence in the optical window at 800 nm.[20]

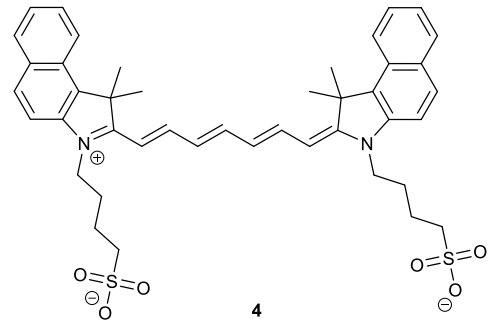

Figure 1.5. The NIR fluorophore indocyanine green (ICG) (**4**), (λ_{Ex} = 785 nm, λ_{Em} = 800 nm).

Fluorescein, **5**, is regularly used in optical angiograms for assessing the vascular structure in the eye.[21,22] It was originally synthesised by Baeyer in 1871 through Friedel-Crafts acylation chemistry (Scheme 1.1)[23] has large quantum yields and extinction coefficients (Φ = 0.95 in aqueous 0.1 M NaOH, ε_{500} 92 300 $cm^{-1}M^{-1}$ in basic EtOH).[14,19] It has an excitation wavelength of 494 nm, with emission at 520 nm, meaning it can be used in parallel with fluorophores such as coumarin and heptamethine dyes. The ubiquitous use of fluorescein is due to several factors, such as its commercial availability, resistance to photobleaching, pH sensitivity, and its high aqueous solubility.

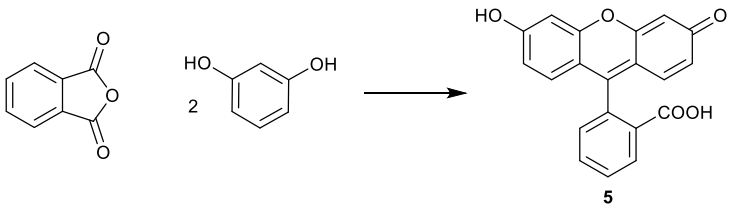

Scheme 1.1. Baeyer's synthesis of the generation of fluorescein (**5**). Reaction conditions: $ZnCl_2$, Δ.

The fluorophores ICG and fluorescein, whilst still popular in medical imaging, lack targeting and cannot be directly attached to a targeting moiety without structural modification. One shortcoming of fluorescein based compounds is the fluorescent emission residing in the same region of the spectrum as tissue

autofluorescence, making it difficult to distinguish background from probe fluorescence.[24]

5-Aminolevulinic acid hydrochloride (5-ALA, Figure 1.6) is a recently approved imaging agent for the detection of glioblastoma tumours during surgery.[25] Oral administration several hours before surgery allows the small molecule to be metabolised (by malignant cells) into the fluorescent metabolite Protoporphyrin IX (Figure 1.6). This metabolite has excitation and emission maxima of 405 nm and 633 nm and is used to elucidate the outer perimeter of the glioblastoma to ensure complete resection of cancerous tissue.[25]

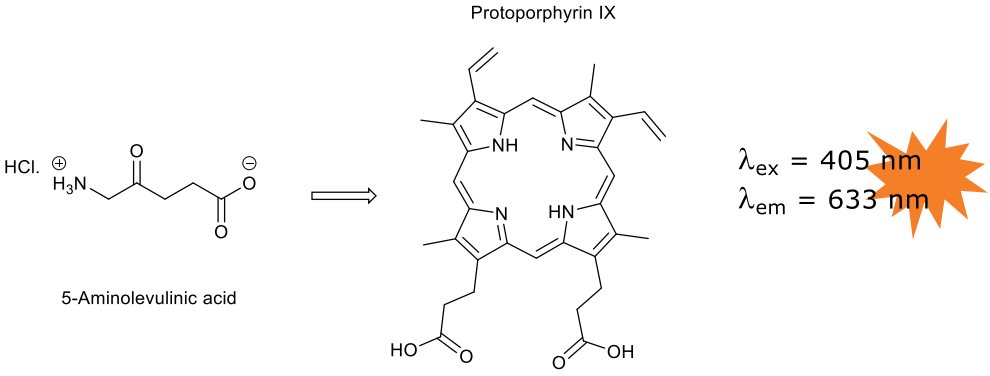

Figure 1.6. The incorporation of 5-aminolevulinic acid into protoporphyrin IX through natural metabolism, to induce a fluorescent signal at 633 nm (when excited at 405 nm).

1.2 Neutrophils

There are two branches of immune system, adaptive and innate, and neutrophils have been implicated in both.[26] The innate immune system is non-specific and is quick acting, within hours, against pathogens, whereas the adaptive is antigen specific and is acquired after interacting with the antigen.[27] There are several types of leukocytes that are constantly monitoring the internal environment (Figure 1.7), with neutrophils acting as the first line of defence. Neutrophils are a type of granophil with a much shorter half-life ($t_{1/2}$

= 5.4 days) than most other leukocytes ($t_{1/2}$ of two weeks or more).[28] It was previously thought to be much less (between 6 and 8 hours) and there is still uncertainty around the study.[29] They are distinguishable by their polynuclear structure and possess numerous membranous sacks of enzymes, or so-called azurophil granules, containing various proteases. The main roles of the neutrophil include immobilisation of bacteria through cleavage of their flagella and subsequent consumption by phagocytosis, as well activating other immune cells, such as macrophages, to direct them to the site of infection.[30] Neutrophils regularly apoptose as a method of maintaining the body's defence system against pathogens.[31]

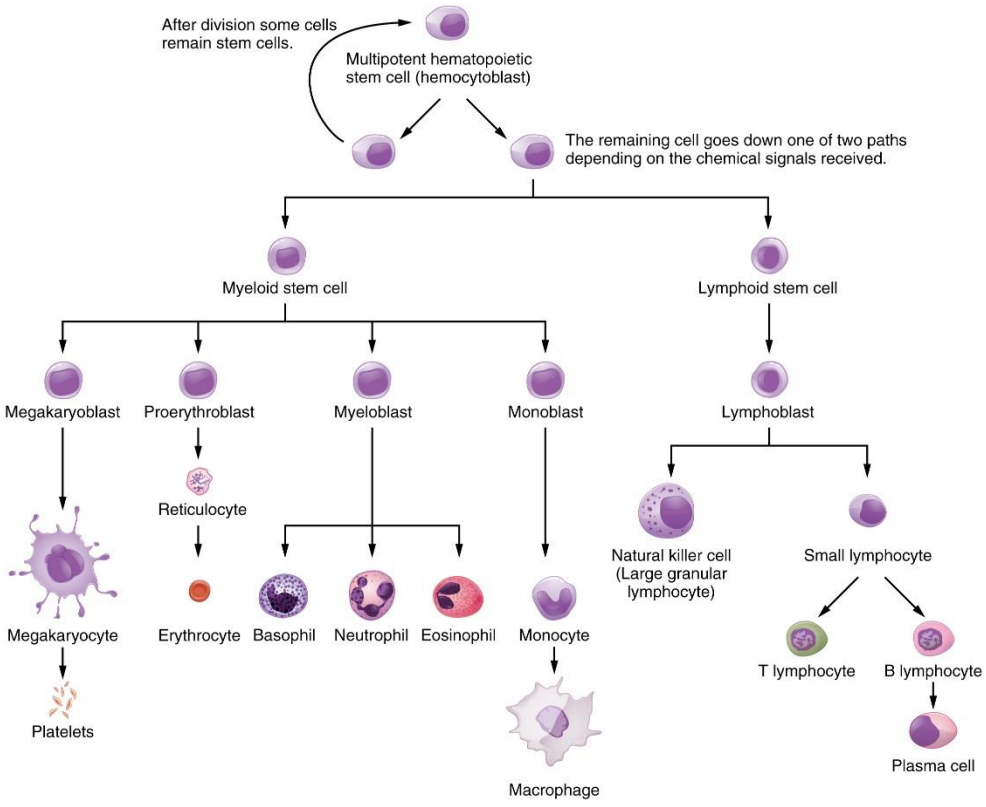

Figure 1.7. The various blood cells that exist within the human immune system. Reprinted with permission from Anatomy & Physiology, Chapter 21, OpenStax, copyright 2016.[32]

The neutrophil contains several degranulative enzymes that aid in decomposing invading organisms, three of which are found in the azurophilic

granules: human neutrophil elastase (HNE), cathepsin G and proteinase 3.[33] There are several methods implemented by the neutrophil to destroy pathogens (Figure 1.8).[34] The enzymes are stored within the granules and are already active and in the first method these remain within the granule. After phagocytosis of the bacteria occurs, it can be 'digested' within the lysosome (A, Figure 1.8). A second route involves activation of neutrophils through activation of the formyl peptide receptor 1 (FPR1) by formylated proteins,[26] whereby the azurophilic granule relocates to the cell membrane and is 'docked', presenting the enzymes extracellularly by anchoring them on the outer membrane (B, Figure 1.8). This method enables the enzymes to be close to the site of inflammation and cover a larger area.

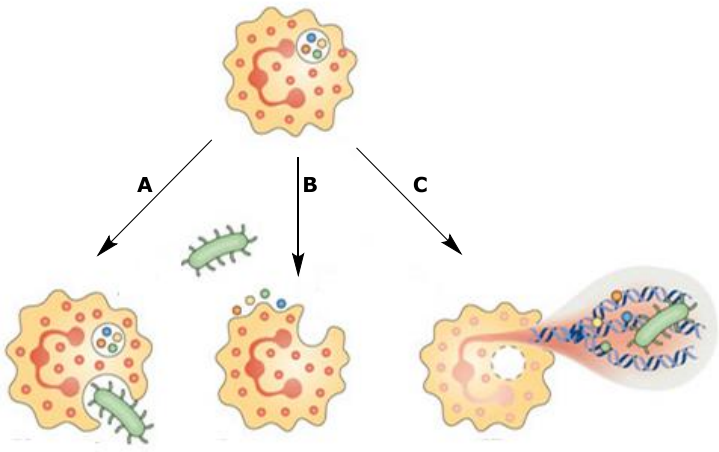

Figure 1.8. Depictions of the methods of pathogen degradation by the neutrophil: A) phagocytosis of the pathogen; B) enzymes within the granule are 'docked' to the outer cell membrane for extracellular attack of the pathogen; C) the use of NETs to release the proteases extracellularly in a self-destructive manner. Adapted by permission from Springer Nature: *Nat. Rev. Immunol.* 2013; **13**(3): 159–175, copyright 2013.[35]

Thirdly, one of the more aggressive methods of bacterial digestion used by the neutrophil is the use of neutrophil extracellular traps (NETs, Figure 1.8 Path C). This is a suicidal method of capture where neutrophils have 'explosions'

of DNA loops with active proteases attached.[36] They act as an extension of the neutrophil and surround the bacterium, resulting in increased levels of degradation. The enzymes are held in place by ionic bonds formed with the chromatin on the DNA loop, preventing them from attacking other endogenous proteins nearby.[36] These however are a last resort for a neutrophil as it induces apoptosis and simultaneously emits signals to other leukocytes for them to consume the apoptotic bodies produced.[37] Alongside digestive enzymes, neutrophils also generate highly reactive oxidative species (such as hydrogen peroxide) in the phagolysosome using NADH oxidase to destroy pathogens.[29,34]

The serine proteases human neutrophil elastase, proteinase 3 and cathepsin G all contain the same catalytic triad (His, Asp and Ser) and mechanism of amide hydrolysis (Scheme 1.2). The active sites of the enzymes are prone to be indiscriminate, to enable their ability to degrade a large range of proteins and many of the pathogens.[33]

1.2.1 Human neutrophil elastase

Many enzymes in the body are classified as proteases, indeed they encompass almost 2% of the human genome.[38] The regulation of these proteases plays a key role in numerous diseases. HNE is a 29 kDa protease that resides in the neutrophil and was originally described by Janoff, who named it after its capability to digest elastin.[39] It was soon established as having other properties such as degrading pathogens. The enzyme is 218 amino acids long (transcribed from chromosome 19) and is comprised of a *C*-terminal α-helix and two β-barrels, each of which contain six antiparallel β-sheets (Figure 1.9). The barrels converge and form the S1 pocket which is hydrophobic due to the presence of the surrounding residues of valine and phenylalanine.[34,40]

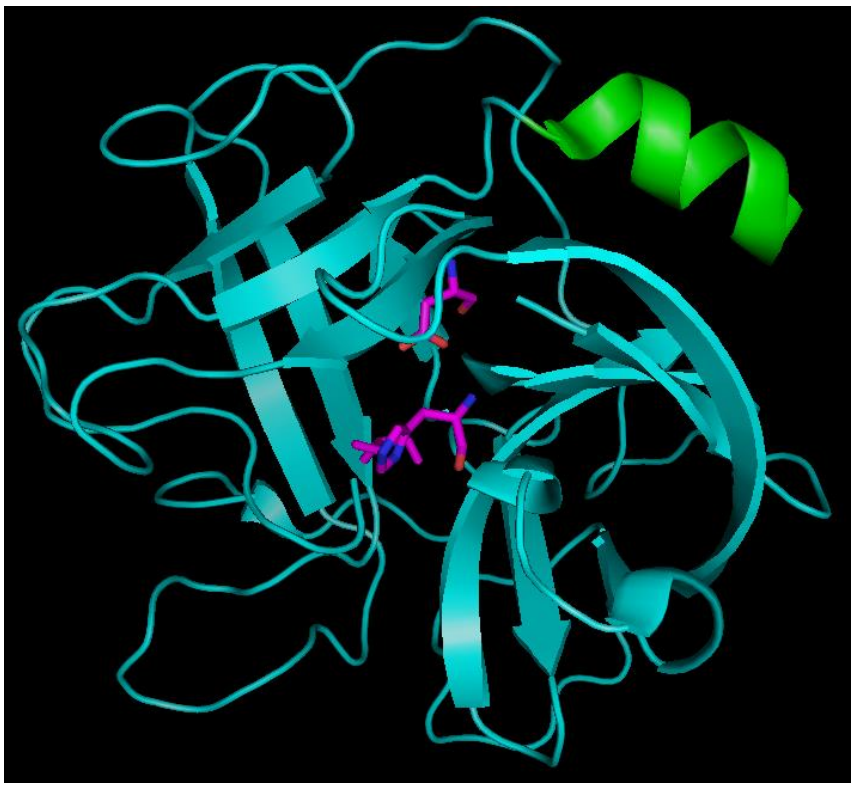

Figure 1.9. The structure of human neutrophil elastase that has been complexed with the GSK inhibitor GW475151. The green feature is an α-helix at the C-terminus connected to six antiparallel β-sheets (blue flat arrows) that form two β–barrels. The magenta residues in the centre depict the catalytic triad.[41]

Neutrophil elastase is capable of digesting a wide variety of proteins such as collagen, fibrin, elastin and fibronectin.[42] Examples of pathogen degradation include the cleavage of the outer membrane proteins of Gram negative bacteria such as *E. coli* and the degradation of the virulence factors for a wide range of enterobacteria preventing them from escaping phagocytosis.[43]

HNE is integral to a plethora of signalling pathways for the immune responses, both anti and pro-inflammatory.[44] The ability to induce a second wave of immune response from leukocytes through the release of interleukin-8 (IL-8) gives a pro-inflammatory response,[27] but digesting the cytokines tumour necrosis factor alpha (TNF-α) and IL-2 (Interleukin-2) can prevent cytotoxic activities and activation of other leukocytes such as T cells, thus

reducing the immune response.[45] The most prominent indigenous promoters are TNF-α, IL-8, C5a (complement protein 5a) and IL-1β. These are used by the immune system to stimulate a response to any form of injury and to induce neutrophil aggregation in the vicinity for a swift response. There are other HNE promoters that include LPS (lipopolysaccharide) compounds present on the outer membrane of Gram-negative bacteria and *N*-formyl oligopeptides that are released by bacteria (a well-established mimic is the tripeptide *N*-formyl-Met-Leu-Phe).

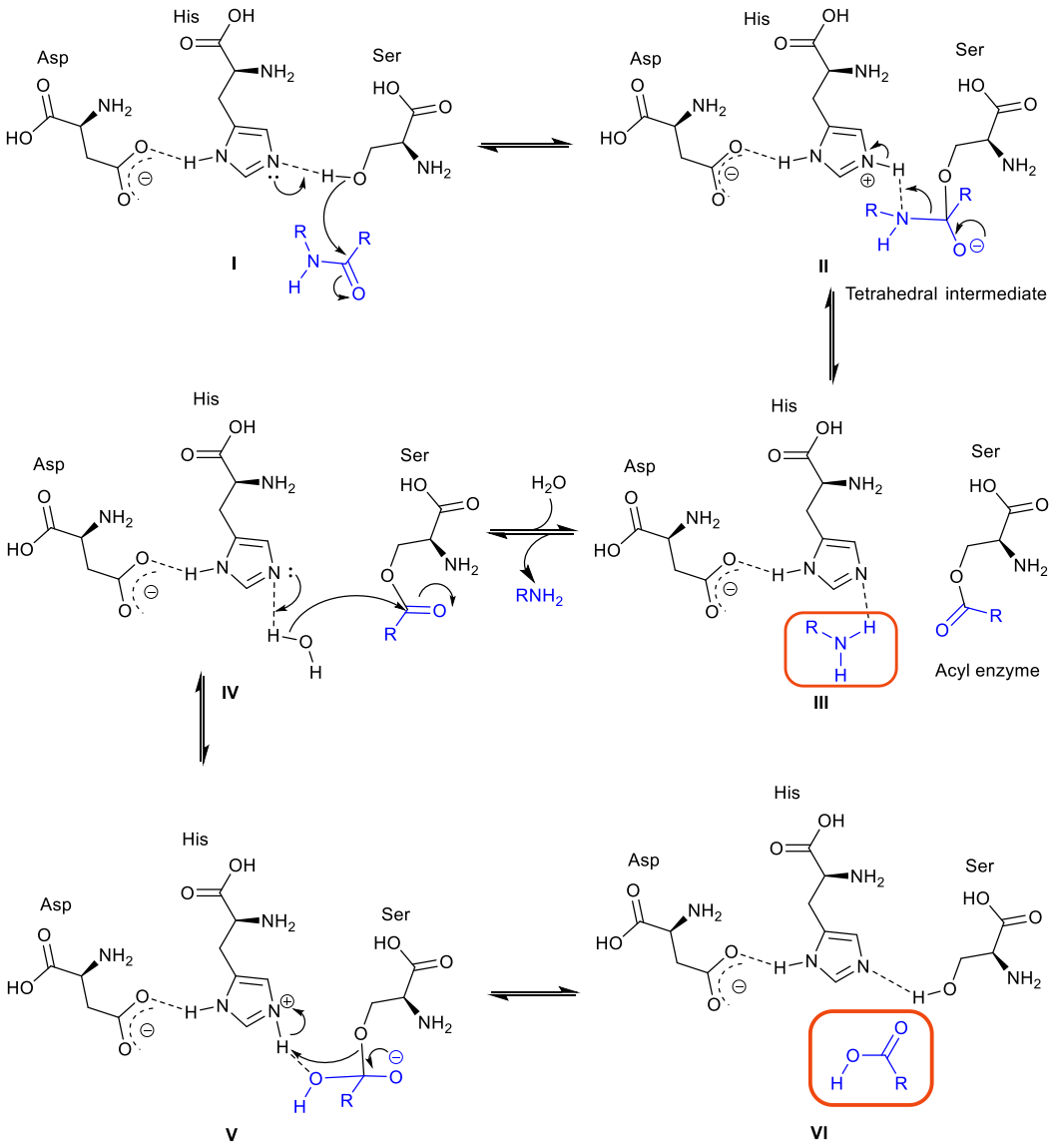

Scheme 1.2. Hydrolysis of amide bonds by the catalytic triad histidine, aspartic acid and serine within the active site of the enzyme human neutrophil elastase. The carbonyl moiety of the peptide undergoes nucleophilic attack from the hydroxyl group of the serine residue (**I**) to generate the tetrahedral intermediate (**II**). The carbonyl is regenerated, breaking the C-N bond to form an acyl enzyme intermediate on the serine and liberate an amine (**III**). The water undergoes nucleophilic attack of the ester (**IV**), hydrolysing the serine ester (**V**), to release the carboxyl acid and regenerate the enzyme (**VI**).

1.2.2 Human neutrophil elastase in disease

Due to the methods of enzyme activation within the neutrophil, the pro-inflammatory response of HNE may be extreme, and this can cause irreversible damage to tissue if uncontrolled. Indeed, overexpression of HNE induces several chronic inflammatory diseases, such as emphysema, chronic obstructive pulmonary disease (COPD), acute lung injury (ALI), fibrosis and acute respiratory distress syndrome (ARDS).[44,46] Other inflammatory diseases with causative HNE levels include psoriasis, where high levels of HNE cleave the interleukin-36 receptor antagonist increasing its biological activity, leading to degradation of the upper dermal layer of the skin, causing patchy flakes of skin and discomfort.[47]

Acute lung injury is a mild variety of acute respiratory distress syndrome, and is defined as clinical syndromes of respiratory failure after an injury or disease, such as sepsis, trauma, acute pancreatitis, etc.[48] The injury induces an exacerbated inflammatory response that causes proteinase concentrations to be unbalanced with excess activated enzymes degrading lung tissue.[49] Since HNE increases the response by releasing chemokine IL-8, ALI can be aggravated over time into a more severe form, ARDS. In a study by Lee, it was found that 52% of ARDS patients had high levels of HNE activity in their bronchoalveolar lavage (BAL).[38] The HNE activity was not reduced by normal levels of α1-antiprotease (α1-AP),[50] one of the main endogenous protease inhibitors.

Currently, the clinical gold standard for HNE detection in the lung is a BAL; a large volume of saline (120 mL) is sprayed into a specific section of the lungs and then removed out. Histology is conducted using a variety of staining techniques and the fluid cultured to detect the pathogens present.[51,52] It can take several days for the results of pathogen identification, and most diagnoses require an additional biopsy, making the procedure less than ideal.

The difficulty in diagnosing pulmonary diseases associated with high levels of HNE leads to vague criteria for a positive diagnosis. Both academia and industry have developed small molecule inhibitors for HNE with the aim of reducing and managing the symptoms of diseases such as COPD and ALI.[53] This need is obvious by the number of patents published in this sector, and has been reviewed succinctly in the last ten years.[54–56] The use of optical probes as a diagnostic tool for clinicians and as a method to validate drugs, would be beneficial to detect certain pulmonary diseases as well to stratify patients, preventing further degradation of lung tissue in patients.

1.3 Optical imaging probes

There is a plethora of enzymes present within the body, all up or down regulated by the enormous ecosystem contained within. It comes to no surprise that the misregulation and overexpression of enzymes has been studied for years as a potential mechanism behind several diseases. Because of this, there have been a wide range of optical probes generated for the investigation and interrogation of isolated proteases, such as caspases,[57] and other cysteine proteases,[58] matrix metalloproteinases, cathepsins,[59–61] not to mention other enzyme families such as esterases,[62] oxidases,[63,64] etc. As HNE has been implicated in a wide variety of diseases, there has been interest in designing optical probes that are diagnostic tools. In addition, inhibitors have been designed as a treatment option for several disease states.[56]

One of the first probes to detect HNE was developed by Powers and was a chromogenic peptide sequence, MeOSuc-AAPV-pNA (Figure 1.10, **6**).[65] The peptide sequence is cleaved by the enzyme, releasing *p*-nitroanilide which is detected by its absorbance at 405 nm. One of the disadvantages of **6** is the requirement for measuring absorbance rather than fluorescence and this can

be circumvented by using its fluorogenic counterpart, MeOSuc-AAPV-AMC (Figure 1.10, **7**). It is an umbelliferone based peptide substrate that has a quenched fluorescent signal until the umbelliferone is released by cleavage of the amide bond. There are still drawbacks of both probes that include their non-selectivity for HNE over other proteases, and the presence of the methyl succinyl ester that will interact with other enzymes in the body, preventing use *in vivo*.

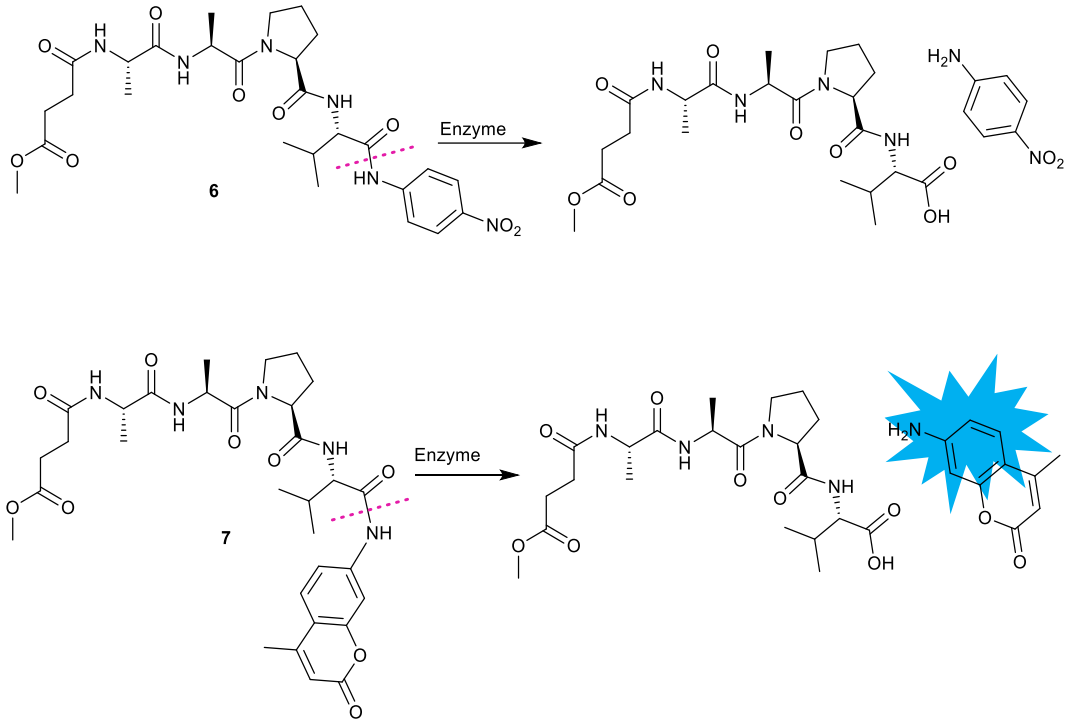

Figure 1.10. The peptide substrates MeOSuc-AAPV-pNA, **6**, a chromogenic substrate used to detect the presence of proteases (HNE, k_{cat}/K_m = 1.2 × 10^5 M^{-1} s^{-1}), and MeOSuc-AAPV-AMC, **7**, its fluorogenic counterpart (HNE, k_{cat}/K_m = 1.1 × 10^4 M^{-1} s^{-1}, λ_{Ex} = 360 nm, λ_{Em} = 460 nm).

There are multiple ways to design an optical probe: activity-based, substrate-based, environmentally sensitive, and always on probes (Figure 1.11). The activity-based probes are frequently designed to be a small molecule attached to a quenched fluorophore; upon interaction with the enzyme in question, the structure alters and the quenching mechanism is inhibited, allowing a

fluorescent signal to be produced.[66] If specific enough it can be incredibly useful for determining the levels of enzyme activity present in both healthy and diseased states, as well as identifying the location of enzyme activity.

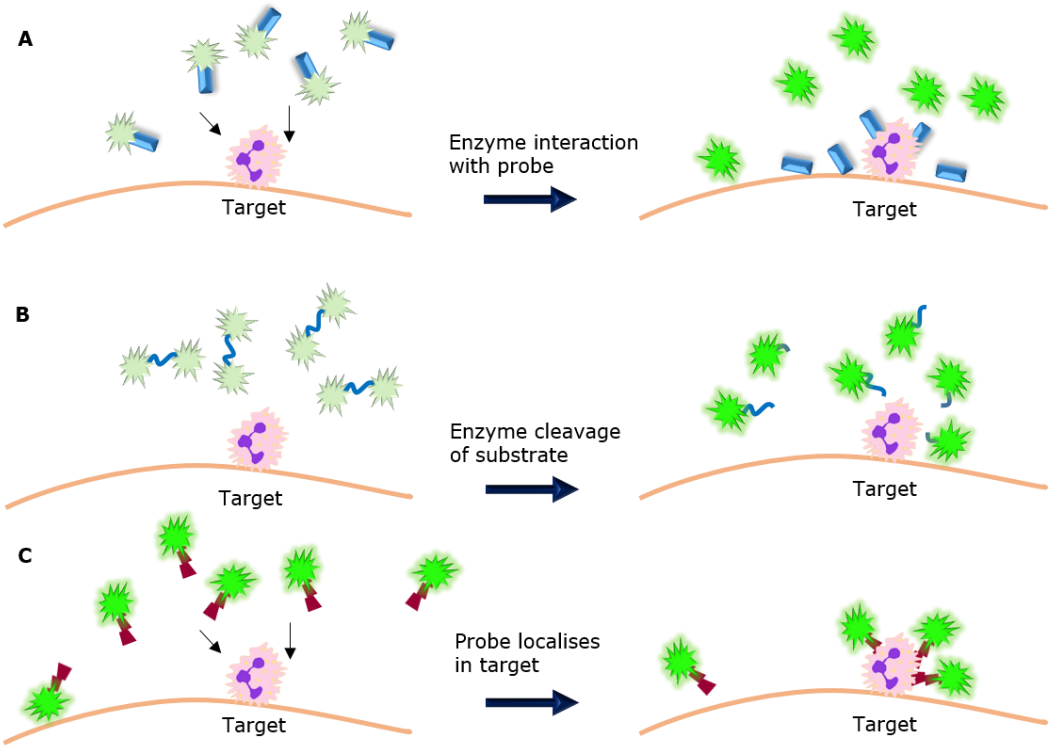

Figure 1.11. Mechanisms of optical probes. A) An activity-based probe, whereby the structure of the probe is modified after interacting with the enzyme, inducing a fluorescent signal; B) A substrate-based probe, a probe with a peptide sequence that can be cleaved to induce fluorescence; C) An always-on probe, where the fluorophore has no quenching, but the probe has a highly specific binding mechanism towards the target.

Secondly, there are substrate-based probes, mostly peptide sequences that are specific to the enzyme of interest (B, Figure 1.11). The peptide might have a fluorophore at one or both termini which self-quench or interact in some way. Upon cleavage of the substrate by the enzyme, the fluorophores will be physically separated, the interaction broken, inducing a signal response from

the fluorophore. Another type of optical probe is 'always-on' probes (C, Figure 1.11). This is when the fluorophore itself has no mechanism of quenching but is directly attached to the targeting group of the compound, giving a signal. The probe is then only bound by the target, fluorescing and can be imaged in its place. This type of probe is beneficial in that it gives more information about the quantity of the target and its location whereas the substrate based, and activity-based probes mostly give a binary response: fluorescence emission if the target is present or no signal. The literature has separated the optical probes into these categories for ease of comparison.

1.3.1 Activity-based probes for elastase detection

The optical probe **8** is an umbelliferone based probe for the detection of HNE, (Figure 1.12).[67] The pentafluoroethyl acetamide group induces photoinduced-electron transfer (PeT) quenching, allowing for an 'off' state of the probe. **8** was further tested after it also showed selectivity towards HNE over other enzymes such as chymotrypsin and trypsin. However, they did not do a screen of other neutrophil-related proteases.

There are several parameters that can be used to describe the efficiency of an enzyme. Km is the concentration of substrate at which the enzyme is at half the maximum velocity and is indicative of how fast the enzyme catalyses the reaction. The number of substrate molecules cleaved per unit time can be defined as k_{cat}.

For optical probe **8** they determined the Km to be 20 μM, and the k_{cat} as 22 min^{-1} with a limit of detection of 68 ng/mL. Compared to the chromogenic substrate MeOSuc-Ala-Ala-Pro-Val-pNA (**6**, Figure 1.10) it was 7-fold slower but they failed to investigate the fluorogenic counterpart MeOSuc-Ala-Ala-Pro-Val-AMC,[68] which has a Km of 140 μM. However, the cost to produce **8**

was far cheaper, as is the advantage of small molecular probes over peptide-based probes.

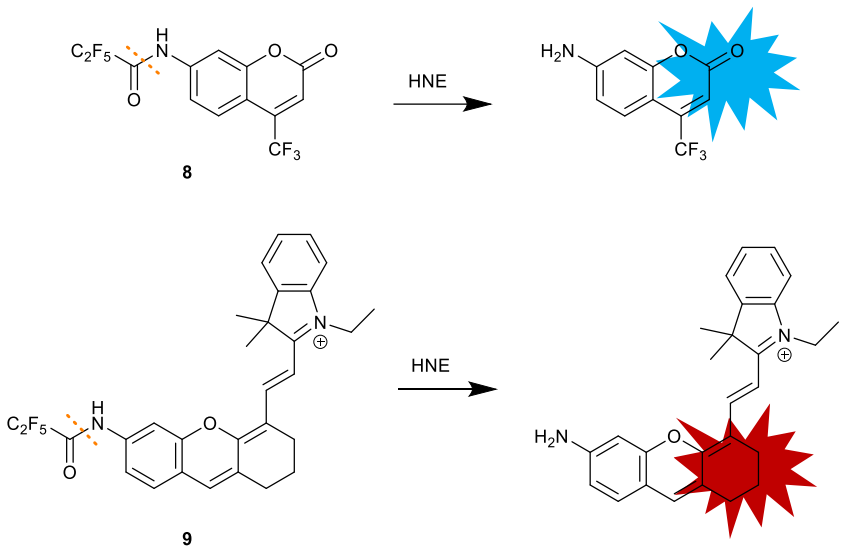

8 9

Figure 1.12. Switch-on optical probes for HNE detection from Yang *et al.* **8** (λ_{Ex} = 490 nm, λ_{Em} = 525 nm) and **9** (λ_{Ex} = 670 nm, λ_{Em} = 700 nm), where the dashed orange lines indicate the enzyme cleaveage.[67,69]

The same group published another paper on HNE detection but in the far-red region.[69] They used a modified Cy7 dye and as before induced self-quenching by placing a pentafluoroethyl acetamide on the aniline to generate **9** (Figure 1.12). However, in a similar manner to their previous paper, they only screen non-related enzymes, such as acetylcholinesterase and carboxypeptidase. They also showed that Sivelestat (a popular HNE inhibitor) reduced cleavage of the probe but it was clear from the images that NIR fluorescence was still generated, presumably due to non-specific cleavage. Issues arise from the types of cell used by the group, A459 and RBL-2H3 cells (basophil line). The cells were first incubated with a solution of isolated HNE before adding the probe. This gives no indication of physiological levels of HNE in either cell line, or that the probe was not targeted by other related proteases present. No information was given regarding the k_{cat} or K_m of this probe.

1.3.2 Substrate-based probes

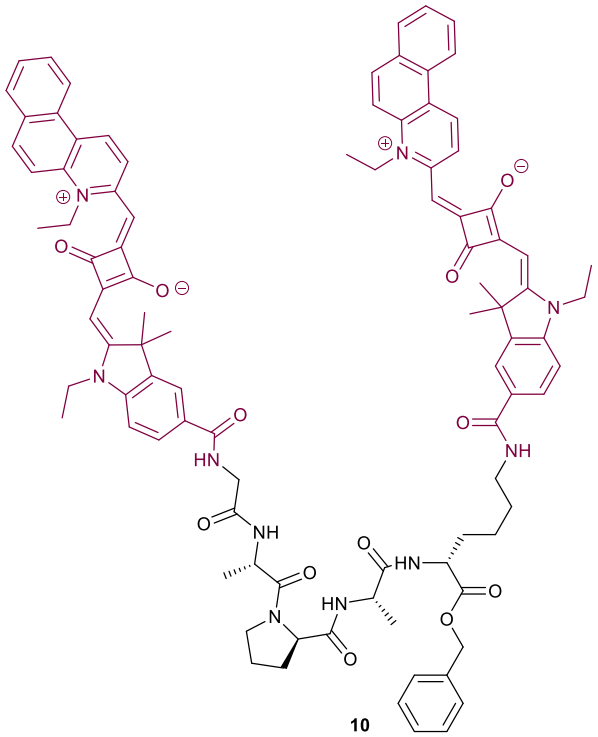

Figure 1.13. Structure of the self-quenching squaraine based optical probe **10** (PBS, λ_{Ex} = 605 nm, λ_{Em} = 658 nm when cleaved).[70]

A peptide-based probe **10** was synthesised by attaching two squaraine based dyes (Figure 1.13).[70] With a highly specific peptide sequence selected, β-Ala-Ala-Pro-Ala-Lys-OBzl, with the two dyes conjugated at the amino terminus and on the primary amine of a lysine residue. This allowed for self-aggregated quenching due to the planarity of the dye. The authors report no kinetics of the HNE cleavage of the substrate, but they did confirm that the fluorescence intensity underwent a significant increase upon interaction with the enzyme. The end goal of the probe was not for use *in vivo*, but to adhere it to a glass slide for microarray analysis. The end goal was to adhere a mixture of different proteases to qualitatively state which enzymes are present in disease states by screening several simultaneously.

Probes **11** and **12** are two FRET (Forster resonance energy transfer) based 'activatable' probes for HNE with each comprising two fluorophores connected by a peptide sequence (Figure 1.14).[71] The optical probe **11** comprises methoxycoumarin (donor, $\lambda_{Ex/Em}$ = 354/400 nm) and coumarin 343 (acceptor, $\lambda_{Ex/Em}$ = 444/490 nm) which are connected by a PEG spacer to enhance the water solubility of the probe. The peptide sequence is cleaved between the two valine residues, and as the fluorophores are separated, illumination at 345 nm results in an emission at 400 nm, and this allowed for quantitative analysis of enzyme activity.

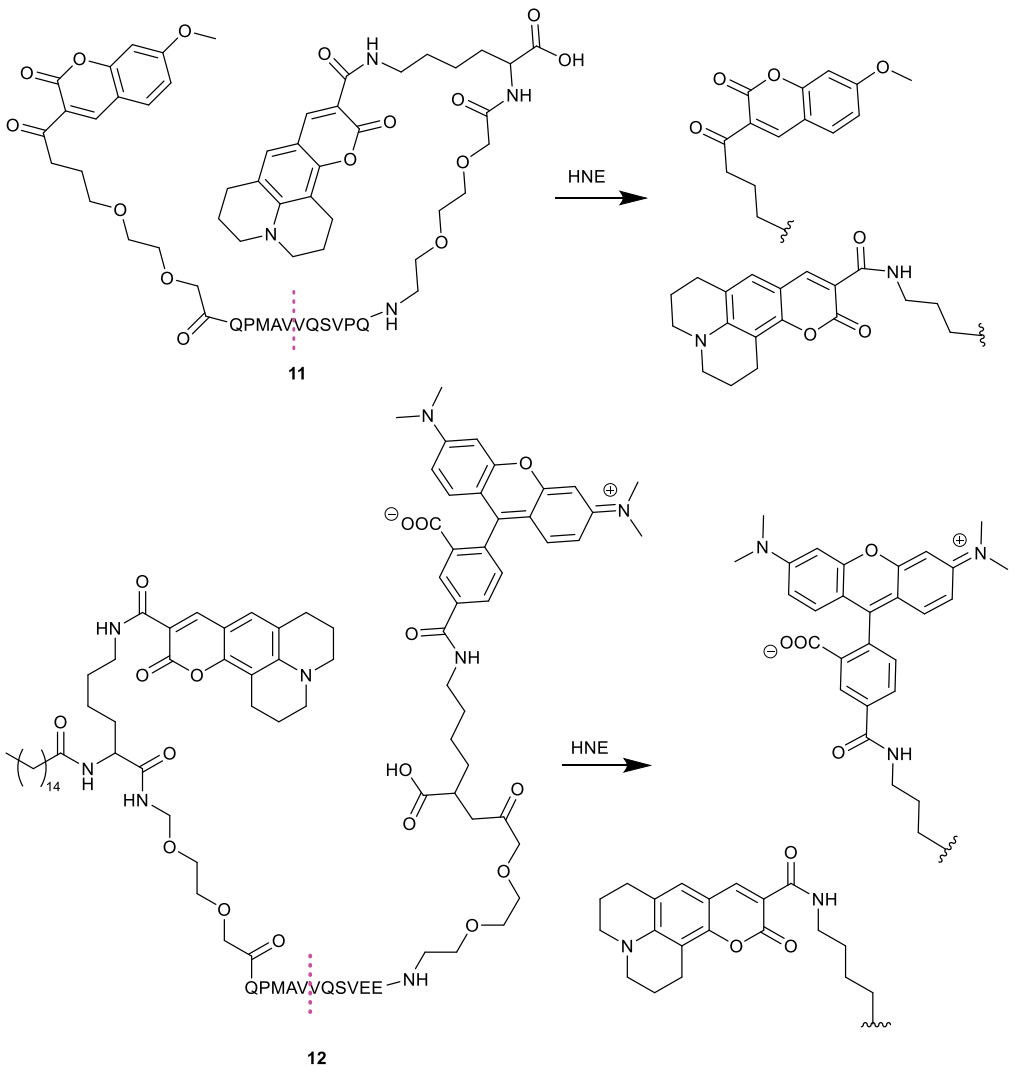

Figure 1.14. Non-cleaved optical probes **11** (non-cleaved λ_{Ex} = 354 nm, λ_{Em} = 490 nm) and **12** (non-cleaved λ_{Ex} = 444 nm, λ_{Em} = 575 nm). The activity probes are cleaved between the two valine residues on the peptide sequences (orange dashed lines).

Probe **12** comprises the fluorophores coumarin 343 (donor, $\lambda_{Ex/Em}$ = 444/490 nm) and TAMRA (acceptor, $\lambda_{Ex/Em}$ = 456/575 nm), connected by a slightly modified peptide sequence to that of **11**. It also contains a C_{15} alkane chain to increase the hydrophobicity of the probe, allowing it to dock to the cell's outer plasma membrane. This permits the probe to only monitor the extracellular HNE activity, whilst securing the coumarin 343 fluorophore in place. As the peptide sequence is cleaved by the enzyme, the TAMRA (5-

carboxytetramethylrhodamine) moiety is released from the cell membrane and coumarin emission observed. The combined use of the two probes has elucidated for the first time that HNE activity is primarily active on the surface of the neutrophil, with biological studies carried out on murine neutrophils taken from a BAL sample.

1.3.3 Always-on probes

The peptide probe **13** contains four unnatural amino acids that had been selected as the substrate with the highest affinity towards HNE during a screening process developed by Kasperkiewicz (Figure 1.15).[72,73] The *C*-terminus was a diphenyl phosphonate moiety that irreversibly binds with the active site, and the *N*-terminus a long PEG chain capped with a biotin. The classical pairing of biotin-streptavidin allows for secondary labelling, as a streptavidin labelled fluorophore would bind the biotin enabling quantitative detection of HNE. There are several advantages of this type of probe, such as the ability to use a wide range of fluorophores conjugated to biotin; to allow a more accurate calculation of HNE and the ability to easily incorporate into gel electrophoresis. However, it cannot be used *in vivo* as a diagnostic tool.

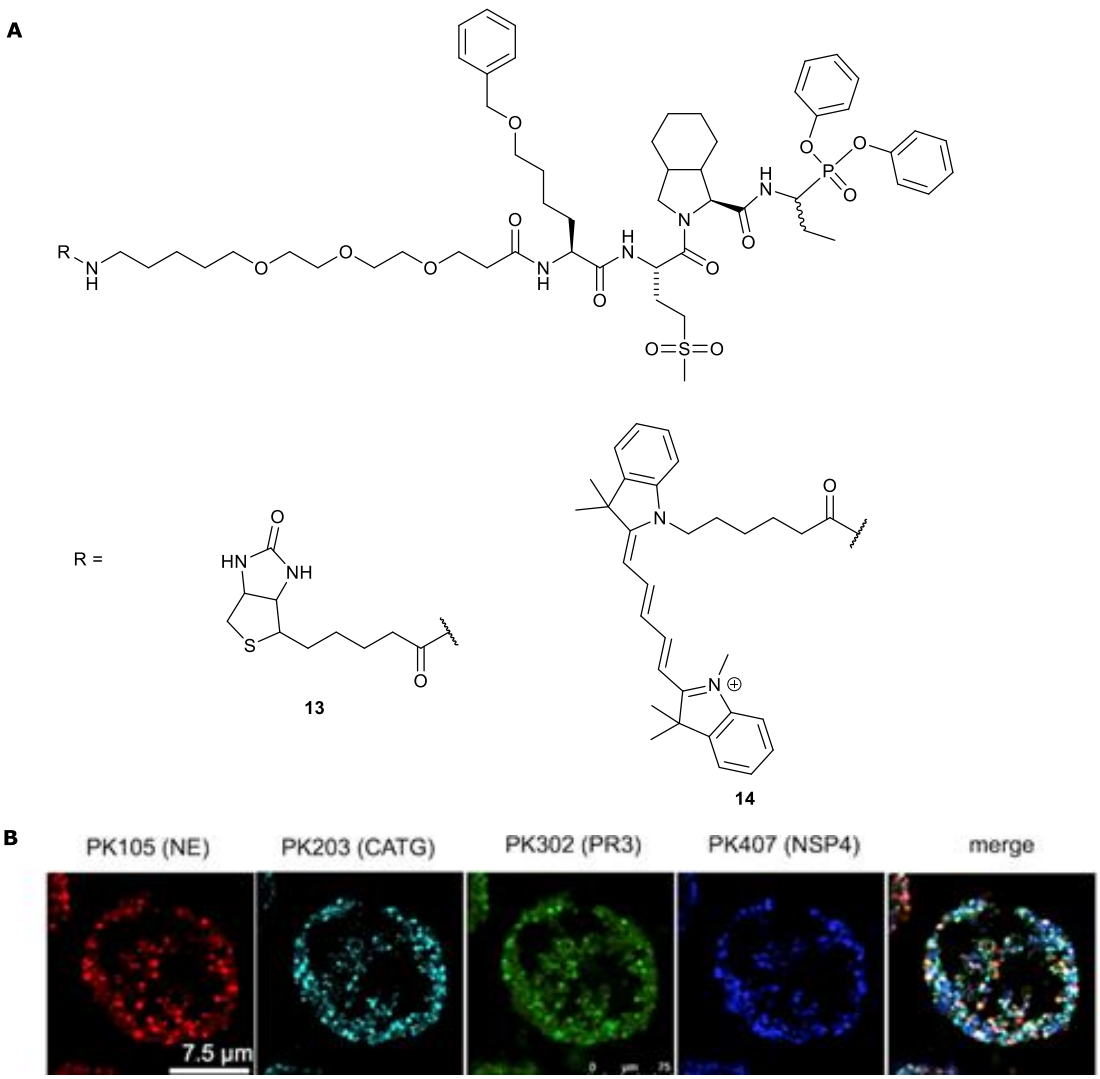

Figure 1.15. (A) Optical probes for the detection of HNE **13** and **14**. (B) Confocal images of a neutrophil labelled with optical probes interrogating the presence of serine proteases (red = HNE, light blue = Cat G, green = Pr3, dark blue = NSP4). Reprinted with permission from J. Am. Chem. Soc. 2017, **139**, 10115-101125. Copyright 2017 American Chemical Society.[73,74]

Since the original research publication of the initial computational screening and cell research,[73,75] the group itself has developed the scope of the probes to include the other serine proteases present in the neutrophil: cathepsin G, proteinase 3 and neutrophil proteinase 4 (Figure 1.15).[74] Peptide sequences incorporating both natural and unnatural amino acids were chosen based on their specificity to the four enzymes: the sequence for HNE was Nle(O-Bzl),-

Met(O)$_2$-Oic-Abu (depicted in Figure 1.15 A), NSP4 was hCha-Phe(guan)-Oic-Arg, Cat G was His(Bzl)-Val-Pro-Phe and Glu(O-Bzl)-Lys(Ac)-hPro(Bzl)-Nva for Pr3.[72] They developed four optical probes for each protease by altering the fluorophore: BODIPY, Cy3, Cy5 or Cy7 (16 probes in total). The Km of the labelled peptides were determined for all enzymes and the fluorophore on each probe were down selected based on their reactivity. The separation in the fluorescent signals from all dyes allowed for multiplexing of the enzymes for simultaneous staining (Figure 1.15, B). The final HNE imaging probe selected based on the best affinity was the Cy5 labelled peptide **14**, which had a k_{cat}/Km of 8.1 × 10^6 $M^{-1}s^{-1}$, but it also had affinity towards Pr3 (k_{cat}/Km = 1.9 × 10^5 $M^{-1}s^{-1}$). The research was transferred to live neutrophils and it is a major step forwards at imaging immune response *in vivo*. Interestingly, they found that the distribution of the proteases within the neutrophil was uneven, as can be seen in B of Figure 1.15 and using image analysis, determined the concentrations of the different enzymes.[53]

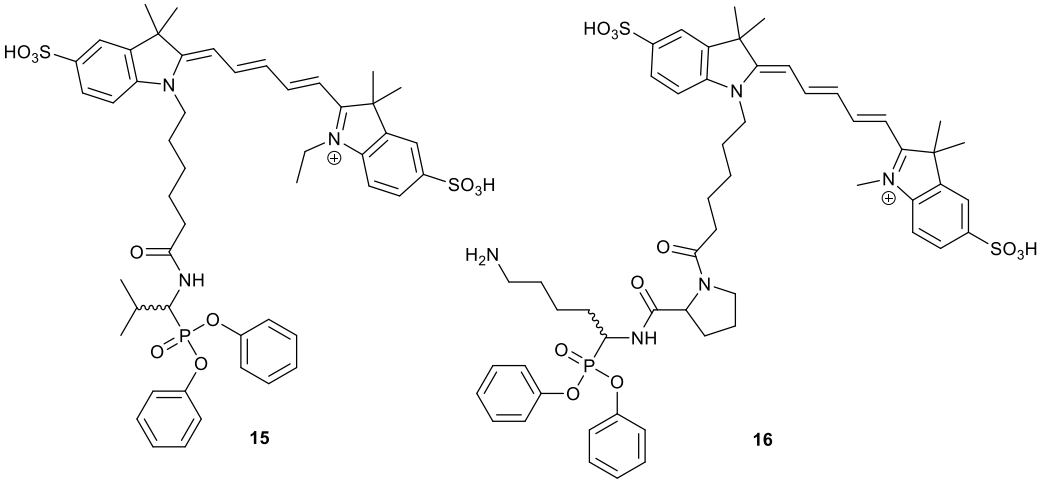

Figure 1.16. Far-red probes **15** and **16** developed by Bunnett.[76]

Further developing the chemistry from Kasperkiewicz, another group used the same diphenylphosphonate warhead, but incorporated only one or two amino acid residues in between the warhead and fluorophore (Figure 1.16), thus **15** contained a valine residue and **16** proline and lysine.[76] They were

developed in the hope that they would be able to detect serine proteases, and after the synthesis, they were screened against a selection such as HNE, Pr3 and trypsin, to confirm their selectivity. **15** labelled both Pr3 and HNE, but **16** showed more affinity towards trypsin and thrombin. Probe **15** was taken through to further investigation, but mostly used in gel electrophoresis experiments, to determine the specificity and dosing requirements. A study on acute pancreatitis was conducted by creating a murine model of the disease through injecting the subjects with the oligopeptide caerulein to induce pancreatic secretion. The optical probe (20 nmol) in a mixture of DMSO and PBS (2:8, 100 μL) was then injected into the subjects and monitored. The negative controls showed no probe had been cleaved within the pancreas, whereas the pancreatitis models show strong levels of fluorescent signal. However, upon gel electrophoresis of cell lysate, no labelled enzyme was seen, indicating that it doesn't irreversibly bind to the probe, or is highly non-specific.

Optical probe **17** (Figure 1.17) was also developed based on the diphenyphosphonate structure but modified to include a methyl thioether in the para position compared to the original **13.**[77] They found that using a mixture of natural and non-natural amino acids in their tripeptide recognition moiety gave a higher affinity towards HNE.

The azido functionalised **17** without a dye had a k_{inac}/K_i value of 3.9×10^5 $M^{-1}s^{-1}$ (*S,R,S*), higher compared to its diastereomer (*S,S,S*) at 1.0×10^3 $M^{-1}s^{-1}$. Upon the addition of the fluorophore to form **17**, the reactivity was reduced to 8.8×10^4 $M^{-1}s^{-1}$, but still higher than (*S,S,S*). The inhibition of the activity of proteases by the three tripeptides showed them to be ineffective against cathepsin B and L, as well as thrombin and trypsin. The peptides were shown to be selective for HNE over its porcine counterpart, porcine pancreatic elastase, but no other serine proteases found in the neutrophil were tested and so it is difficult to determine their selectivity. The peptide was not used in cell imaging, but used

in gel electrophoresis, where they saturated HNE with the probe before running the gel. The azido group gave rise to the ability to attach different fluorophores depending on which excitation and emission wavelengths were required. This was achieved by using Huisgen's copper catalysed azide alkyne cycloaddition (CuAAc or click).[78] This approach is appealing as it is high yielding, can be completed in mild conditions and enables the use of most fluorophores that are alkyne functionalised, but further testing would be required to determine if the peptide is specific enough for the enzyme targeted.

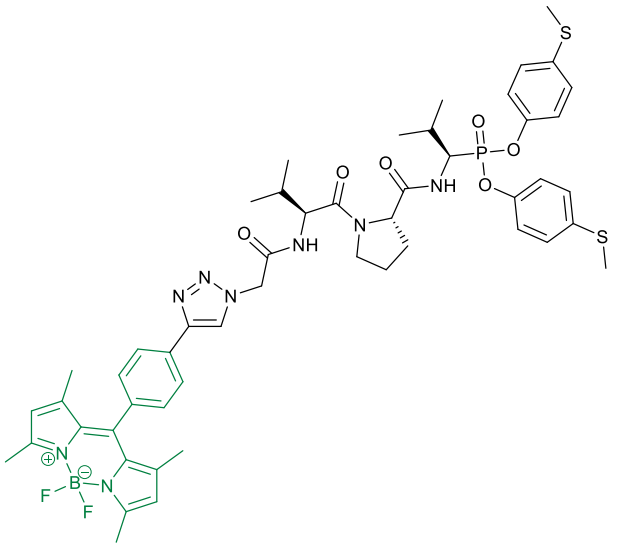

17

Figure 1.17. Structure of the BODIPY based optical probe **17** (H_2O, λ_{Ex} = 509 nm, λ_{Em} = 513 nm).[70]

1.4 Previous research

The Bradley/ Dhaliwal team has long been interested in HNE due to the damage that it can inflict on the lung by its overexpression, and so two previous optical probes were developed, **18** and **19** (Figure 1.18).[79] The probes

were based on peptides with a known specificity towards HNE and were tri-branched to induce self-quenching of the fluorophore, (carboxyfluorescein, $\lambda_{Ex/Em}$ = 490/525 nm). Upon peptide cleavage, the carboxyfluorescein molecules are released inducing a fluorescence signal (4-fold for **18**, 2-fold for **19**).

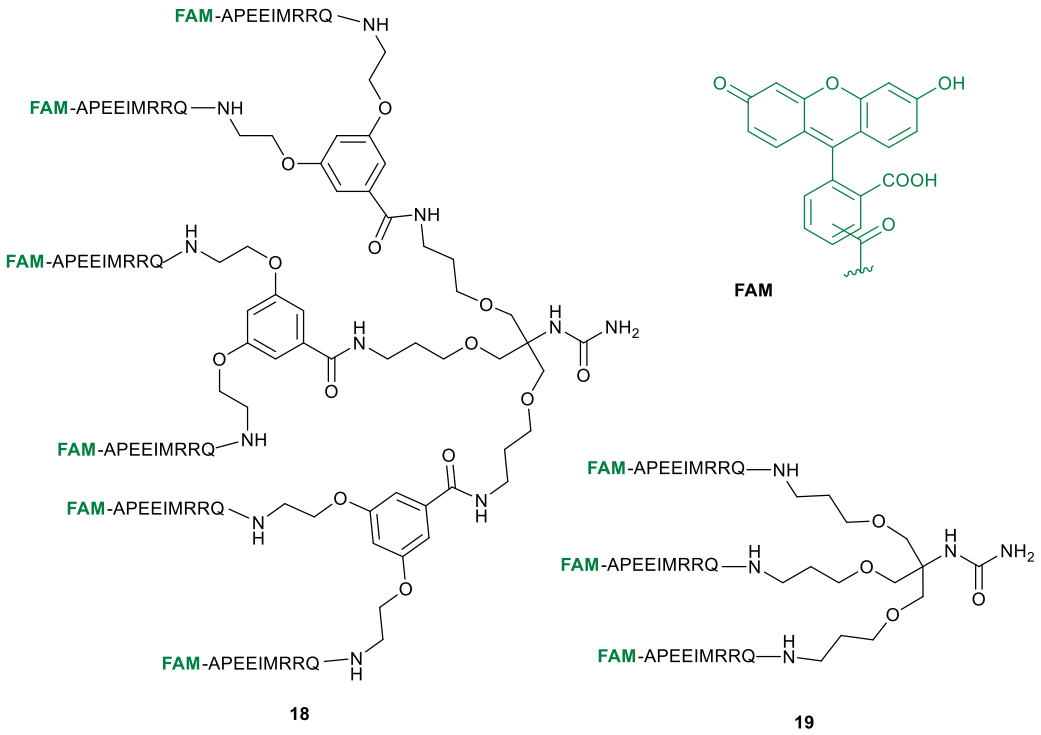

Figure 1.18. Peptide based activatable probes, **18** and **19**, developed by Avlonitis[79] (λ_{Ex} = 490 nm, λ_{Em} = 525 nm). The peptide sequence is cleaved between the methionine and arginine residues.

Further developed from this design was the optical probe **20** (NAP, Figure 1.19). This has the same motif of self-quenching carboxyfluorescein moieties which fluoresce after the peptide sequence is cleaved ($\lambda_{Ex/Em}$ = 490/525 nm). The probe also includes a PEG motif as a spacer between the peptide sequence and the fluorophore. Carboxyfluorescein emits fluorescence in the green region, and so the turn-on activity of the probe can be difficult to distinguish in pulmonary tissue due to the high background autofluorescence of the tissue

(340–405 nm). Regardless of this, it is currently in first-in-man studies, with the potential to be used as a diagnostic probe.[80]

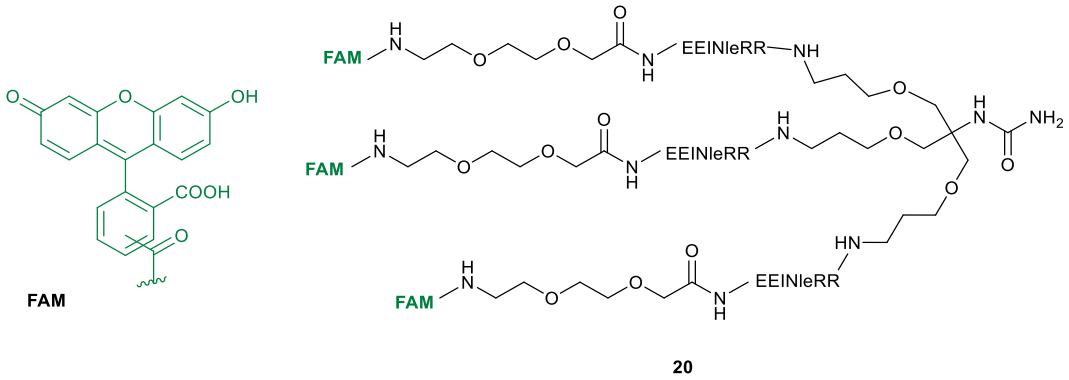

20

Figure 1.19. Optical probe **20**, NAP, with a similar design to **18** and **19**, with the inclusion of a PEG spacer between the targeting motif and the fluorophore (λ_{Ex} = 490 nm, λ_{Em} = 525 nm).

The most recent publication was a tri-branched peptidic optical probe **21** (Figure 1.20) designed to interrogate HNE *in vivo*.[81] It has been demonstrated previously that HNE is anchored on the extracellular membrane of the neutrophil as well as within the azurophilic granule.[71] This activity-based probe contains three fluorescein molecules that are each quenched with a methyl red. The activation of the probe is induced by cleaving off the methyl red labelled peptide, to relieve the tri-branched PEG type compound containing three FAM molecules, inducing an 8.5 fold increase in fluorescence. The activity of **21** was confirmed by adding it to neutrophil lysate, but by incubating the lysate in Sivelestat beforehand, no signal was observed, thus indicating the signal was HNE dependent. Following this, they also demonstrated a limit of detection as 10 nM, with no additional haemotoxicity to the solvent PBS. Confocal imaging of the probe *in vivo* within isolated human neutrophils was also used to confirm the signal uptake from the neutrophil. The neutrophils were also incubated with two inhibitors, α-PI and Sivelestat, before the addition of **21**. The method of inhibition of α-PI involves inhibiting extracellular HNE, whereas Sivelestat crosses through the

membrane and inhibits intracellular HNE. By alternating these, the fluorescence was only present when α-PI was used, inferring the probe detected only intracellular levels of HNE. The addition of the membrane stain Calcein was used to confirm the co-localisation of vesicles and HNE, demonstrating that phagolysosomes contained active HNE.

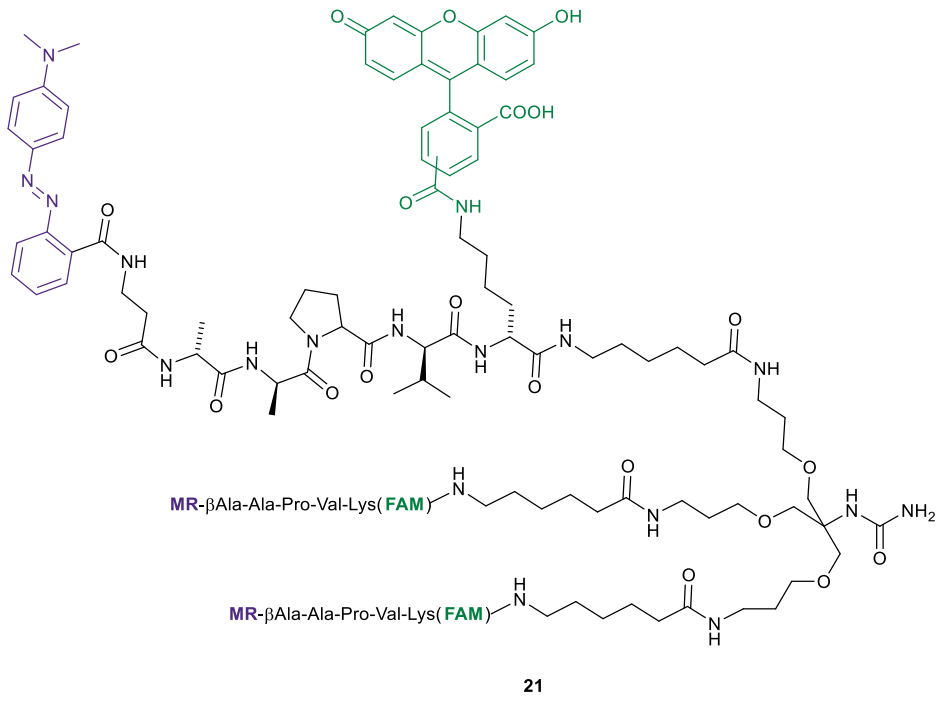

21

Figure 1.20. The 'silent' optical HNE probe **21** from Craven.[81] The probe is a tri-branched peptide with the fluorophore 5,6-carboxyfluorescein (green, FAM) and the quencher methyl red (purple, MR).

1.5 Aim of the thesis

The aim of this thesis was to develop optical probes for the identification and visualisation of elevated levels of HNE. This would aid rapid diagnosis of selected pulmonary diseases *in vivo*. In short, this was to be achieved by:

- Synthesis of multiple biocompatible fluorophores on gram scale
- Synthesis of several HNE inhibitors, and the generation of optical probes through conjugating the molecules to fluorophores

The optical probes generated were then evaluated for their biological applicability by measuring cytotoxicity, affinity towards HNE and live cell imaging in neutrophils.

Chapter 2 Synthesis of fluorophores

2.1 Introduction

The use of fluorophores has been long established as a method to elucidate mechanisms of biological processes.[82,83] Several hundred, if not thousands of different fluorophores have been reported, with fluorescent properties over a wide variety of wavelengths from across the spectrum.[15,84,85] The sheer quantity gives great scope for chemists and biologists alike to select the optimal molecules for imaging while tuning the inherent properties of the fluorophore such as quantum yield, Stokes shift, excitation and emission wavelengths to the biological question under investigation.

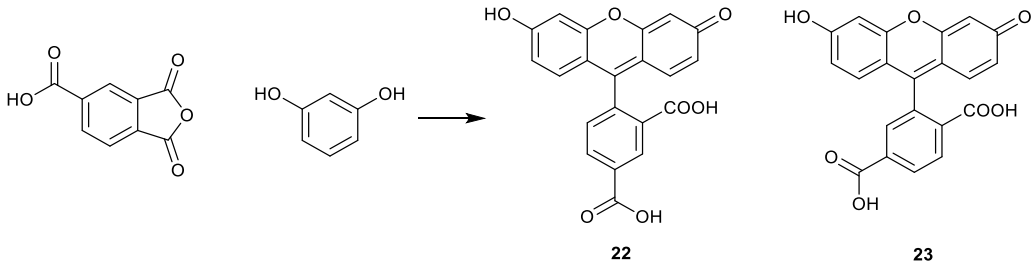

Scheme 2.1. The synthetic pathway for the two regioisomers of carboxyfluorescein: 5-carboxyfluorescein (**22**) and 6-carboxyfluorescein (**23**). Reaction conditions: $ZnCl_2$, Δ.

Carboxyfluorescein (**22**, **23**) is a derivative of fluorescein and can be easily synthesised by incorporating a carboxylic acid group onto the naphthalic anhydride, however this gives a mixture of regioisomers (5 & 6, Scheme 2.1). Carboxyfluorescein is easily incorporated into imaging probes, as the free carboxyl group can be conjugated to a variety of biologically targeting moieties through amide bond formation. Altogether, these properties make it an excellent fluorophore to be incorporated into optical probes.

One shortcoming of fluorescein based compounds is the fluorescent emission resides in the same region of the spectrum as tissue autofluorescence, possibly making it difficult to distinguish background from probe fluorescence.[24] Far-red fluorophores (>650 nm) can be used to avoid this issue as tissue autofluorescence is negligible in this region of the spectrum.

Cyanine dyes are made up of a conjugated backbone with two indole capping groups, although other aromatic heterocycles have been used (Figure 2.1). The wavelengths absorbed and emitted by the cyanine dyes are 'tuneable' by altering the unsaturated carbon chain length from 3 carbons (550-570 nm) to 5 (650-670 nm) to 7 (750-780 nm). Due to the extended conjugation present in cyanine dyes, they are lipophilic, but this can be remedied by modifying the structure to incorporate hydrophilic functional groups (e.g. sulfonates).

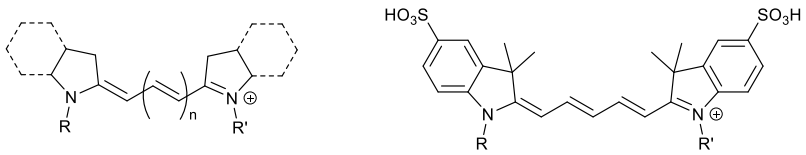

Figure 2.1. Basic structure of cyanine dyes (left) where n = 1, 2 or 3. Basic pentamethine dye structure used in this thesis (right), where R and R' are alkyl groups of varied lengths and functional groups.

Pentamethine, or Cy5, dyes (Figure 2.1) have been frequently used for imaging biological processes as emission is in the far-red region of the spectrum (630-700 nm), thus having the ability to enable contrast against tissue autofluorescence, which frequently occurs in the 'green' region of the spectrum (510-560 nm).[86] They also have relatively high extinction coefficients and reasonable quantum yield (*c.a.* 0.25), giving them 'good brightness'.

2.2 Aims of chapter 2

For the synthesis of optical probes to allow the *in vivo* detection of human neutrophil elastase (HNE) within the lungs, a fluorophore had to be conjugated to the targeting moiety. With this in mind, the aims of this chapter were to synthesise several biocompatible fluorophores with a range of wavelengths, on a large scale.

2.3 Preparation of single isomers of 5 and 6-carboxyfluorescein

Carboxyfluorescein is a common commercially available fluorophore, typically sold as a mixture of regioisomers. It is preferable to have single isomers of dyes to aid purification of imaging compounds, due to possible resulting diastereomers. Additionally, the presence of just a single isomer is advantageous for compounds targeting clinical use, simplifying the regulatory aspects. Previously in the group, a simple procedure was used to separate the two regioisomers of carboxyfluorescein, in addition to forming the active esters, in preparation for conjugation to an amine (Scheme 2.2).[87]

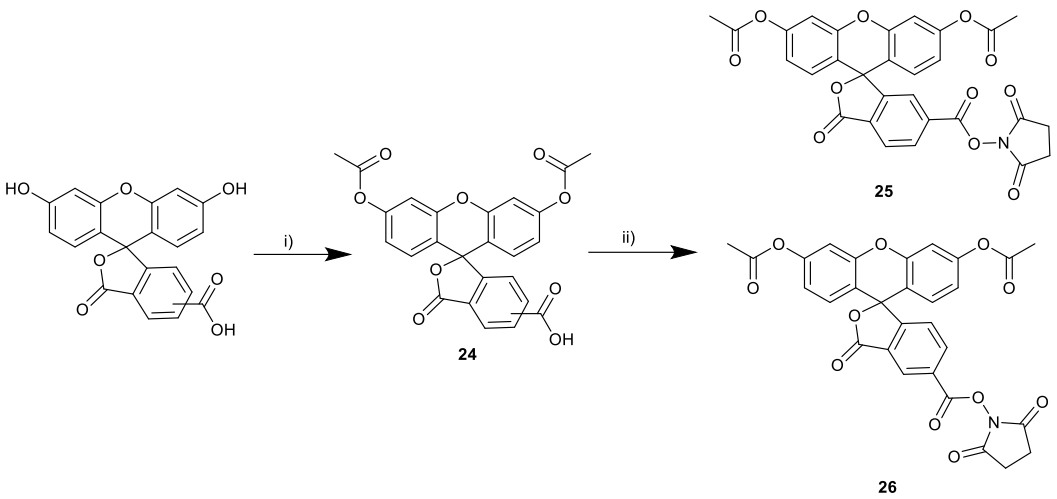

Scheme 2.2. Synthetic route to 5 and 6-carboxyfluorescein diacetate *N*-hydroxyl succinimide esters, **25** & **26**. Reaction conditions: i) Ac_2O, pyridine, 110 °C, 3 h, 100% conversion by HPLC; ii) NHS, DIC, DCM, 0.5 h, yield **25** 36%, **26** 24%.

Separation by column chromatography took place after two steps: acetylation of the phenols followed by activation of the carboxylic acid. The two phenol functionalities were deprotonated by pyridine driving the lactone formation, with the phenolate anions reacting with acetic anhydride, giving the phenol acetates (Scheme 2.3). Using acetic anhydride in large excess ensures this occurs on both phenols to generate **24**.

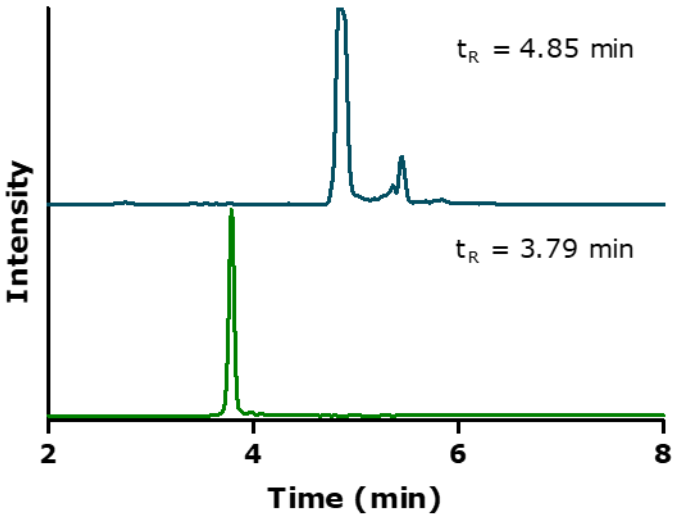

Figure 2.2. HPLC ELSD traces of 5(6)-carboxyfluorescein (green trace) and 5(6)-carboxyfluorescein diacetate (blue trace).

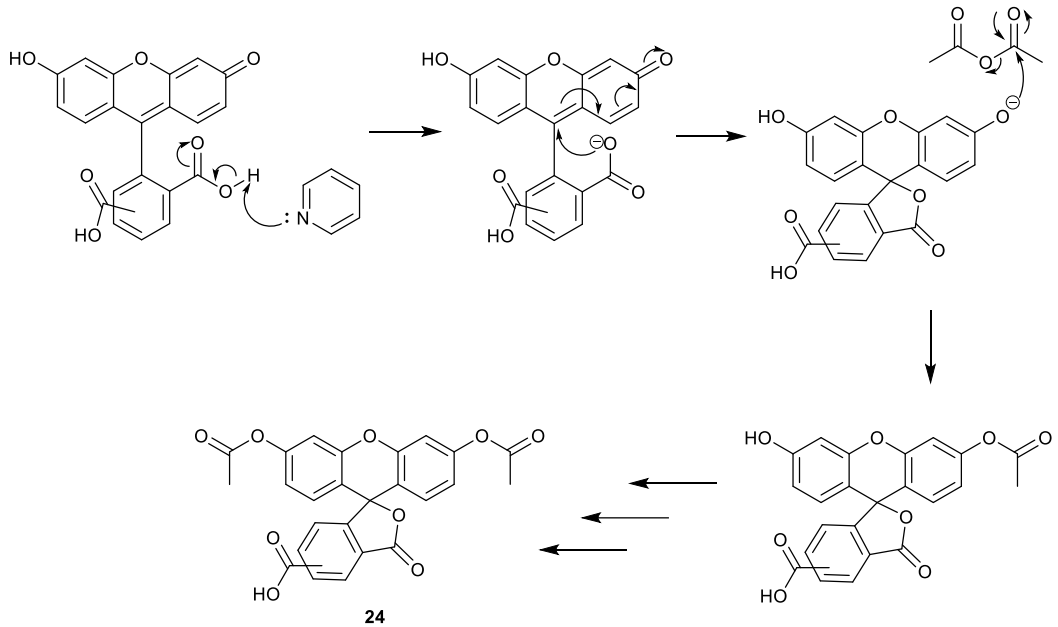

Scheme 2.3. Proposed mechanism of acetylation of the phenols on 5(6)-carboxyfluorescein.

In the second step, activation of the carboxyl group through the addition of *N*,*N*′-diisopropylcarbodiimide (DIC) and subsequent reaction with *N*-hydroxysuccinimide (NHS) generates a *N*-hydroxylsuccinimide active ester. This ester allows for nucleophilic attack by an amine to give an amide. The carboxyl group reacts with DIC to generate the *O*-acylurea. This is attacked by the nucleophilic hydroxyl group of the NHS, to generate the active esters **25** and **26** with *N*,*N*′-diisopropylurea as a by-product (Scheme 2.4).

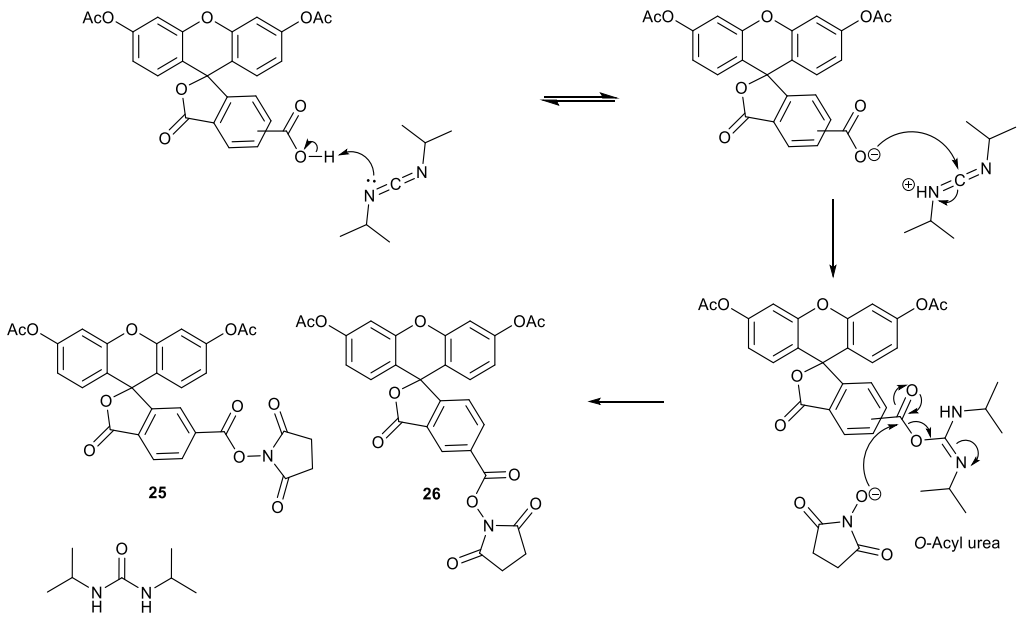

Scheme 2.4. Formation of *N*-hydroxylsuccinimidyl esters of 5 & 6-carboxyfluorescein diacetate, **25** and **26**.

The consequence of both acetylation and activation of carboxyfluorescein makes it possible to separate the two isomers using simple flash column chromatography. The products were separated using an isocratic gradient with the solvent system toluene and ethyl acetate to generate the activated isomers in yields of 36% for **25** and 24% for **26**. Purity was assessed by HPLC where the isomers were shown to be successfully separated (Figure 2.3), the reaction was scaled up to 40 mmol (15 g) with similar yields. It was possible to store the products in the freezer for several months with minimal degradation.

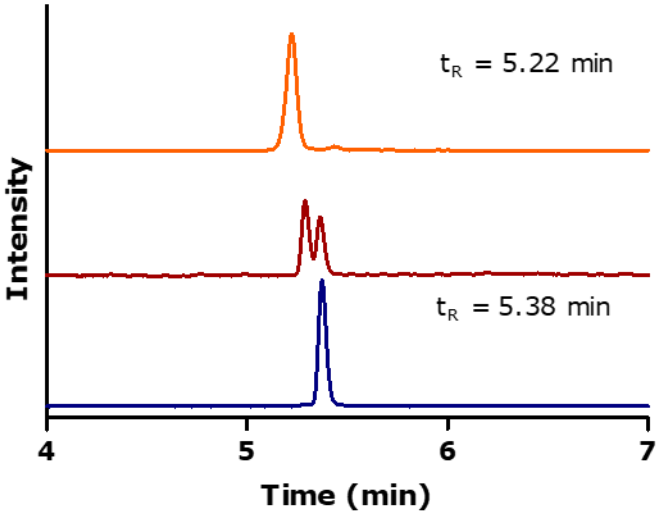

Figure 2.3. RP-HPLC traces of 5-carboxyfluorescein NHS ester (blue), mixture (red) and 6-carboxyfluorescein NHS ester (orange), confirming their separation (ELSD channel), analysed by analytical HPLC.

Due to the presence of acetyl groups on the phenolic hydroxyl groups of carboxyfluorescein, the final compounds **25** and **26** were more fluorescent after deprotection during the conjugation chemistry (Figure 2.4 shows one isomer).

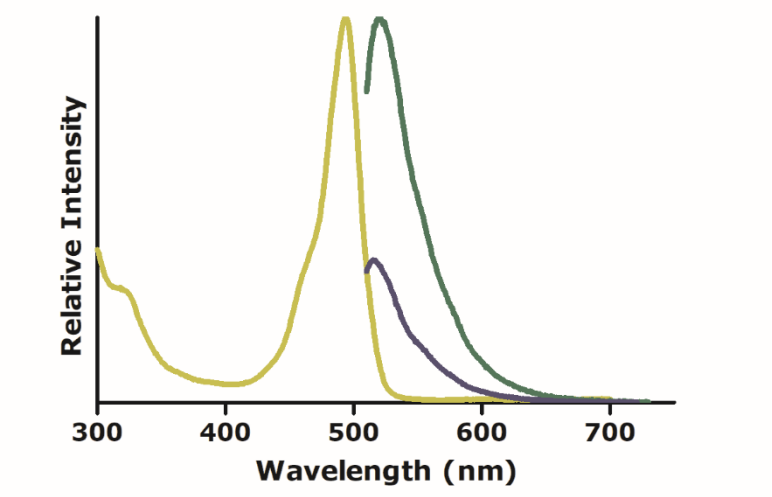

Figure 2.4. Absorption (yellow, λ_{Ex} = 494 nm) and emission (green, λ_{Em} = 521 nm) spectra of 6-carboxyfluorescein NHS ester after the addition of triethylamine (excitation at 480 nm) and emission before the addition of triethylamine (blue, λ_{Em} = 515 nm). 1 μM solutions were made up of 10% DMSO in PBS.

2.4 Synthesis of pentamethine dye 27

To generate several optical probes in the far-red region of the spectrum, a far-red dye was required, and on large scale to allow sufficient amount of probe for testing. Several Cy5 dyes are available but are expensive (Alexafluor 647, 1 mg = £302, October 2018),[88] and as such, synthesis of a dye was required. The Cy5 **27** (Figure 2.5) was selected as it had been incorporated into several optical probes with clinical applications.[89–91] The dye has several sulfonate groups increasing its solubility, in addition to containing a carboxylic acid at the end of a six carbon chain, available for conjugation to an amine.

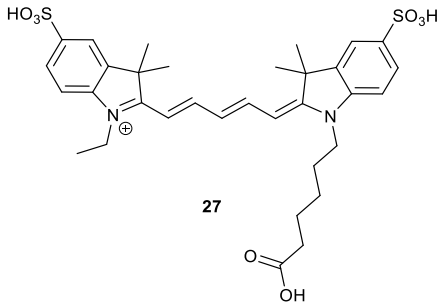

Figure 2.5. Pentamethine dye **27**.

The most common method of disconnection for cyanine dyes is between the two head groups. The indoles can be identical to generate a symmetrical Cy5 dye, or different, such as in **27**, for an unsymmetrical Cy5.

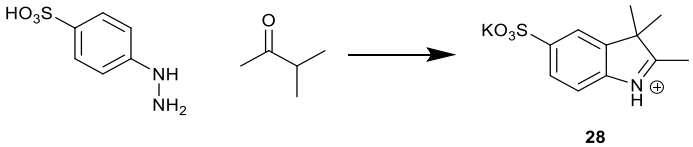

Scheme 2.5. Synthesis of indole **28**. Reaction conditions: AcOH, reflux, 4 h, 78%.

Indole **28** was synthesised by a Fischer indole reaction, using 4-hydrazinobenzenesulfonic acid and 3-methylbutan-2-one under acidic conditions (Scheme 2.5). This afforded **28** in a high yield (78%) and was easily purified through precipitation with Et_2O as a potassium salt (Scheme 2.6).

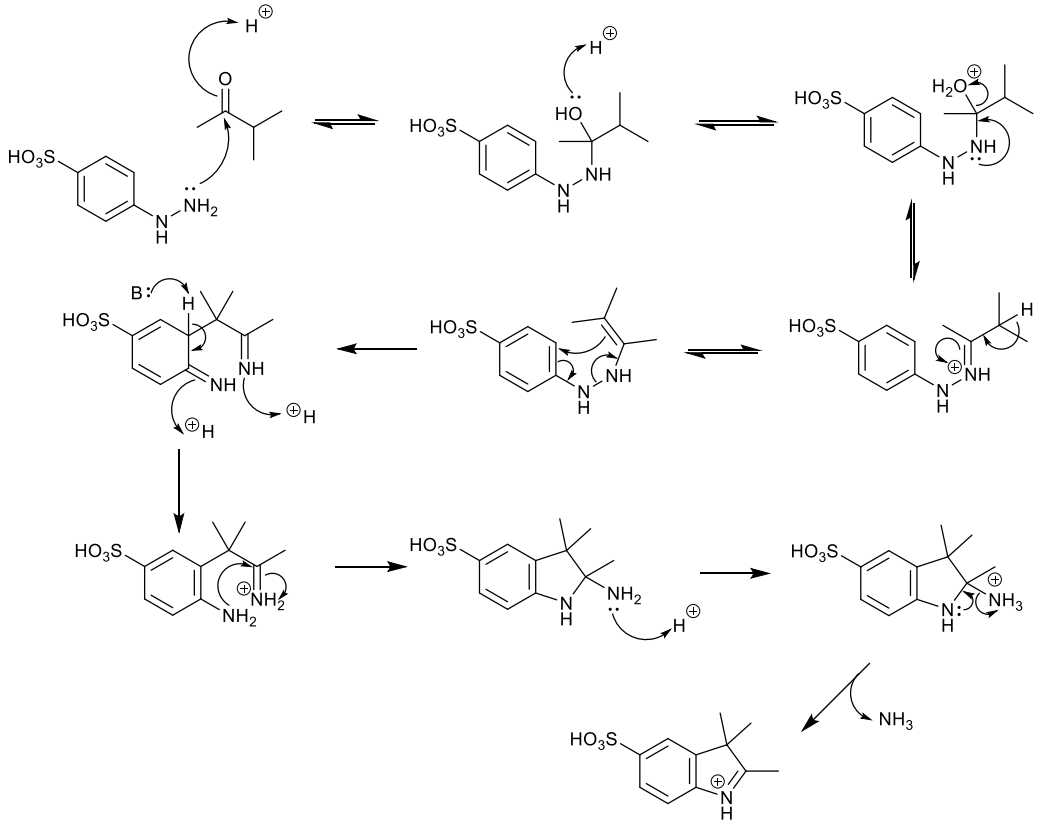

Scheme 2.6. Postulated mechanism for Fischer Indole synthesis of indole **28** under acidic conditions, where the indole was drawn as a sulfonate for ease.[92]

Compound **28** was used in two ways, both with S_N2 quaternisation reaction of the amine group of the indole. Thus compound **28** was added to neat bromoethane and heated to reflux for 24 hours, until complete conversion seen by HPLC, to give **29** in a high yield (98%) (Scheme 2.7).

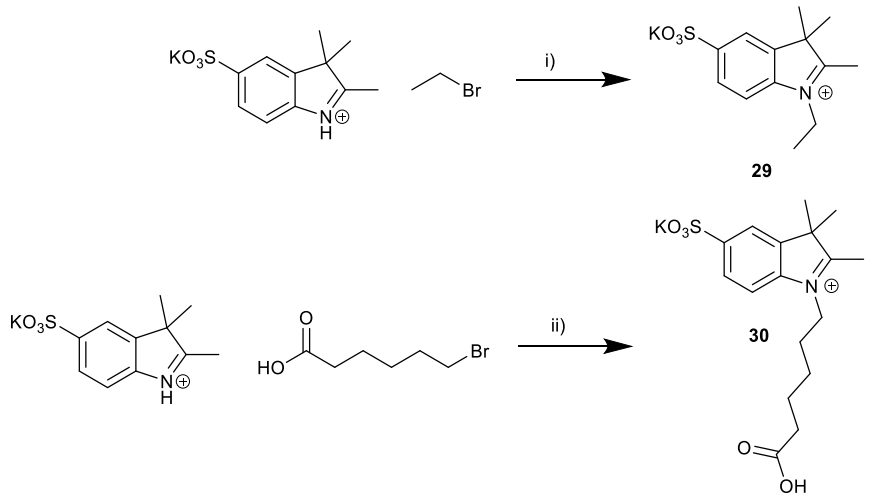

Scheme 2.7. Synthesis of indoles **29** and **30**. Reaction conditions: i) reflux, 24 h, 98%; ii) DMF:MeCN (9:1), 150 °C, 4 h, μw, 60%.

For **30**, indole **28** was reacted with 6-bromohexanoic acid diluted in a mixture of DMF and acetonitrile (9:1), with the reaction taking four hours in a microwave reactor at 150 °C. Previously, it had been found that, conventional heating required 48 hours for good conversion. Indoles **29** and **30** were purified by removal of the reaction solvent before re-dissolving the crude product in a minimal amount of acetonitrile, and crystallisation from diethyl ether.

Upon formation of the functionalised indoles, **29** was added to malonaldehyde bis(phenylimine) hydrochloride and heated to reflux to form the conjugated anilide intermediate **31** (Scheme 2.8). Purification of this intermediate was time consuming as the excess bisphenylamine had to be removed through rigorous washing. The crude intermediate was dried at 40 °C with a vacuum overnight to give **31** in 64% yield.

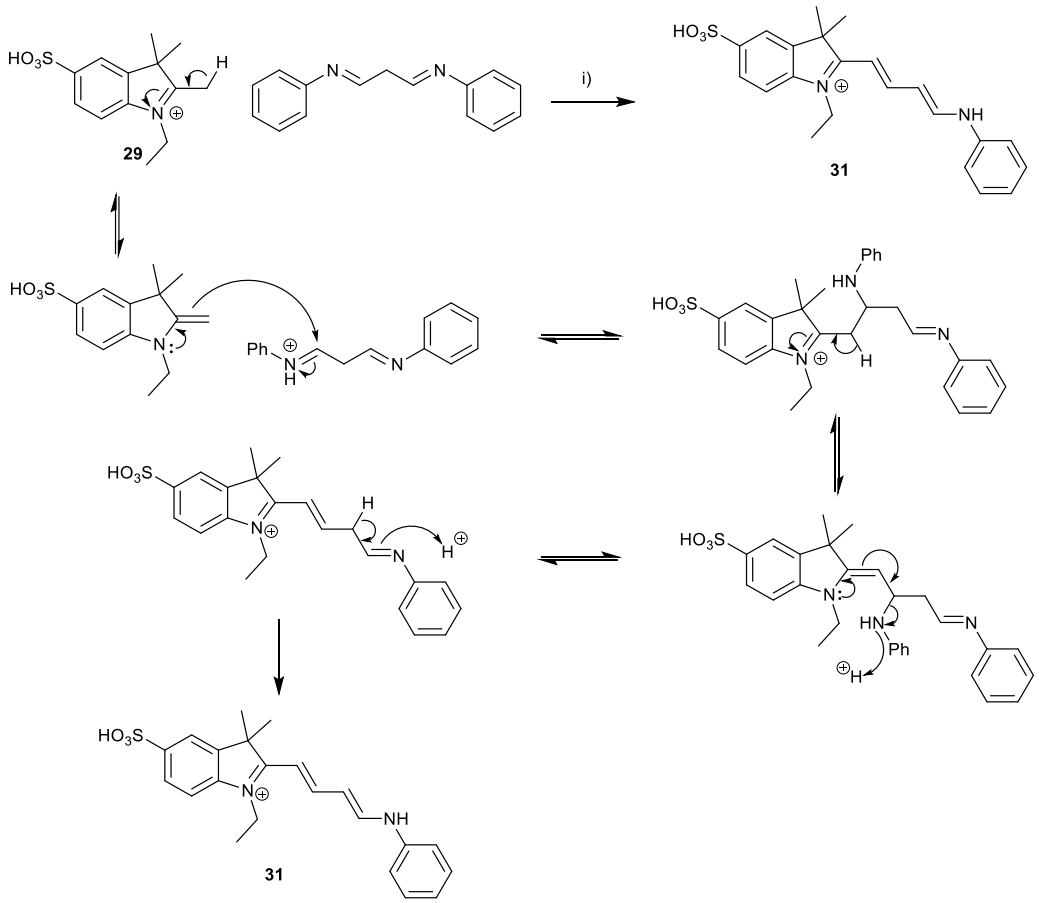

Scheme 2.8. Postulated mechanism for the formation of **31**. Reaction conditions: i) AcOH, Ac_2O, NaOAc, reflux, 3 h, 26% after purification. All sulfonate groups are shown as sulfonic acids for simplicity.

Indole **29** was reacted with **30** and sodium acetate in a solvent system of acetic anhydride and acetic acid (2:1) to generate the conjugated Cy5 dye (Scheme 2.9). The reaction could be monitored by HPLC, as the formation of the product had a wavelength of 650 nm (Figure 2.6). After the reaction was complete, the crude product was analysed by HPLC and LCMS and shown to contain **27** in addition to the two symmetrical dyes of the two functionalised indoles (**32** and **33**, Figure 2.7). The crude mixture was purified by reverse phase preparative HPLC to give Cy5 **27** in a moderate yield (26%).

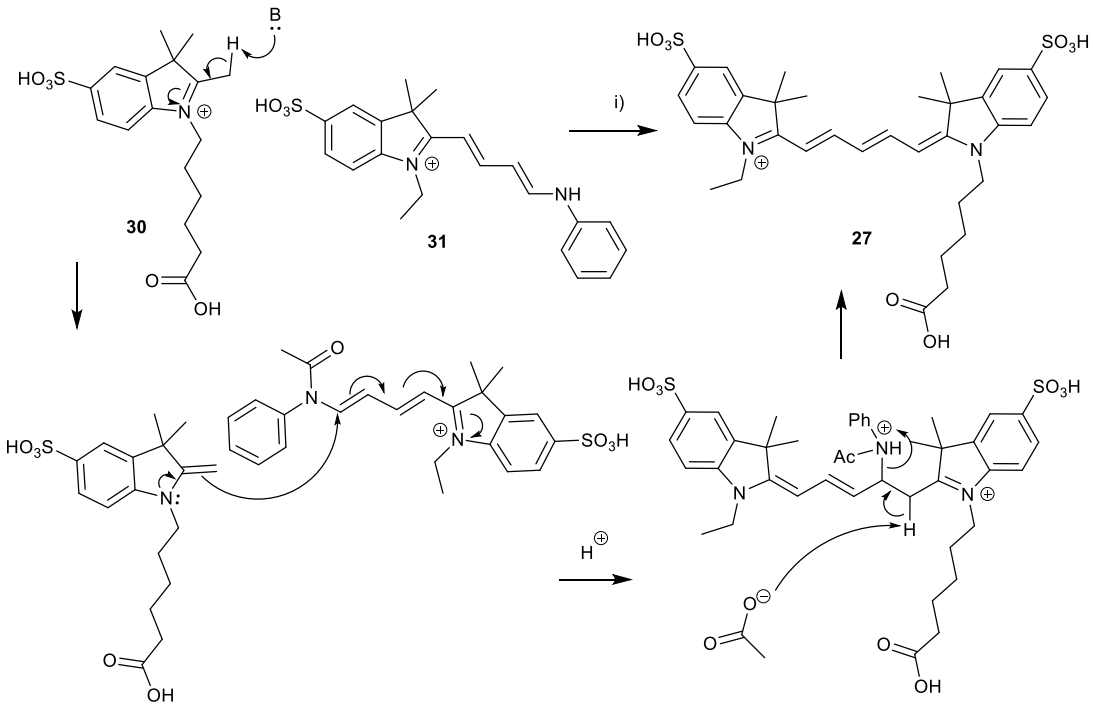

Scheme 2.9. Cy5 dye synthesis: i) AcOH: Ac_2O (2:1), NaOAc, reflux, 3 h, 26% after purification. Mechanism of conjugation of indole **30** and **31** to form pentamethine dye **27**.

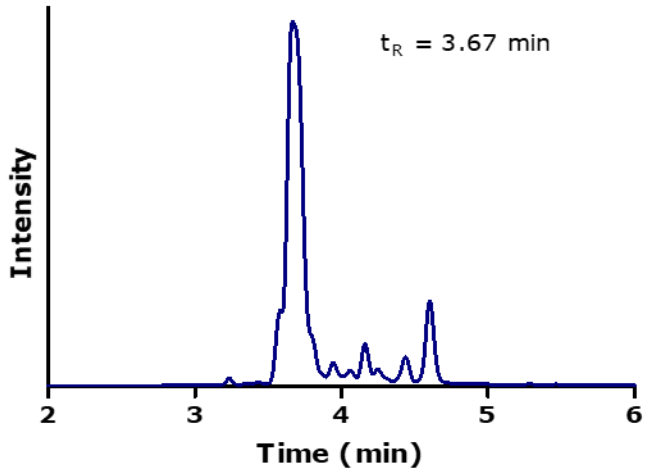

Figure 2.6. HPLC trace of the reaction mixture (Scheme 2.9) for the formation of **27** (650 nm), showing the product at t_R = 3.67 min, with several other by-products.

The dye was synthesised on a large scale, whereby 1.4 mmol of one indole was used to generate some 0.5 g of the final Cy5 dye after purification. The excitation and emission of the dye were examined as having an excitation maximum of 650 nm and emission maximum 666 nm (Figure 2.8).

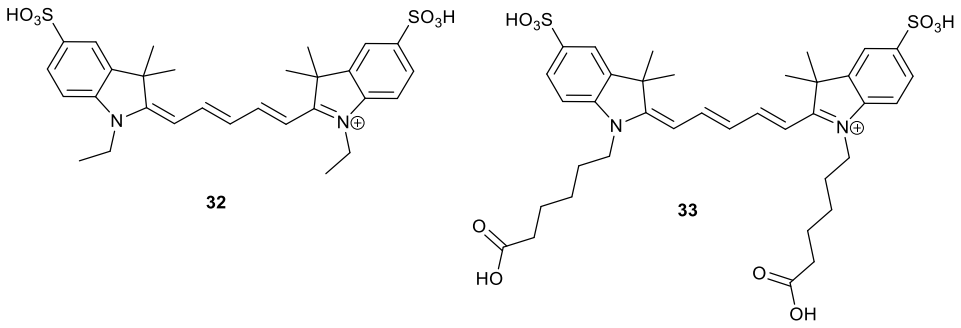

Figure 2.7. The two symmetrical Cy5 dyes **32** and **33** produced as by-products from the formation of Cy5 **27**.

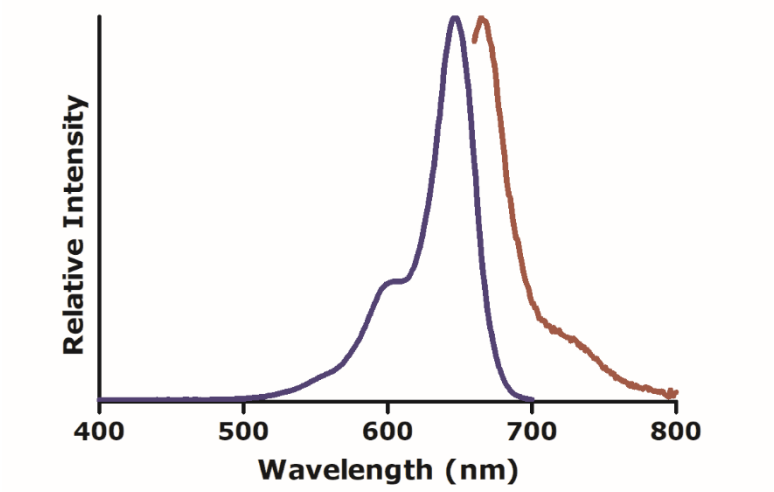

Figure 2.8. Absorption (blue) and emission (red) spectra of Cy5 **27** in PBS (1 μM), with both sets of data normalised to 1. Emission recorded after excitation at 630 nm.

2.5 Synthesis of pentamethine dye Cy5**

Cy5** (**34**, Figure 2.9) is an asymmetric, water soluble pentamethine dye that has been incorporated into several optical probes and used *in vivo*. Patents have been filed for optical probes containing the dye with the aim of using them in several diseases, such as dysplasia, tumours with high c-Met expression and lymphomas.[93–95] A study was published in 2015 detailing the use of a Cy5** labelled peptide in patients for the location of cancerous polyps in the colon.[96] The combination, highlights the versatility of the dye and its advantageous application in humans.

Cy5** has been used frequently because of its desirable properties, such as high water solubility, good brightness, and photostability under ambient light.[96,97] In particular, the dye has been shown to achieve clearance from the body, predominantly through the renal system. The precedent in clinical use made it attractive to synthesise and use in optical probes for HNE detection.

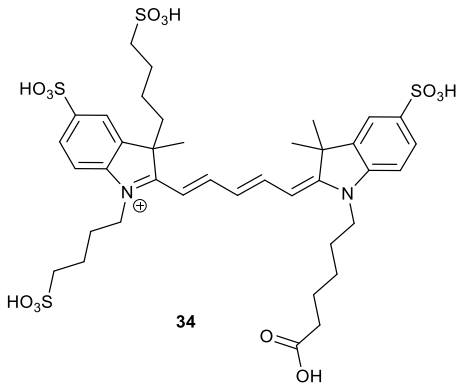

34

Figure 2.9. Pentamethine dye Cy5** **34**.

In order to synthesise the trisulfonated indole **39** (Scheme 2.12), a sulfonated ketone was required that could be incorporated into the indole (**37**, Scheme 2.10). The alpha proton of acetoacetate **35** was deprotonated by a hydride, and the enolate produced used to attack 1,4-butane sultone inducing ring opening and creating a terminal sulfonate group on **36**.

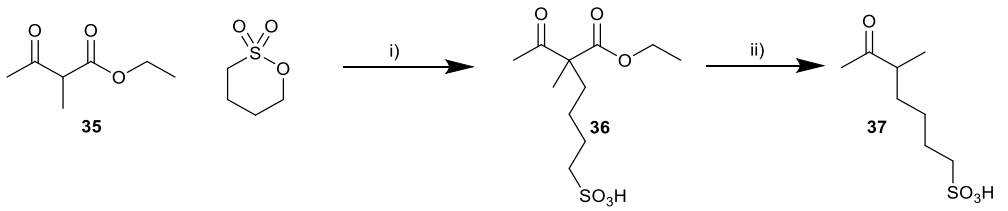

Scheme 2.10. Synthesis of intermediate **37**. Reaction conditions: i) NaH, DMF, 0 to 5 °C for 1 h, then 50 °C for 18 h; ii) NaOH, H_2O, 90 °C, 18 h, acid workup with HCl.

The ethyl ester was removed by saponification with sodium hydroxide and loss of CO_2 to generate **37**, which was carried through to the next reaction without purification (Scheme 2.10). Base mediated hydrolysis of the ester occurs to generate a carboxylic acid (Scheme 2.11), which then loses CO_2. The reaction induces decarboxylation and the product, an enolate, tautomerises upon work up.

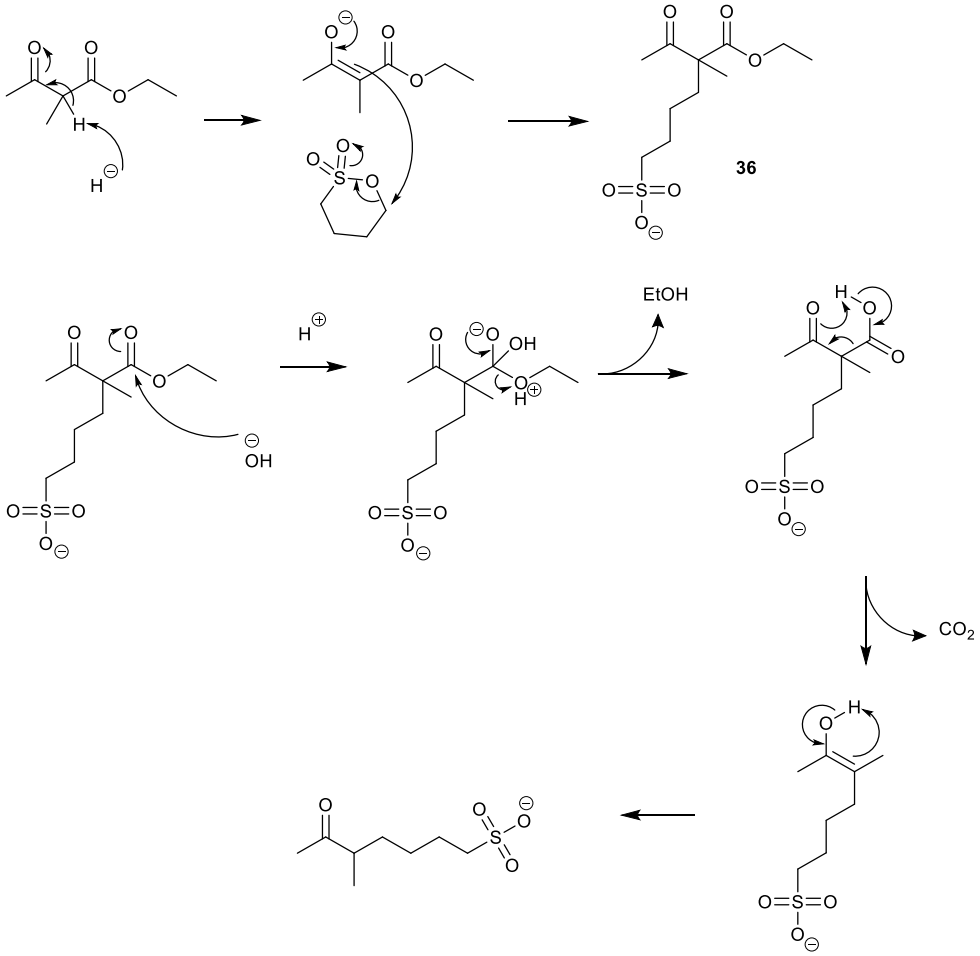

Scheme 2.11. Proposed mechanism of formation of **37**.

Sulfonated ketone **37** then underwent Fischer indole chemistry with 4-hydrazinobenzenesulfonic acid to generate the disulfonated indole **38** in a similar fashion to Cy5 **27** (Scheme 2.12). The product required purification, before reacting with 1,4-butane sultone in excess, to force completion of the S_N2 quaternization on the amine. The yield of trisulfonated **39** was moderate (51%) in comparison to previously synthesised indoles and required 48 h for the reaction to proceed. It was also attempted in a microwave reactor, but the yield remained unimproved.

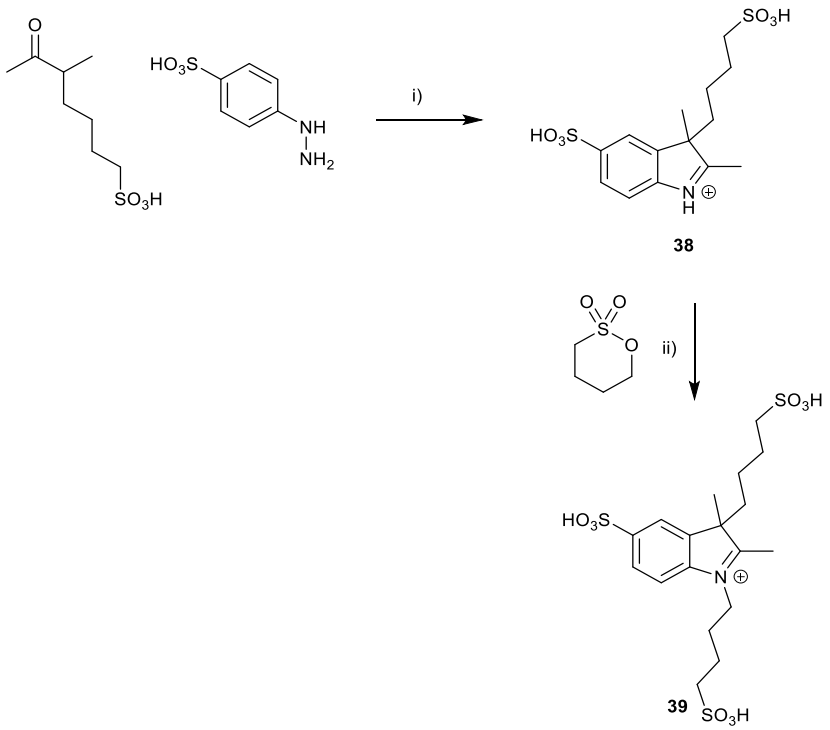

Scheme 2.12. Final synthetic steps towards trisulfonated indole **39**. Reaction conditions: i) AcOH, 105 °C, 12 h, 41% from **35** to **38**; ii) dimethyl acetamide, reflux, 24 h, 51%.

With both indoles in hand, the synthesis was completed by conjugating the two indoles (Scheme 2.13). The carboxyl modified indole **30** to an alkene, which undergoes nucleophilic attack on a bisphenylanilide to form **40**. Upon purification, **40** was reacted with indole **39** and heated to reflux. As with Cy5 **27**, the reaction was monitored by HPLC at 650 nm, where the formation of product **40** could be seen, alongside the two symmetrical Cy5 dyes (Figure 2.10). After the reaction was complete, the crude product required preparative HPLC due to the water solubility of **34**, giving a yield of just 12%.

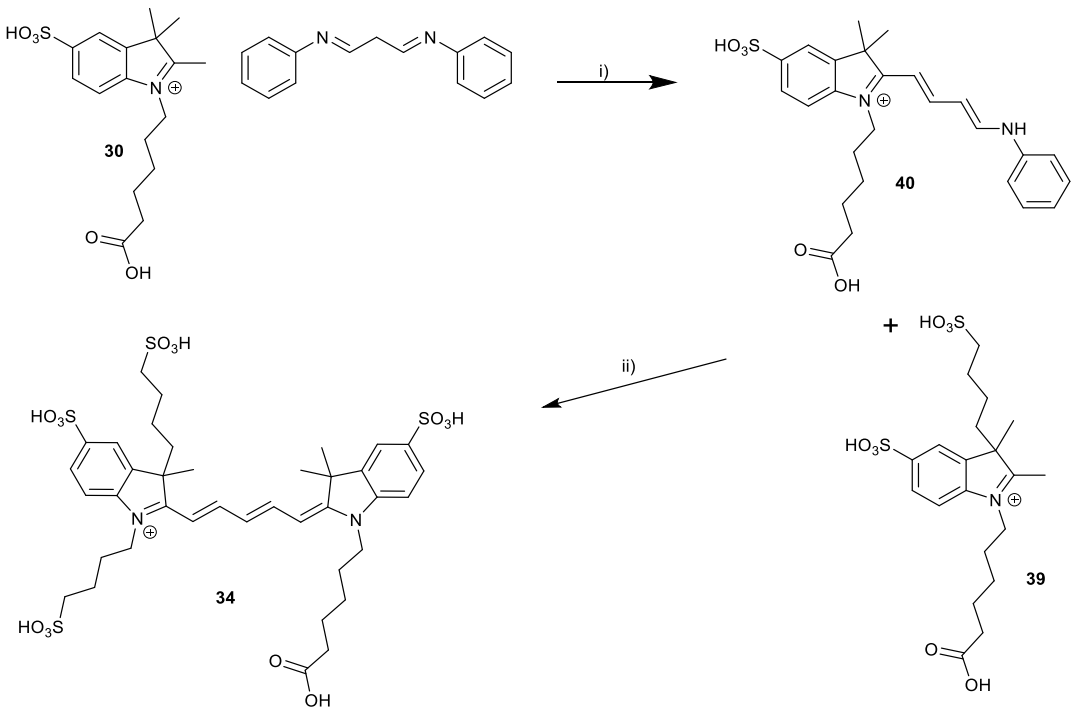

Scheme 2.13. Final steps towards the synthesis of Cy5** **34**. Reaction conditions: i) Ac_2O, acetic acid, reflux, 4 h; ii) Ac_2O, acetic acid, NaOAc, reflux, 3 h, 12% after purification.

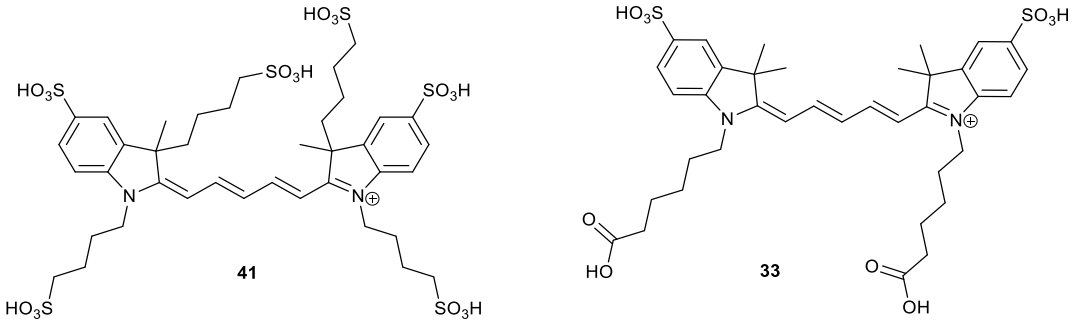

Figure 2.10. Two symmetrical Cy5 dyes **41** and **33** produced from the final conjugation reaction.

Dye **34** was analysed by UV-vis spectroscopy and fluorimetry to identify its excitation and emission maxima. The excitation maximum was 666 nm and it had a far-red emission at 673 nm upon excitation at 650 nm (Figure 2.11), confirming its possible use in the desired optical window.

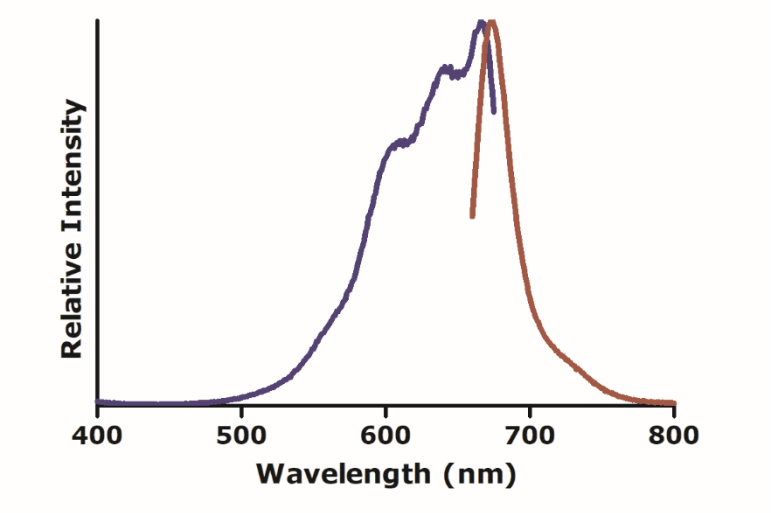

Figure 2.11. Absorption (blue, λ_{Ex} = 666 nm) and emission (red, λ_{Em} = 673 nm upon excitation at 660 nm) spectra of Cy5** **34** in PBS solution (1 μM), with both sets of data normalised.

2.6 Conclusions

Optical medical imaging requires dyes that can be used within the biological environment and biological window, and with functional groups available for reacting with the targeting moiety. Herein, several water-soluble dyes were successfully synthesised containing carboxyl groups available for conjugation to a recognition element that targets HNE.

The pentamethine dye Cy5** whilst synthesised on a large scale in industry, it was not reported in large scale elsewhere. A paper referenced during the synthesis had a starting mole of 0.3 mmol, and yield of 11%, whereas this thesis used 1.6 mmol and a yield of 12%.[98] Cy5 **27** was synthesised in a similar manner to Cy5** and whilst literature used a larger scale, it didn't report the yield for this particular dye, but the yield of another non-symmetrical dye was 5%.[99] Another literature search gave a patent stating their yield as 22%, but this thesis reported a 26% yield.[100]

The mixture of regioisomers for 5 and 6 carboxyfluorescein were successfully modified with acetyl groups and activated allowing separation of the isomers in yields of 36% and 24%. Two variations of water soluble asymmetric pentamethine dyes, **27** and **34**, were synthesised and purified using reverse phase preparative HPLC, in quantities (500 mg of **27** and 200 mg of **34**).

Chapter 3 Oxo-β-lactam based optical probes

3.1 Introduction

Research into the overexpression or overactivation of human neutrophil elastase (HNE) has implicated its involvement in a wide range of diseases, making it an ideal drug target, particularly for pulmonary diseases.[101,102] The Moreira group has developed a portfolio of HNE inhibitors based on a common binding scaffold (Figure 3.1).[103] Screening a large range of aryl groups based on inhibitor **42**, they found that compounds 2-mercaptobenzoxazole **43** and 2-mercaptobenzothiazole **44** had the highest affinity towards HNE.

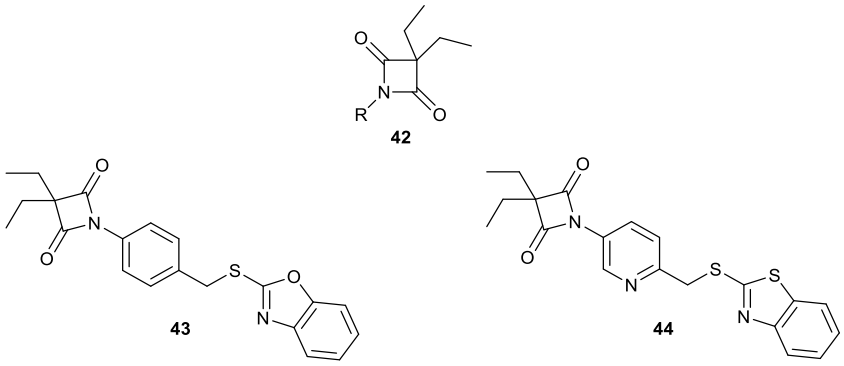

Figure 3.1. The key motif found in the HNE inhibitor, **42**, and the structure of the first generation inhibitors **43** and **44**, which displayed a high affinity for HNE.[103]

The inhibition constants, or Ki, values for the inhibitors were found to be as low as 0.34 nM (**43**) and 0.50 nM (**44**). In addition to the compounds having high affinity for HNE, they also showed little to no affinity for other related serine proteases associated with neutrophils, cathepsin G and proteinase 3.

Both showed no inhibition when incubated with proteinase 3 (Pr3) but **43** had a k_{obs} value of 4080 $M^{-1}s^{-1}$ for cathepsin G (Cat G), much larger in comparison to **44** at 29.6 $M^{-1}s^{-1}$.

The postulated mechanism of inhibition by the oxo-β-lactams involved nucleophilic attack by the hydroxyl group of the serine present within the active site (Scheme 3.1). This induces ring opening of the azetidine-2,4-dione and formation of an ester bond between one of the carbonyl groups and the serine residue. The stability of this intermediate can be dependent on the R group on **42**.

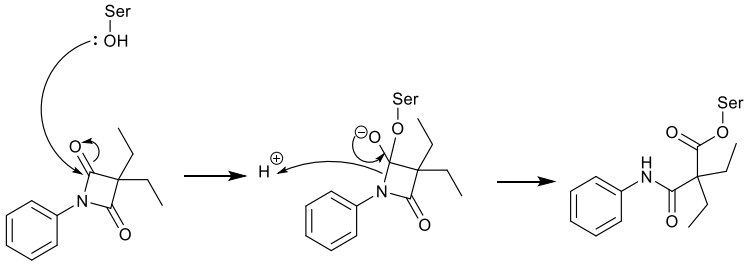

Scheme 3.1. Postulated mechanism of inhibition by the oxo-β-lactams with HNE modification of Ser195 within the active site of the protease.

Another inhibitor of HNE generated was probe **45**, with a sulfonyl group (Figure 3.2), with a Ki determined to be 0.63 nM and k_{on} 1.46×10^6 $M^{-1}s^{-1}$, it also had a higher affinity towards HNE than other serine proteases.[104] The k_{on} value for **45** and Pr3 was 4.99×10^3 $M^{-1}s^{-1}$ but much lower for Cat G at 41.4 $M^{-1}s^{-1}$, indicating that the selectivity was big enough to take it through for further testing. The *in vitro* data led to *in vivo* murine studies to determine the efficacy of the molecule as a drug. However, the half-life of the probe was very short, showing poor stability in PBS ($t_{1/2}$ = 1 h), and faring even worse in human plasma ($t_{1/2}$ = 6 min) and led to the inhibitor being discarded as a potential drug, due to its instability.

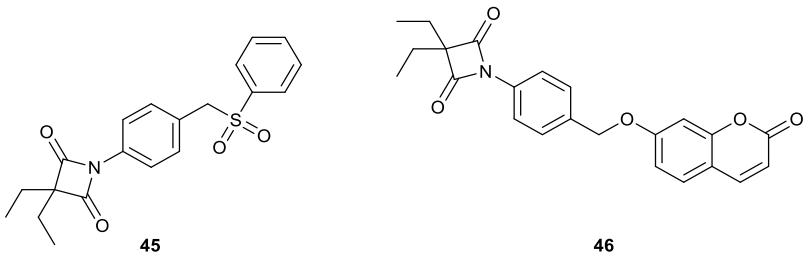

45 46

Figure 3.2. Second generation inhibitors based upon the oxo-β-lactam motif.[104,105]

The same group also developed an oxo-β-lactam **46** that is conjugated to an umbelliferone scaffold, and encapsulated it into starch nanocapsules to allow slow release of the inhibitor as a treatment option for psoriasis, another disease where HNE has been demonstrated to be at high levels.[36,105,106] The inhibitor was shown to have an IC_{50} of 0.67 nM, and studies were used to determine the concentration required for the most effective treatment against HNE damaging the upper dermal layer of skin.

Another set of HNE inhibitors with incorporated fluorophores and oxo-β-lactam warhead were compounds **47** and **48** (Figure 3.3). These inhibitors were formed by reacting azide functionalised fluorophores with a propargylated oxo-β-lactam in a copper catalysed azide-alkyne cycloaddition (CuAAC).

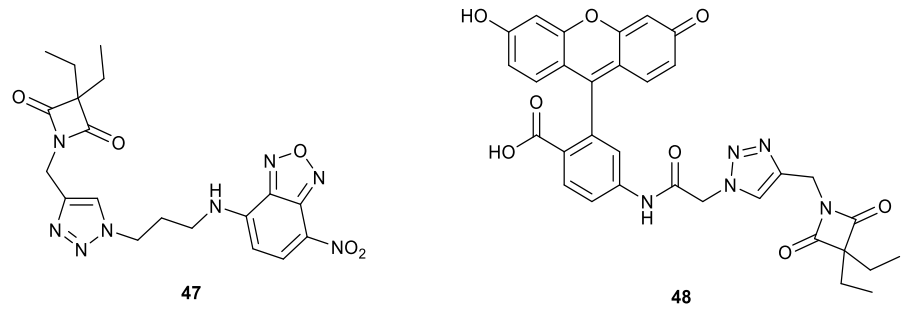

47 48

Figure 3.3. Fluorescent compounds with the same warhead from Ruivo *et al.*, targeting the detection of HNE.[107]

The probes were analysed against HNE to generate their IC_{50} values, inhibitory constants, and were found to be 56 nM (**47**) and 66 nM (**48**).

Interestingly, they only screened **47** against other serine proteases including Pr3 (IC_{50} = 3 μM), thrombin (1 μM) and chymotrypsin (23 μM) but not Cat G. The probes were shown to bind to HNE by gel electrophoresis and were used to elucidate enzyme activity *in situ*, by indicating the presence of HNE within neutrophils.

The facile method of altering the R group present on compound **42** without a evident loss of activity makes this an attractive HNE targeting element to be incorporated into optical probes.[104]

3.2 Aims of chapter 3

HNE is a serine protease found within the azurophil granules in neutrophils and mis-regulation has been correlated with several pulmonary diseases, with high levels of the enzyme in the lung causing irreversible tissue damage. Many pulmonary diseases can be difficult to diagnose due to ambiguous symptoms, particularly differentiating between bacterial infection and an autoimmune response in diseases such as COPD and fibrosis.

The aim of this chapter was to generate several fluorescent optical probes with a range of wavelengths to allow the detection of the presence of HNE *in vivo*. To interrogate the correlation between structure and affinity, two types of spacers between the oxo-β-lactam and fluorophore were used. The optical probes were evaluated for their activity and affinity towards HNE, incubated with neutrophils and used to determine the presence of HNE with the target of developing *in vivo* optical imaging of neutrophils for rapid disease diagnosis.

3.3 Synthesis of aromatic oxo-β-lactam based optical probes

The synthesis of the oxo-β-lactam motif was adapted from the work of Moreira, starting from *N*-Boc-aminobenzylamine that undergoes cyclisation with diethylmalonyl chloride forming lactam **49** (Scheme 3.2).[103]

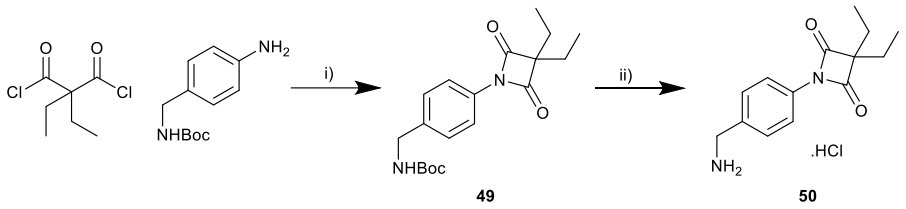

Scheme 3.2. Synthesis of HNE targeting compound **50**. Reaction conditions: i) TEA, dioxane, -10 °C to rt, 18 h, 25%; ii) 4 M HCl in dioxane, 6 h, quant.

The initial addition of the amino group to the acid chloride could be achieved without base, but for the second substitution, an equivalent of base was required to ensure reaction. The low yield (25%) is due to the majority of the compound forming a dimer, whereby the diacid chloride undergoes two consecutive intermolecular reactions instead of the required second intramolecular cyclisation (Figure 3.4).

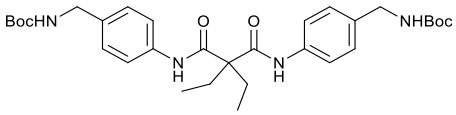

Figure 3.4. Main product of the reaction in Scheme 3.2.

The reaction was initially carried out using the same reaction conditions as in the literature[107] but the product was obtained in poor yield (4%). The yield was increased by decreasing both the temperature and base equivalents, from rt to 0 °C, and from 3.7 equivalents to 2.4. The product and by-product were easily separated by normal phase chromatography. The subsequent reaction was to

cleave the Boc protecting group using acidic conditions, with the product forming in a quantitative yield without requiring further purification.

The primary amine could then undergo amidation with a fluorophore. This was firstly completed using 5-carboxyfluorescein (Scheme 3.3).

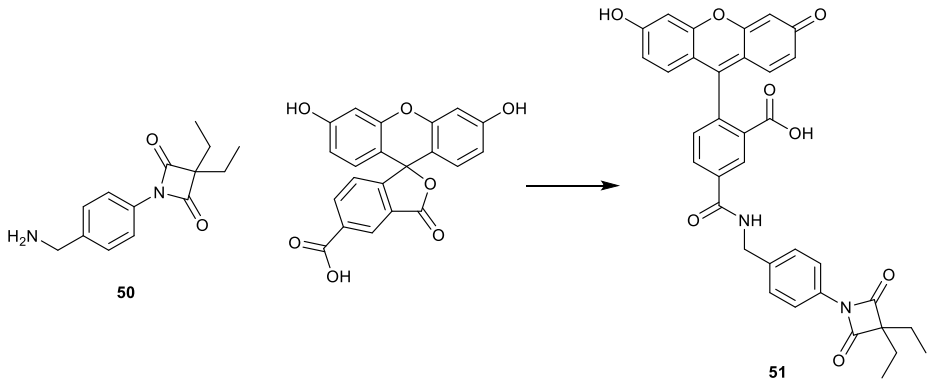

Scheme 3.3. Synthesis of the carboxyfluorescein based optical probe **51**. Reaction conditions: DIPEA, PyBrOP, DMF, 24 h, 31%.

The activation of the carboxylic acid on the fluorophore was achieved by the coupling reagent PyBrOP, to generate *in situ* an acid bromide, a labile leaving group for nucleophilic attack by the amine (Scheme. 3.4).

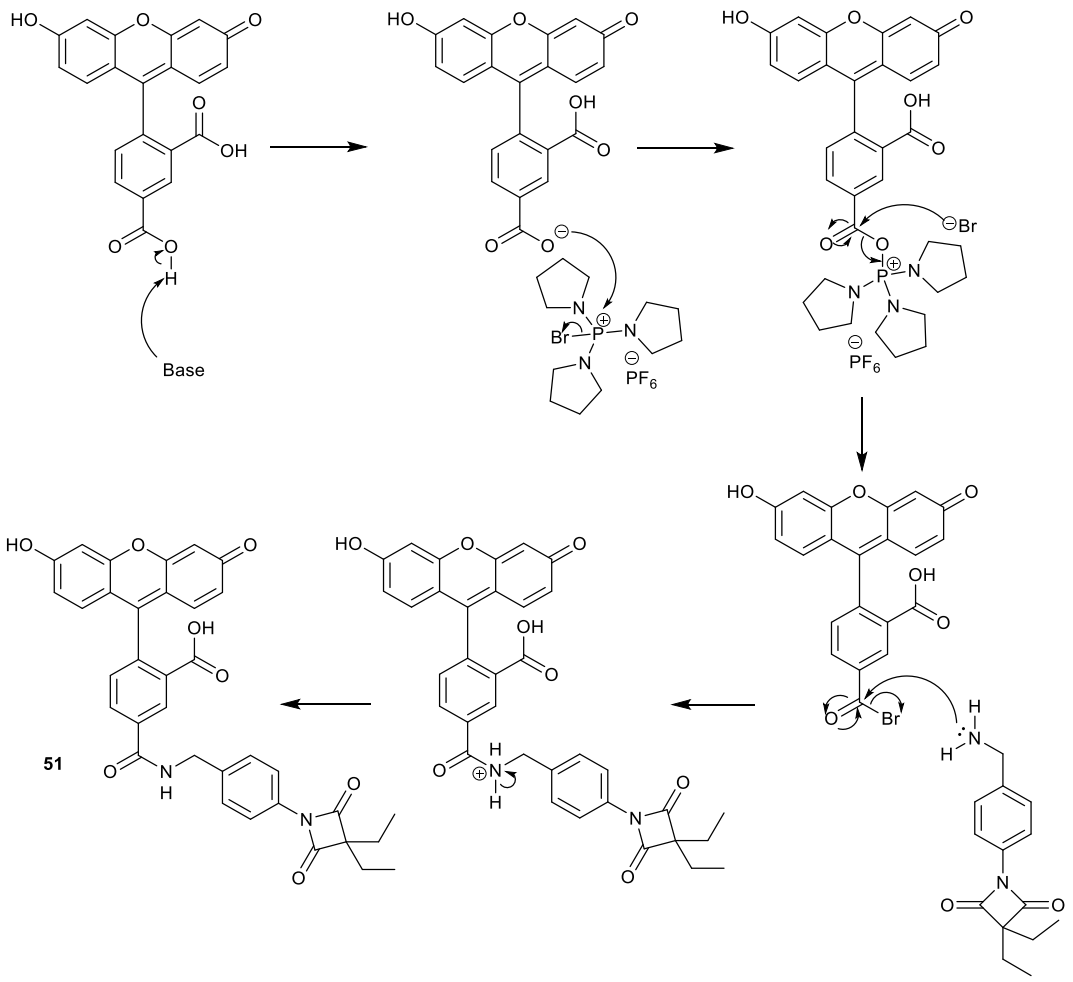

Scheme 3.4. Mechanism of activation of 5-carboxyfluorescein using PyBrOP.

The optical probe **51** was formed in a moderate yield of 31% after purification, the excitation and emission maxima were determined to be 494 and 523 nm (Figure 3.5).

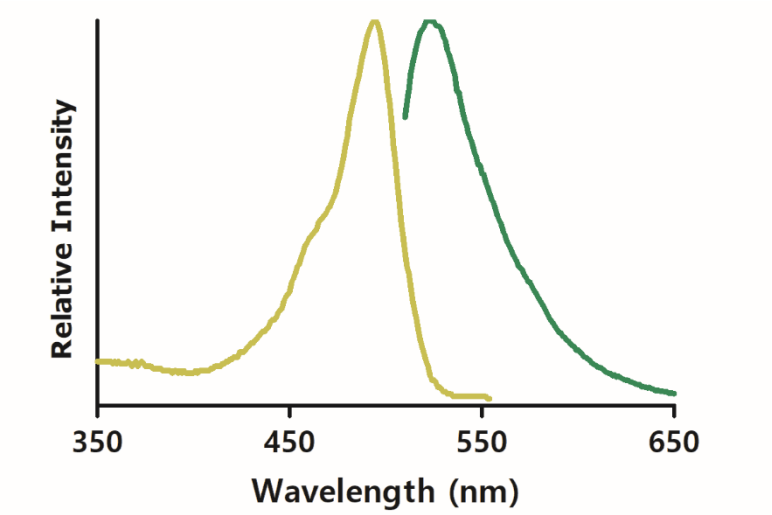

Figure 3.5. Absorption (yellow) and emission (green) spectra of **51**. Solutions were 1 μM in PBS (pH 7.4), and the data normalised.

Subsequently, the inhibitor **50** underwent amidation with Cy5 dye **27** (Scheme 3.5). The carboxylic acid group on the dye also required activation *in situ* before the addition of the amine. In this particular reaction, the preferred coupling reagent was HSPyU that forms a succinimide ester (Scheme 3.6).

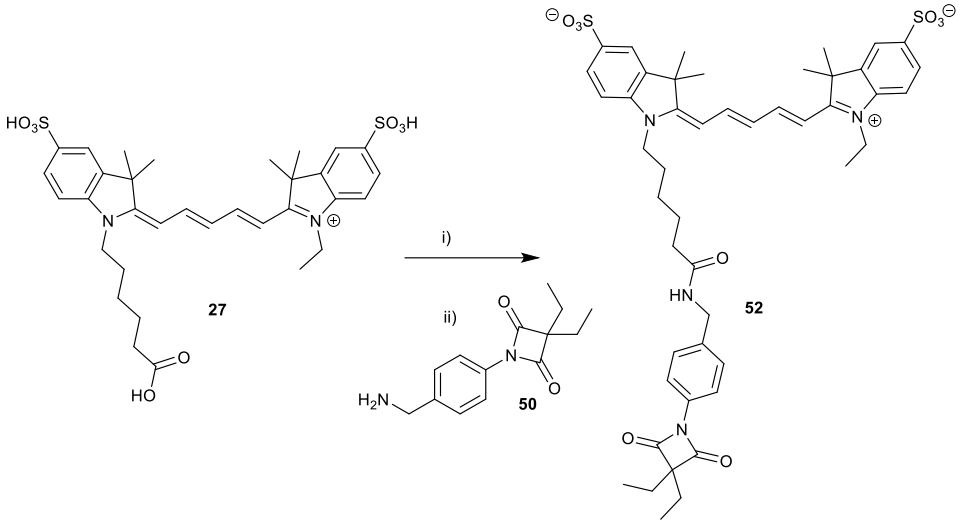

Scheme 3.5. Generation of NIR optical probe **52**. Reaction conditions: i) HSPyU, DIPEA, DMF, 3 h; ii) **50**, DIPEA, 18 h, 27% after purification.

The activation of the dye was monitored by HPLC, as the retention time shifts significantly upon formation of the succinimide ester and after which the inhibitor (**50**) was added. The amidation was monitored until the activated dye was shown to be fully consumed, after which the solvents were removed, and the product purified by reverse phase column chromatography.

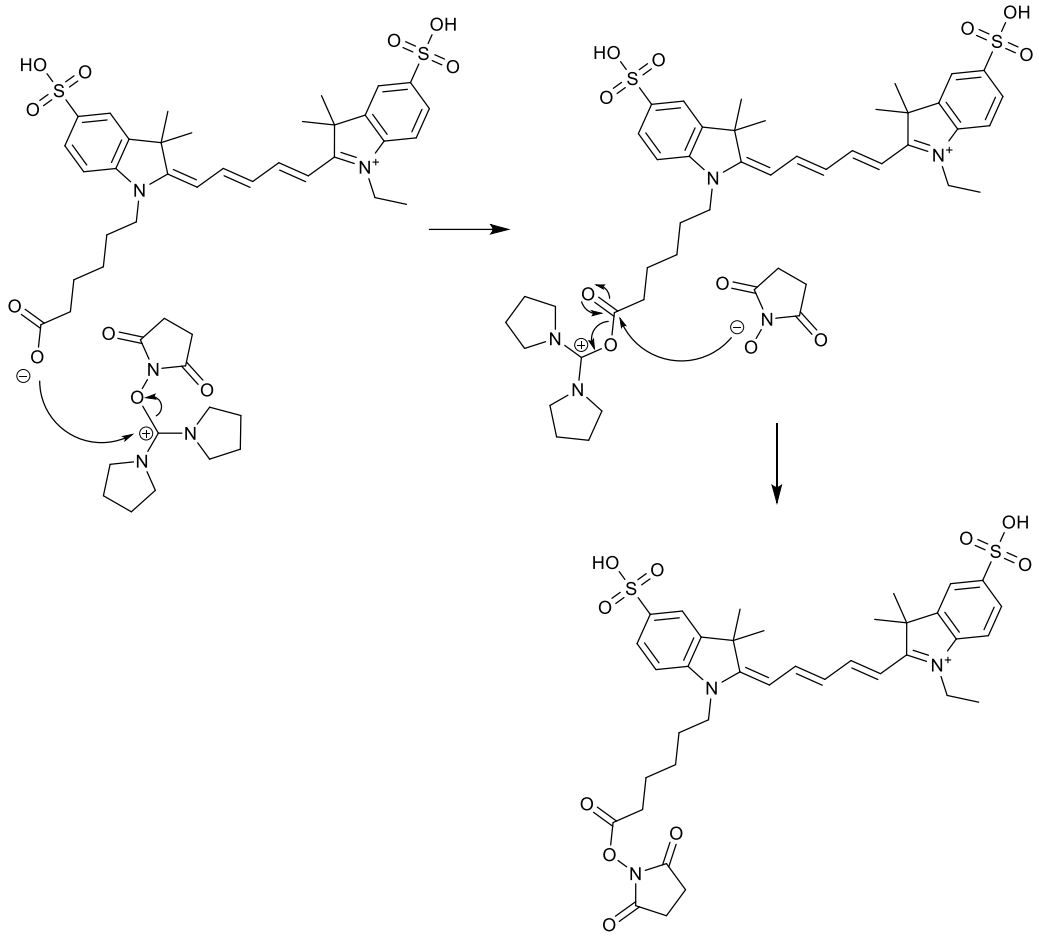

Scheme 3.6. Activation mechanism of the cyanine dye **27** with HSPyU.

The excitation and emission spectra of probe **52** was then analysed (Figure 3.6). Probe **52** underwent a slight bathochromic shift from the original Cy5 dye **27** by 2 nm, the new excitation wavelength being 649 nm with the emission maximum at 667 nm (upon excitation at 630 nm).

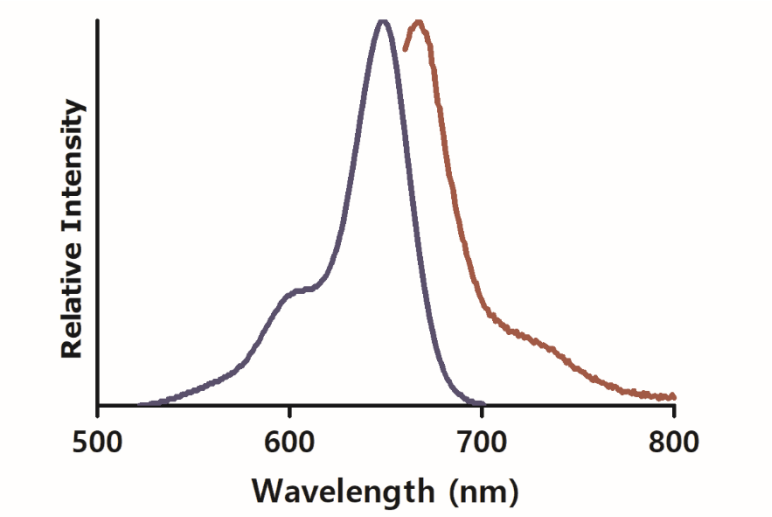

Figure 3.6. Absorption (blue) and emission (red) spectra of probe **52**. Solutions were 1 μM in PBS, and the data normalised.

3.4 Synthesis of oxo-β-lactam optical probes containing an ethyl spacer

The second oxo-β-lactam based HNE inhibitor generated contained an ethyl moiety linking the warhead to the fluorophore in place of the phenyl group on **50**. The synthesis was similar in that another Boc-protected primary amine was used for cyclisation with the diacid chloride (Scheme 3.7).

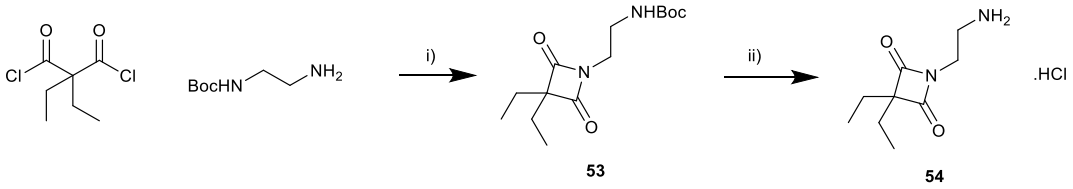

Scheme 3.7. Synthetic route for HNE targeting compound **54**. Reaction conditions: i) TEA, dioxane, -10 °C to rt, 18 h, 22%; ii) 4 M HCl in dioxane, 4 h, quant.

The cyclisation reaction was initially achieved at room temperature, but this gave a low yield of 14%. Cooling the reaction to -10 °C, increased the yield to

22%. The Boc protecting group was then removed using hydrochloric acid, to unmask the primary amine, for amidation with a fluorophore.

The first fluorophore to be used was the protected and activated 5-carboxyfluorescein **25** (Scheme 3.8). This was carried out using DIPEA (9 equiv) as the phenols were deprotected *in-situ* by deacetylation in addition to the amidation reaction.

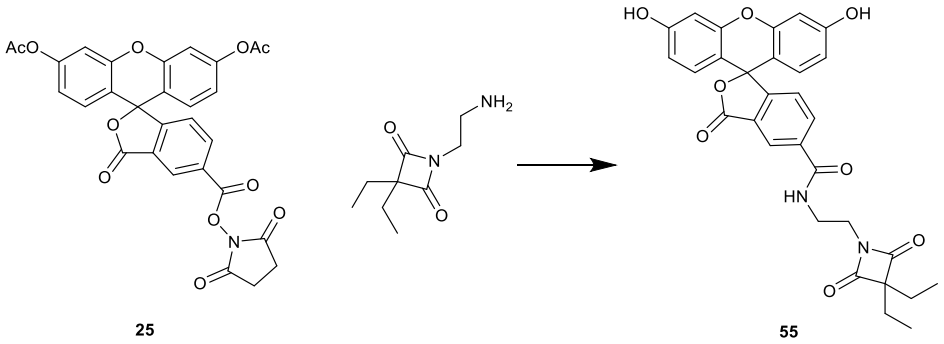

Scheme 3.8. Synthetic route to the generation of carboxyfluorescein based probe **55**. Reaction conditions: DIPEA, DMF, 18 h, 21% after purification.

In a similar fashion to probe **49**, optical probe **53** required purification using reverse phase chromatography. The excitation maximum of **53** was 494 nm, with a slight bathochromic shift of the emission maximum to 525 nm (Figure 3.7).

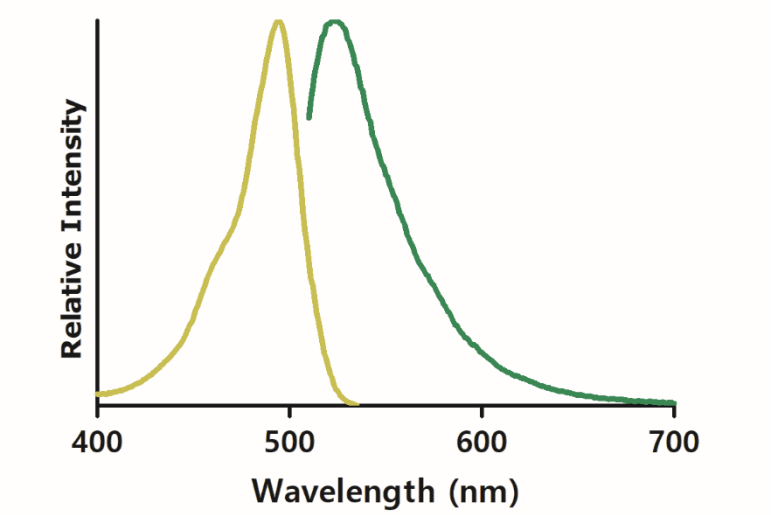

Figure 3.7. Absorption (yellow) and emission (green) spectra of probe **55**. Solutions were made up of PBS (pH 7.4, 1 μM), and the data normalised. The emission was collected with excitation at 480 nm.

The subsequent fluorophore used was Cy5, and in the same fashion as probe **52**, with the carboxylic acid activated *in situ* using HSPyU (Scheme 3.9). Amidation was likewise monitored by HPLC and compound **56** was purified using reverse phase preparative HPLC to obtain the optical probe in 45% yield.

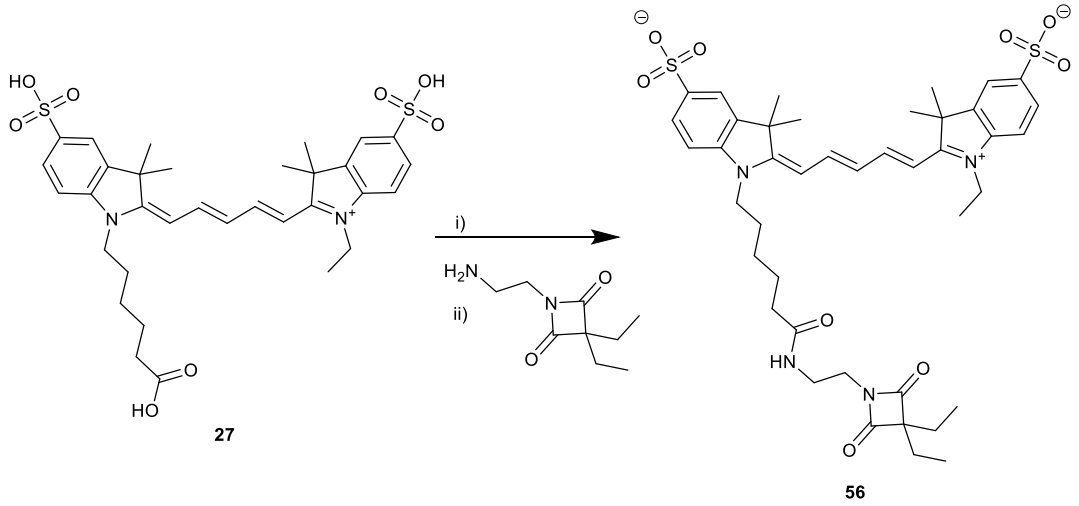

Scheme 3.9. Final synthesis steps of probe **56**. Reaction conditions: i) HSPyU, DIPEA, DMF, 3 h, ii) **54**, DIPEA, 18 h, 45% after purification.

Probe **56** was then analysed to show its excitation and emission maxima, at 650 nm and 666 nm respectively (Figure 3.8), confirming emission in the far red and in the desired optical window.

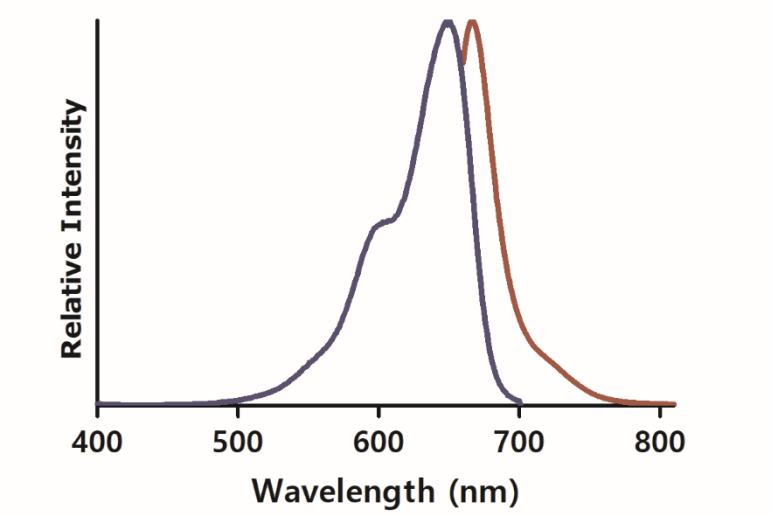

Figure 3.8. Absorption (blue) and emission (red) spectra of **56**. 1 μM solutions were made up in PBS (pH 7.4), and the data normalised. Emission was recorded after exciting at 630 nm.

With four optical probes in hand, the next step was to evaluate their biological properties and potential as imaging agents for detecting HNE *in vivo*.

3.5 Biological evaluation of optical probes

The optical probes required evaluation to indicate whether they were suitable in a biologically relevant setting. This involved determining the stability, affinity towards HNE, its toxicity towards mammalian cells, and the concentration required for visualisation of the optical probes *in vitro*.

3.5.1 IC50 determination of optical probes

The half maximal inhibitory concentration, or IC_{50}, is used to determine relatively how potent a drug is. There are many methods that can be used to determine an IC_{50}. In this thesis, it was achieved using the well-known chromogenic peptide-based substrate, *N*-methoxysuccinyl-alanine-alanine-proline-valine-amido-4-methyl coumarin (MeOSuc-AAPV-AMC, Scheme 3.10).

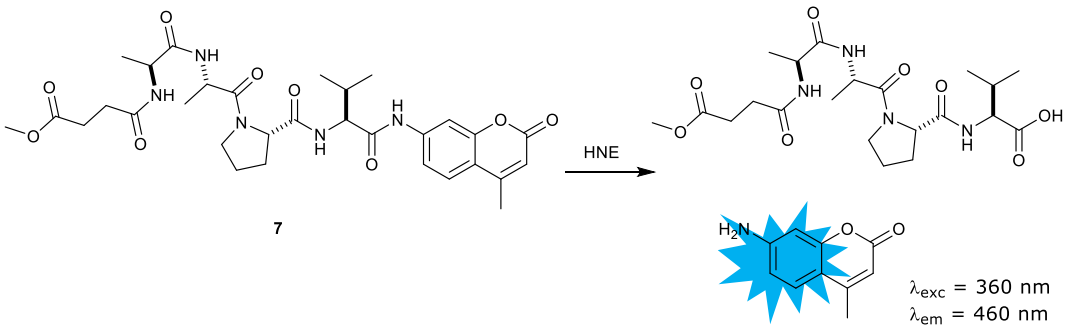

Scheme 3.10. HNE substrate *N*-methoxysuccinyl-alanine-alanine-proline-valine-amido-4-methylcoumarin **7** and the mechanism of fluorescence upon peptide cleavage.

7 is a tetrapeptide which has been modified on both terminals. The *N*-terminus has been capped with methoxy succinate and the *C*-terminus reacted with the fluorophore amino-4-methylcoumarin. The enzyme HNE cleaves the amide bond between the peptide and fluorophore, releasing coumarin, enabling a fluorescent signal to be detected as a signal of enzyme activity.

The enzyme was incubated with a variety of concentrations of the probes for 30 minutes, after which the substrate was added. The initial velocity of the reaction was calculated and plotted against the inhibitor concentration to determine at which concentration the enzyme activity was reduced by 50%, when compared to the enzyme alone (negative control). The graphs are shown in Figure 3.9.

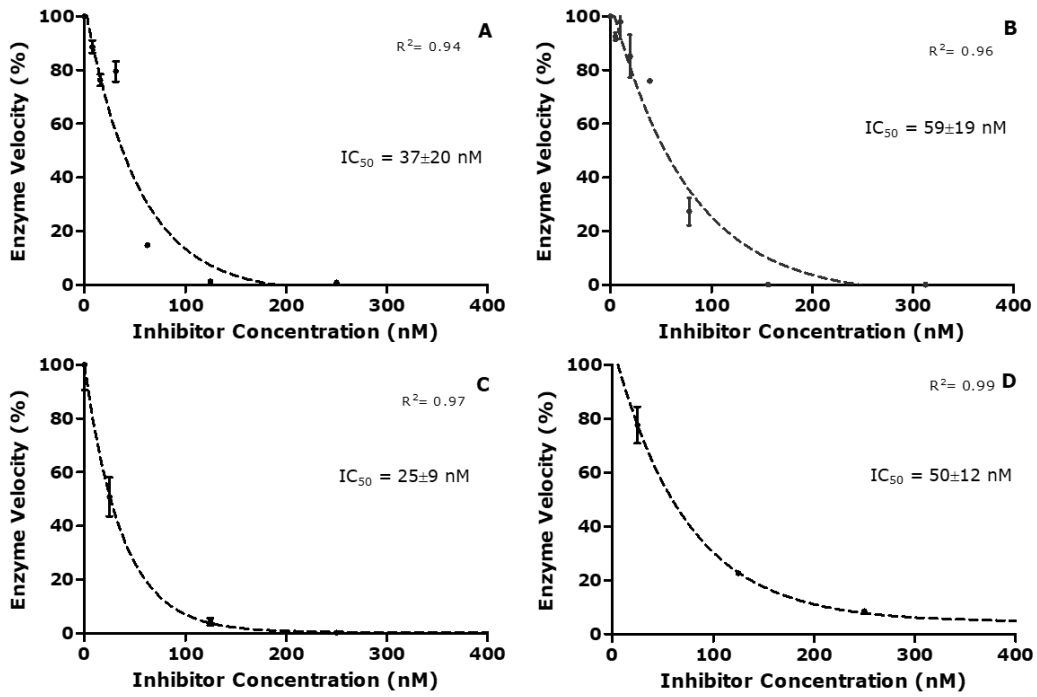

Figure 3.9. IC_{50} graphs of optical probes **51** (A), **52** (B), **55** (C) and **56** (D). Data was collected using a plate reader and measuring fluorescence of substrate **7**. The optical probes were incubated with HNE for 0.5 h before the addition of the substrate, at various concentrations (n=3, except for A where n= 2).

Interestingly, the two carboxyfluorescein based probes had lower IC_{50} values than the Cy5 based probes, probe **51** having an IC_{50} of 37 nM and **55** an IC_{50} of 25 nM (Figure 3.9, A and C). The two Cy5 probes (**52** and **56**) still had respectable IC_{50} values of 59 and 50 nM, indicating good affinity towards the enzyme.

This confirmed the addition of the fluorophores didn't strongly affect the activity of the oxo-β-lactam scaffold towards HNE and provided some confidence in the potency of the optical probes.

3.5.2 K_i determination for the optical probes

The K_i was to be determined in a similar manner as the IC_{50} values (Figure 3.9) but without incubating the enzyme and probes before the experiment. This was to determine the rate of inhibition, however, there were many issues in replicating this data. When using the same stock of serial dilutions varying results were observed, with some showing strong inhibition, and some almost none. This was a common occurrence for all probes, making reproducible K_i data problematic. It is also possible that the measurable inhibition was playing a complicated role

3.5.3 Stability of optical probes in solution

The difficulties in collecting reliable data for the Ki constants led to the stability of the probes in aqueous media being examined, as the decrease in activity could be a cause in the change in progress curves over time. Additionally, stability of the compounds in biological environment is also a significant requirement of a probe used in a clinical setting.

The optical probes were incubated at 37 °C in PBS and analysed by HPLC over 24 hours to determine the level of degradation (Figure 3.10). Most of the probes were relatively stable under these conditions, except for probe **51**, which had a half-life of 22 hours. These values indicate that the stability of the probes in PBS had no bearing on the difficulties in determining their Ki values, as the solutions were only made up for a few hours. However, they do show that the probes robustness could allow for clinical use due to their reasonable lifetime in solution.

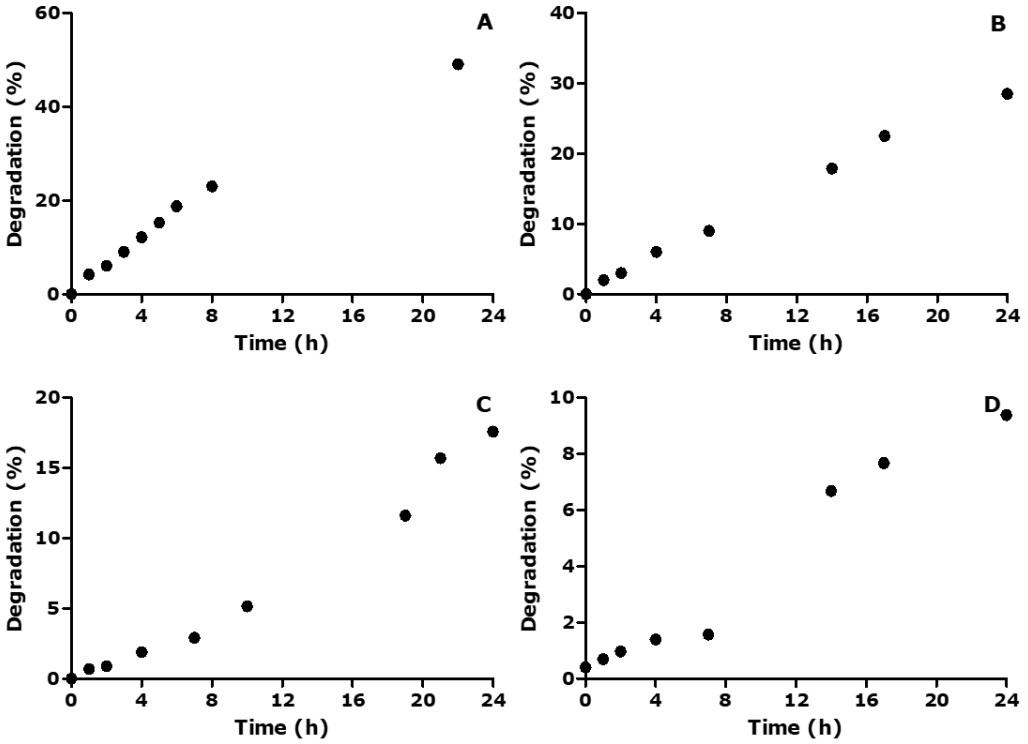

Figure 3.10. Stability study of optical probes (60 μM) in PBS at 37 °C (n=1). Degradation of the samples were analysed by analytical HPLC at 254 nm for **51** and **55** (A and C) or 650 nm for **52** and **56** (B and D).

A similar experiment was completed by incubating the optical probes in Dulbecco's Modified Eagle's Medium (DMEM) at 37 °C (Figure 3.11).

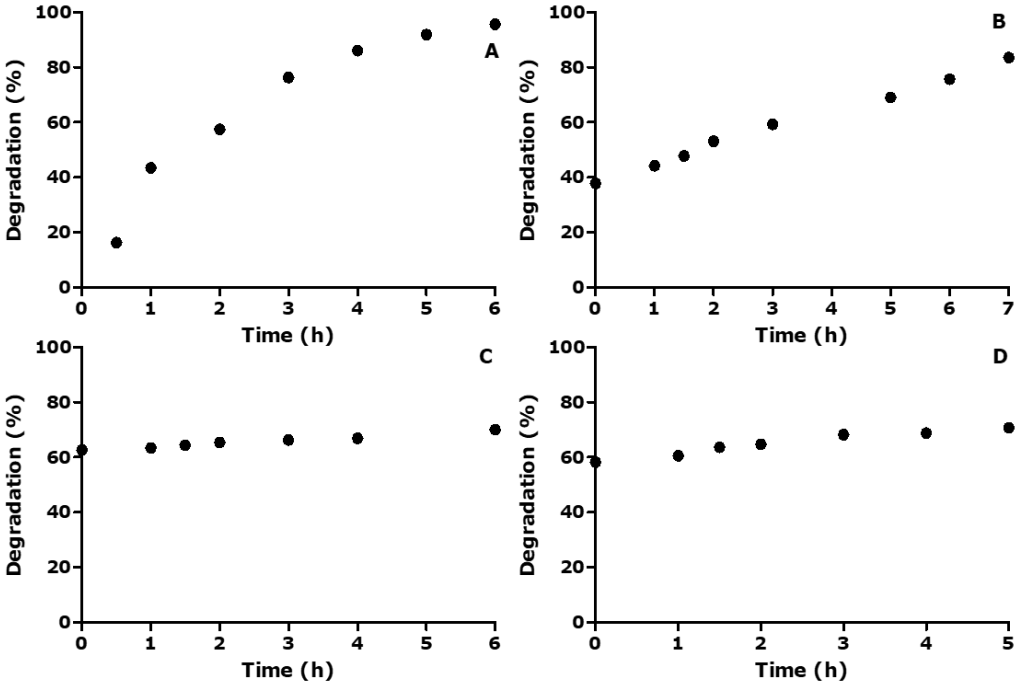

Figure 3.11. Degradation of optical probes (60 μM) over time at 37 °C in DMEM media (n=1). The formation of by-products and degradation was monitored using analytical HPLC at 254 nm for **51** and **55** (A and C) or 650 nm for **52** and **56** (B and D).

The probes **51** and **52** exhibited longer half-lives than **55** and **56**, with $t_{1/2}$ values falling between 1 and 2 hours, in comparison to probes **55** and **56**, where degradation from the initial measurement was determined to be 60% by-product. They exhibited almost instantaneous degradation, as HPLC traces of almost all compounds at t=0 h had large amounts of by-product, which was absent in the PBS traces of the same stock solutions (Figure 3.12). The instability of the optical probes in media is unsurprising due to the number of enzymes present in the solution, as well as the fact it is unnecessary, as neutrophils do not require media after isolation, if anything the media would activate the neutrophils and cause them to self-destruct before imaging can occur.

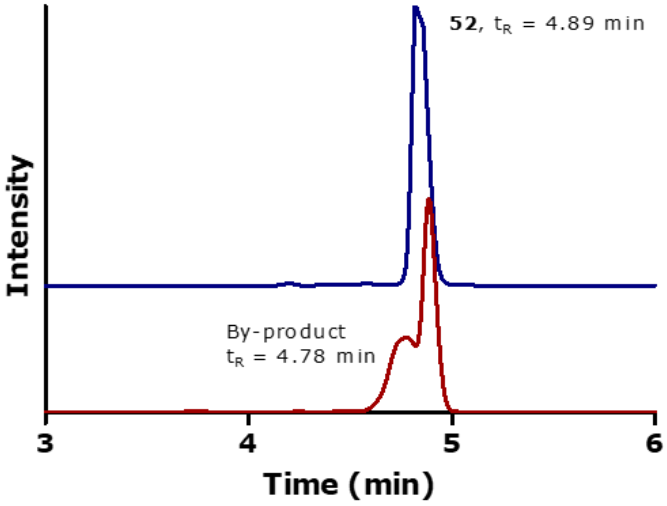

Figure 3.12. Example of the observed 'instant degradation' of an optical probe in media. The probe **52** at t= 0 h, in PBS (blue) and media (red), analysed by HPLC in the 650 nm channel.

3.5.4 Gel electrophoresis of the optical probes and human neutrophil elastase

To confirm that a covalent bond was formed between the probes and HNE, the probes were incubated with enzyme for 5 mins before undergoing gel electrophoresis. The gel was first imaged in different fluorescent channels to visualise the presence of the fluorophores, before being stained with Coomassie blue to confirm the presence of the protein (Figure 3.13).

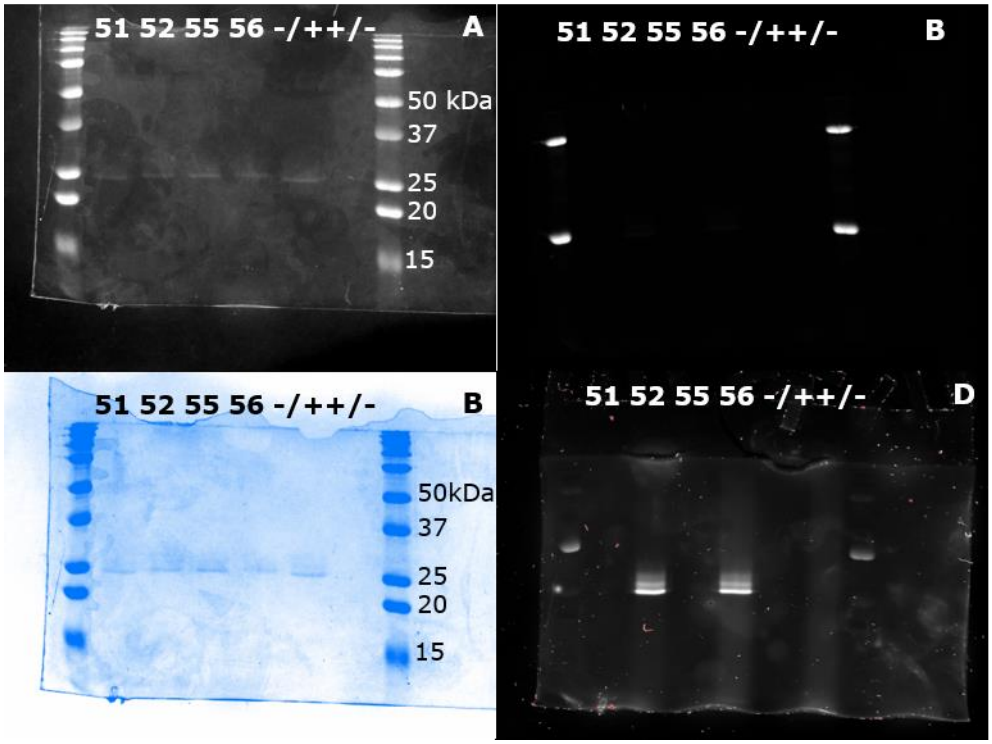

Figure 3.13. Imaging of human neutrophil elastase incubated with the optical probes **51**, **52**, **55** and **56** by SDS-PAGE. Imaged using coommassie blue staining (A is in greyscale and C), the fluorescein channel (B) and the 625 nm channel (D), (-/+) HNE with no optical probes, and (-/+) optical probes without HNE. The outermost lanes are kaleidoscope ladder from Biorad.

Interestingly, the two far red probes can be distinguished (Figure 3.13 D) but no fluorescence was detected from the optical probes using the 495 nm channel (Figure 3.13 C), which may have been caused by a number of factors. Possible reasons include: the concentration of the optical probes was too low at 2.5 μM, the fluorophore had been photobleached and were not bright enough for a detectable fluorescent signal or the ester bond formed was destroyed by the denaturation technique, but unlikely as the far-red probes were stable. Further research would be required to elucidate the cause.

3.5.5 Toxicity of optical probes

As the probes were designed with the intention for use *in vivo*, a vital characteristic was a lack of toxicity towards mammalian cells. One of the more

common methods of assessing cytotoxicity is an MTT assay but this is primarily used on tumour cells and would be a skewed representation of cytotoxicity on the epithelial cells within the lungs. As such, a different cell viability study was targeted, a haemolysis assay, as the cells targeted are red blood cells, and haemolytic activity would prevent clinical use of the optical probes.

The assay was achieved by incubating the probes for an hour at 37 °C with erythrocytes at two different concentrations and monitoring the concentration of porphyrin released after an hour, compared to a known standard curve (Figure 3.14). This was repeated with three samples from different volunteers and on different days.

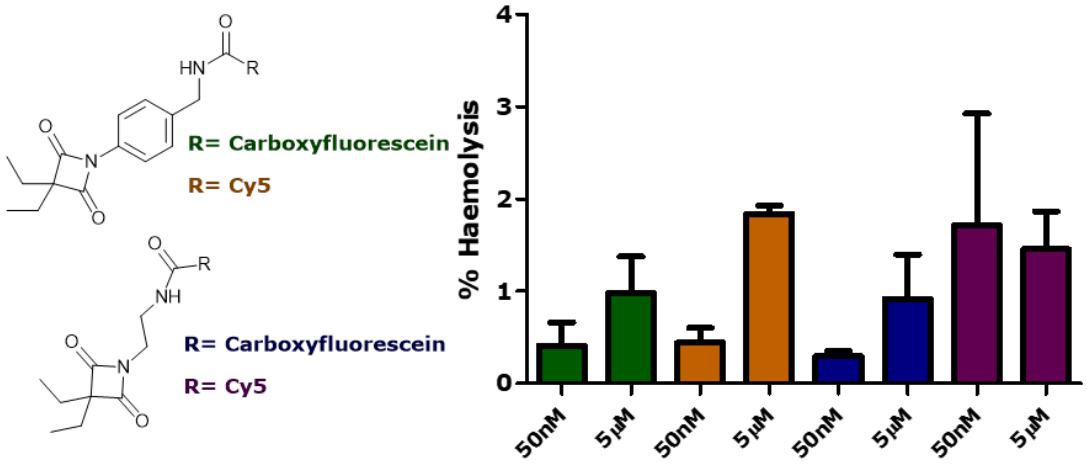

Figure 3.14. Haemolysis assay of the optical probes **51** (green), **52** (orange), **55** (blue) and **56** (purple), at two concentrations 50 nM and 5 μM, with the data compared to a standard curve of controlled haemolysis, n=3.

The haemolysis assay determined that all probes had a cytotoxicity of less than 2% at 5 μM, a concentration ten-fold higher than needed, making them acceptable for *in vivo* imaging.

3.5.6 Confocal imaging of optical probes

After confirming the optical probes bound to HNE and could be detected with fluorescent imaging after gel electrophoresis (Figure 3.13), the next step was to image the probes on human neutrophils.[#] This was achieved by first isolating the neutrophils from a donated whole blood sample using a previously stated protocol.[24,108] The neutrophils were then incubated with a calcium ionophore to activate them before adding the optical probes for 10 min. The cells were then imaged using confocal microscopy. In addition to the probes, they were also stained with Hoechst 33342, a UV-active dye that is specific for the nucleus (Figure 3.15). In imaging **55**, an additional imaging agent was used, an HNE specific antibody with a far-red fluorophore. This allowed for confirmation of staining the enzyme, as the two HNE probes would be seen to co-localise.

[#] The human neutrophils were sourced ethically, and their research use was in accordance with the terms of the informed consents

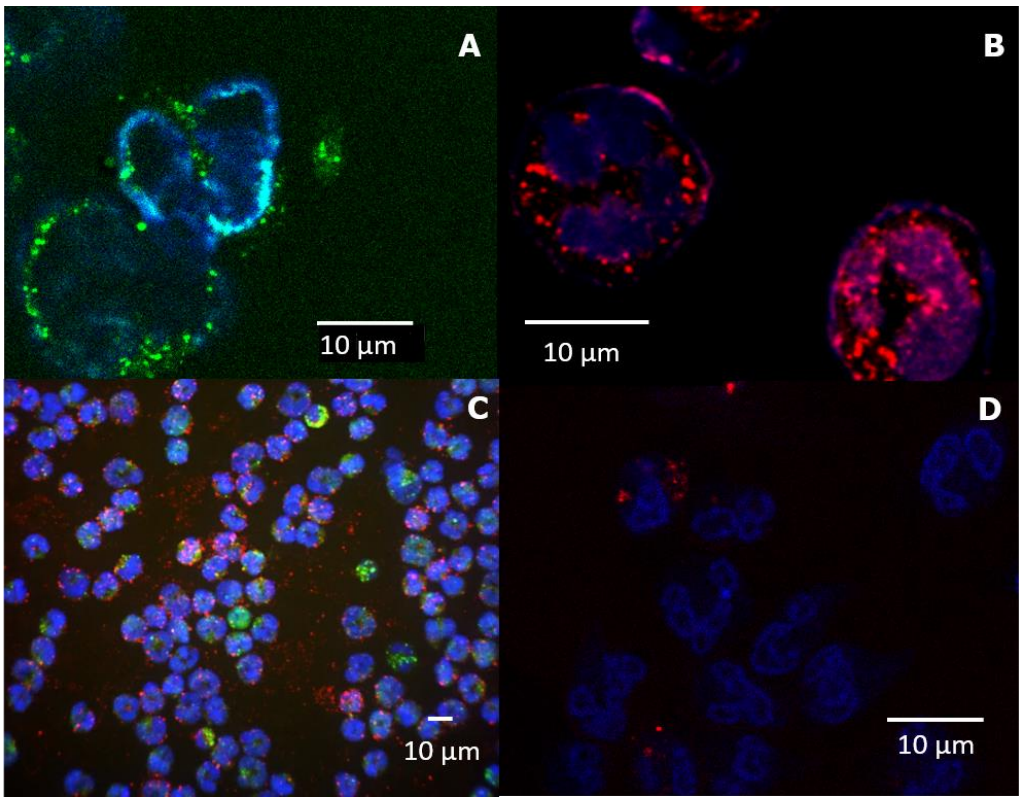

Figure 3.15. Live confocal imaging of activated human neutrophils incubated with the optical probes (500 nM, 10 min) and nuclear stain Hoescht 33342 (blue, 405 nm laser line). Image (A) was stained with **51** (green, 488 nm laser line), (B) was stained with **52** (red, 630 nm laser line), (C) was stained with **55** (green), in addition to an HNE specific antibody (red) and (D) was stained with **56** (red).

3.5.7 Flow cytometry of **55**

The confocal images confirm uptake of the probes by neutrophils, but flow cytometry provides a quantitative method. Neutrophils were isolated from human blood using a previously described method to purify whole blood by fractional density with Percoll, then resuspended in PBS.[108] The cells were separated into various wells: a control with no activation or probe, and cells activated and cells without activation. Two different concentrations of optical probes were analysed to compare the concentration effect as well as the effect of activation of the neutrophils (Figure 3.16). In addition to the neutrophil isolation, they were also labelled with a neutrophil specific antibody, CD66b,

to confirm the cells were neutrophils. The cells were incubated with probe **55** for one hour at 37 °C, and half of which were activated using a tripeptide, fMLF, a commonly used activator of leukocytes.

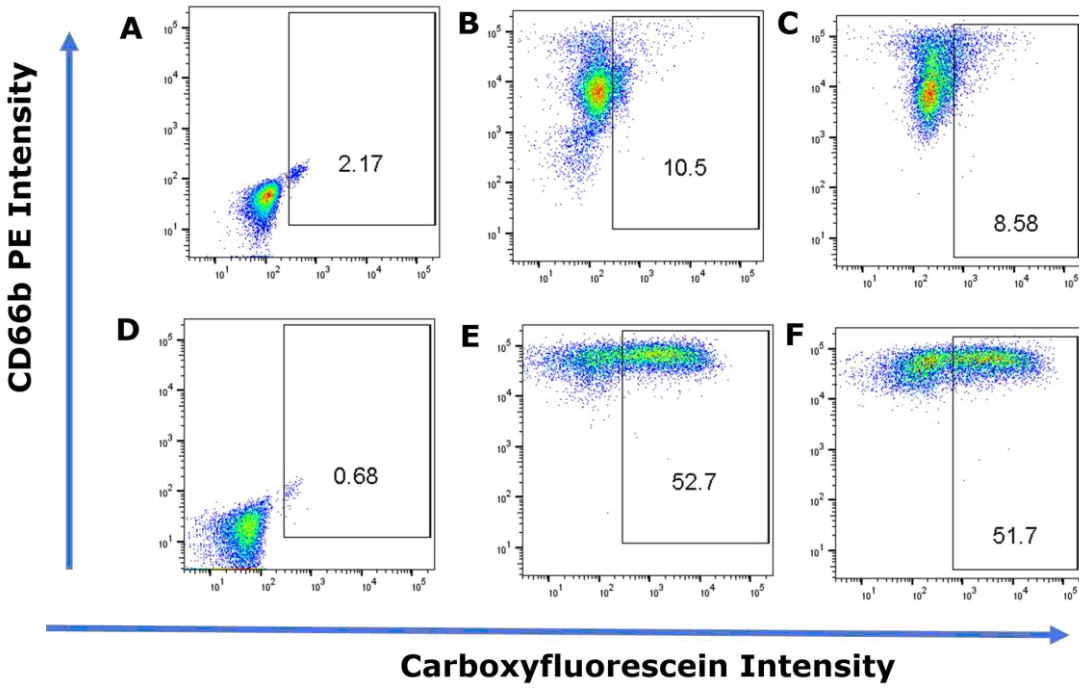

Figure 3.16. Labelling of neutrophils with probe **55**. Flow cytometry density plots of neutrophils after being incubated with a labelled CD66b antibody (15 min) and optical probe **55**, whereby the boxed data indicate a positive result. A and D represent a population of neutrophils after incubation with labelled CD66b, with a control population (A) and an activated population with 1 μM fMLF (D); (B) and (E) are neutrophils incubated with 250 nM **55**, where E has also been incubated with activation agent fMLF; C and F are neutrophils after 0.5 h incubation with 500 nM **55**, where F was also incubated with the activation agent fMLF. All density plots had a cut off after 10 000 counts, with n = 1.*

The control density plots (Figure 3.10 A and D) confirmed the gating required for the successive plots as they indicate where healthy cells reside. Strangely, A and D should be on a similar plane in the y axis to the rest of the plots. This

* Data collected and analysed with Dr Richard O'Connor at Queens Medical Research Institute

is to indicate positive labelling of neutrophils with the specific neutrophil antibody CD66b. The other sets of neutrophils show a higher concentration of CD66b labelling, which may be due to the length of time the different sets of cells were incubated with the antibody and would require further experiments to confirm this.

Two sets of neutrophils were incubated with probe **55** (Figure 3.10, B and C) but not activated by the tripeptide, and hence the small values, 10.5% and 8.6%, were expected when comparing to the same conditions but in presence of the tripeptide as an activation agent (Figure 3.10, E and F). The wide spread of counts in the density plots of the activated sets would require further investigation but at this stage, the confirmation of increased labelling with activation, was a good indication that **55** labelled HNE.

3.6 Conclusions

HNE inhibitors with high water solubility are ideal to microdose in the lung (through a bronchoscope) to identify potential inflammatory sites, or to aid in rapid diagnosis of pulmonary diseases. Here, four optical probes were successfully synthesised and purified in moderate yields and validated on the green and red channels to confirm the presence of human neutrophil elastase.

In addition to two different fluorophores, two different spacer groups between the oxo-β-lactam warhead and the fluorophore were also incorporated, allowing comparison of the reactivity of the probes. The aryl spacer was shown to have a higher affinity towards HNE over the alkyl spacer, in addition to having a lower affinity towards other serine proteases. There was no noticeable difference in their cytotoxicity, the optical probes with an aryl space showed a slightly longer half-life in DMEM media over the ethyl spaced

probes **55** and **56**. However the optical probes with an alkyl spacer demonstrated a longer half-life in PBS over **51** and **52**.

The optical probes were determined to have IC_{50} values between 25 and 60 nM, and their half-lives in PBS were at least 22 hours but lacked stability in DMEM media. The two Cy5 probes **52** and **56** were confirmed to have formed a covalent bond with HNE via gel electrophoresis, and flow cytometry was used to confirm probe **55** was labelling activated neutrophils. The probes were used to image live neutrophils and highlight puncta areas of the cells.

Chapter 4 GSK drug-based elastase targeting optical probe

4.1 Introduction

To develop a useful always-on optical probe, a highly specific targeting moiety is required, which is selective for human neutrophil elastase (HNE) over other analogous serine proteases. For the probe to be applicable *in vivo*, biocompatibility is essential, in addition to excellent clearance by the metabolic system. Given HNE has been correlated with a wide range of chronic pulmonary diseases, pharmaceutical companies have used the enzyme as a potential treatment target. To generate a highly specific optical probe, an HNE targeting drug can be incorporated into the structure. This is advantageous as a vast number of initial screening has been done before, including the specificity and affinity studies for HNE over other related serine proteases.

HNE inhibitors slow down the enzyme activity which reduces the degradation of the pulmonary tissue. To date, there is only one commercially available treatment for the inhibition of HNE activity, Sivelestat, **57** (Figure 4.1). The drug has been surrounded by vague and contradictory results regarding it as a treatment option for ALI. Sivelestat was approved for two clinical trials: one in Japan and the STRIVE study, a Europe wide study. The Japanese study gave a positive outcome of reducing the number of days a patient requires ventilation, whereas the STRIVE study was terminated early due to the mortality rate of both the placebo and drug group being equivalent. As a result, **57** is only available as a treatment in South Korea and Japan.[109–111]

In addition to the controversy regarding Sivelestat, the mechanism of the drug is slowly reversible, making it unsuitable for manipulation to become an optical probe, due to the possibility of dissociation.

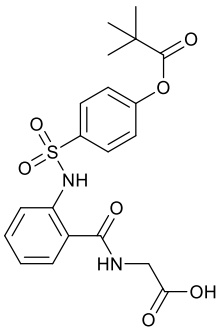

57

Figure 4.1. Structure of the HNE inhibitor Sivelestat (ONO-5046), **57**, Ki = 200 nM, IC_{50} = 44 μM.[112]

HNE has been a popular drug target for chronic obstructive pulmonary disease (COPD) after several years of research found a link between the two.[54-56] A library of second-generation inhibitors for the enzyme were developed by GSK; suicidal small molecules designed to bind irreversibly in the active site. The inhibitors all comprised the same motif: a 'warhead' attached to a long hydrophilic tail that interacts with the tunnel of the active site in the enzyme. The warhead consists of a pyrrolidine *trans*-lactam which covalently binds to the hydroxyl group of the serine residue in the active site (Ser203) (Figure 4.2).

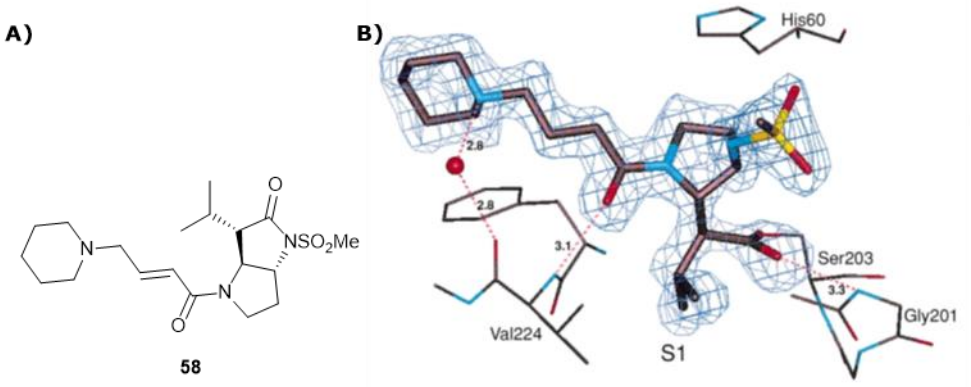

58

Figure 4.2. A) The HNE inhibitor GW311616A, **58**;[113] B) crystal structure of **58** complexed in the active site of porcine pancreatic elastase. The structure has dotted lines to represent bonding between the substrate and enzyme, at the active site and channel towards it.

The library of inhibitors was published in 2002 and, **58** was demonstrated to be highly potent to HNE, and selective over other serine proteases.[41] The IC_{50} of **58** towards HNE was 22 nM compared to other serine proteases such as chymotrypsin (3 μM) and trypsin and cathepsin G (above 100 μM). The combination of selectivity towards HNE and the versatility of altering the 'tail' with different functional groups made it a suitable candidate as the targeting moiety for the optical probe.

4.2 Aims of chapter 4

HNE has long been a drug target due to its overexpression being symptomatic of several diseases including COPD and cystic fibrosis. The GSK inhibitor **58** has proven to be specific towards HNE over other familial serine proteases, as well as compatible *in vivo*, due to rigorous testing required for pharmaceuticals. Due to the advantages of this inhibitor, the aim of this chapter was to synthesise the compound but include a slight modification to allow for the addition of a fluorophore. After formation of the modified inhibitor, a dye was to be conjugated to form a highly specific far-red probe. The probe was to undergo cursory biological studies including the affinity towards HNE as well as imaging the probe *in vitro*.

4.3 Synthesis of elastase targeting warhead

The GSK inhibitor **58** can be disconnected to form two separate moieties: the warhead and the tail (Scheme 4.1). The tail can be easily modified to incorporate a fluorophore by substituting the piperidine for a piperazine, enabling an amine for the conjugation to a fluorophore.

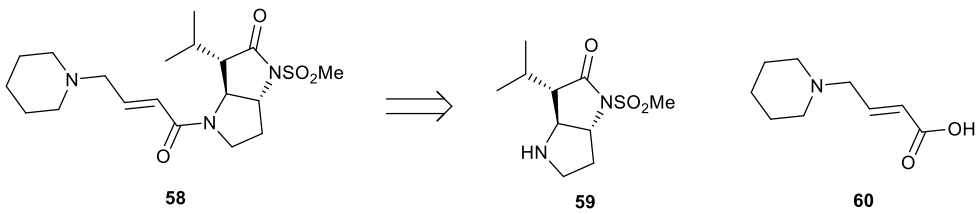

Scheme 4.1. Disconnection of GSK inhibitor **58**, to the warhead **59** and the hydrophilic tail **60**.

The synthesis of inhibitor **58** was developed by GSK, by starting with L-methionine (Scheme 4.2). The first reaction involved the Boc protection of the α-amino group with Boc anhydride under basic conditions.

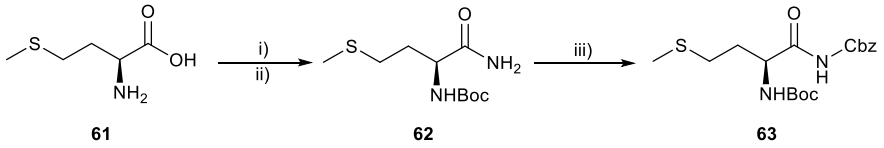

Scheme 4.2. First two steps towards the synthesis of **59**. Reaction conditions: i) 1.25 M NaOH, Boc_2O, dioxane, 0 °C to rt, 3.5 h; ii) pyridine, NH_4HCO_3, Boc_2O, DMF, 18 h, 50% over i) & ii); iii) *n*-BuLi, benzyl chloroformate, THF, -70 °C, 1.5 h, 96%.

The subsequent step involved amidation of the carboxylic acid. Firstly, the free carboxylic acid was activated to give a mixed anhydride that then reacted with ammonia to generate the carboxamide **62** (Scheme 4.3). The generation of the by-product CO_2 was observed by effervescence throughout the reaction. The presence of product **62** was confirmed by the presence of the characteristic two amide protons in the ^1H NMR spectrum.

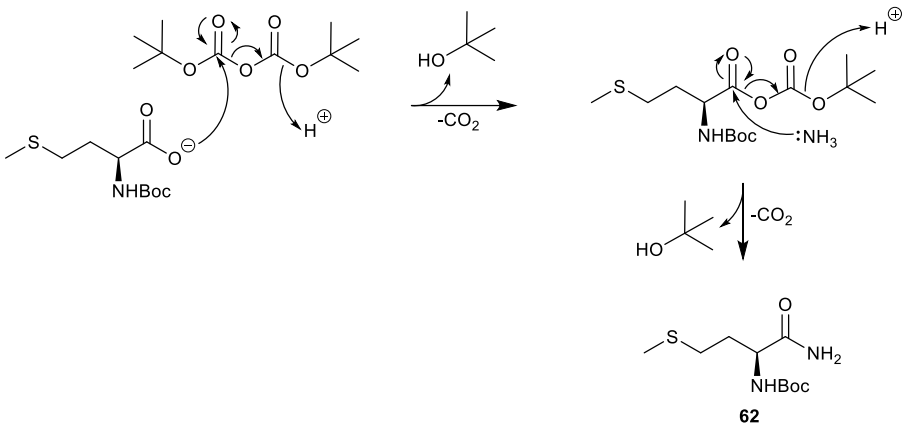

Scheme 4.3. Proposed mechanism for the amidation of Boc protected L-methionine to form **62**.

An orthogonal protecting group was introduced onto the newly formed amide moiety in the form of a benzyl carbamate to generate **63**. This was achieved by deprotonation of **62** by *n*-BuLi which enabled nucleophilic attack on benzyl chloroformate with subsequent elimination of the chloride yielding in the desired carbamate. As the reaction required low temperatures (-70 °C) and was highly water sensitive, scale up proved challenging but several small-scale reactions gave **63** largely in quantitative yield.

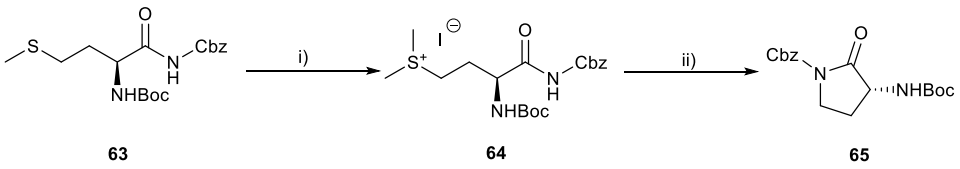

Scheme 4.4. Synthesis of lactam **65**. Reaction conditions: i) MeI, acetone, rt, 3 d, dark, 78%; ii) Amberlite IRA-410 (hydroxide form), MeCN, 4 Å molecular sieves, 45 °C, 4.5 h, 42%.

To generate lactam **65**, the protected methionine amide **63** was methylated to generate the sulfonium ion as a leaving group (Scheme 4.4). Subsequent reaction of **64** generated dimethyl sulfide, upon nucleophilic attack by the amide anion on the gamma carbon. The purification of **64** was difficult to achieve on a small scale. The published procedure indicated precipitation

should occur during the reaction and the product recrystallized with diethyl ether, but this was not reliable. Due to the difficulty in obtaining pure product, the crude **64** was carried into to the following step.

The cyclisation step to generate the pyrrolidone **65**, involved using a resin, Amberlite IRA-410 in its strongly basic form (Scheme 4.5). The Amberlite resin was functionalised with 10 M NaOH before washing with H_2O, MeCN and drying with diethyl ether. Following the reaction, the mixture was filtered through a plug of silica to remove the physical contaminants as well as the positively charged **64** and the crude product crystallised to give **65** in an average yield of 47% (Scheme 4.5).

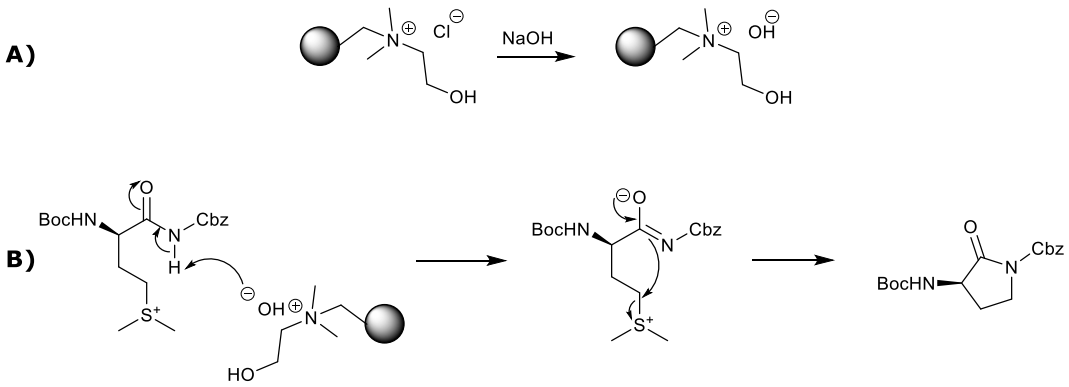

Scheme 4.5. Functionalisation of Amberlite IRA 410 (A) and proposed mechanism of cyclisation of **64** using hydroxyl functionalised Amberlite IRA 410 (B).

The reaction mechanism was postulated to be a deprotonation of the amide by the functionalised resin to form an iminolate, allowing the double bond present on the nitrogen to attack the gamma carbon, releasing dimethyl sulphide. The positive charge on the sulfur makes this reaction possible. The positively charged starting material to the relatively hydrophobic product, makes the reaction easy to monitor by HPLC, as well as the distinctive odour of the by-product (Figure 4.3).

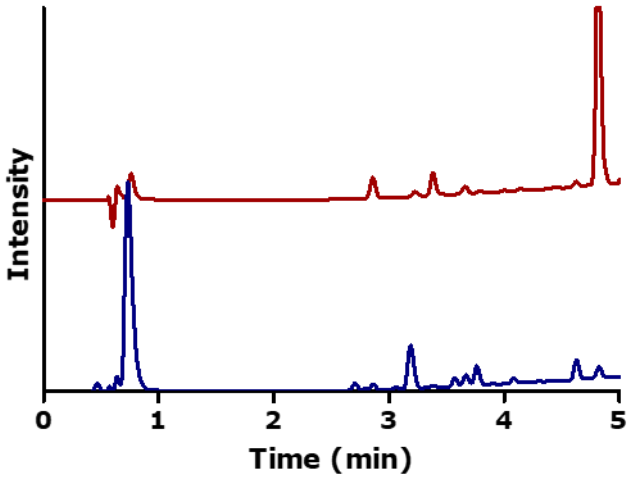

Figure 4.3. HPLC traces showing the conversion of **64** (blue trace, t_R = 0.73 min) to **65** (red trace, t_R = 4.82 min), using the wavelength 254 nm.

Functionalisation of pyrrolidone **65** was carried out in preparation for the synthesis of the bicycle system in **58** (Figure 4.2).

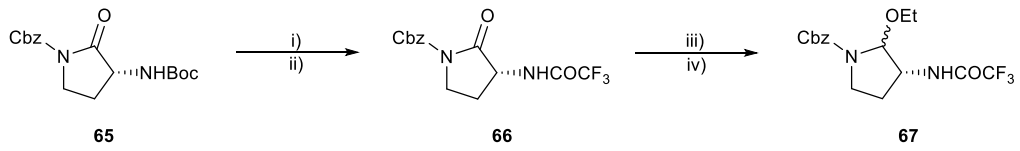

65 **66** **67**

Scheme 4.6. Synthesis of **67** from **65**. Reaction conditions: i) 4 M HCl, dioxane, 2.5 h; ii) *N*-methyl morpholine, methyl trifluoroacetate, DCM, MeOH, 18 h, 51% over steps i & ii; iii) $LiBH_4$, THF, -35 °C, 3.5 h; iv) EtOH, H_2SO_4, -20 °C to rt, 3.5 h, crude 94% over steps iii & iv.

Thus, the acid labile Boc protecting group was replaced with a trifluoroacetamide group by a two-step procedure: deprotection of the Boc group using HCl in dioxane, followed by reaction with methyl trifluoroacetate under basic conditions leading to the trifluoroacetamide **66** in moderate yield (51%) (Scheme 4.6). The trifluoroacetamide protecting group enables the amino group to be protected against the acidic conditions in the subsequent reactions.

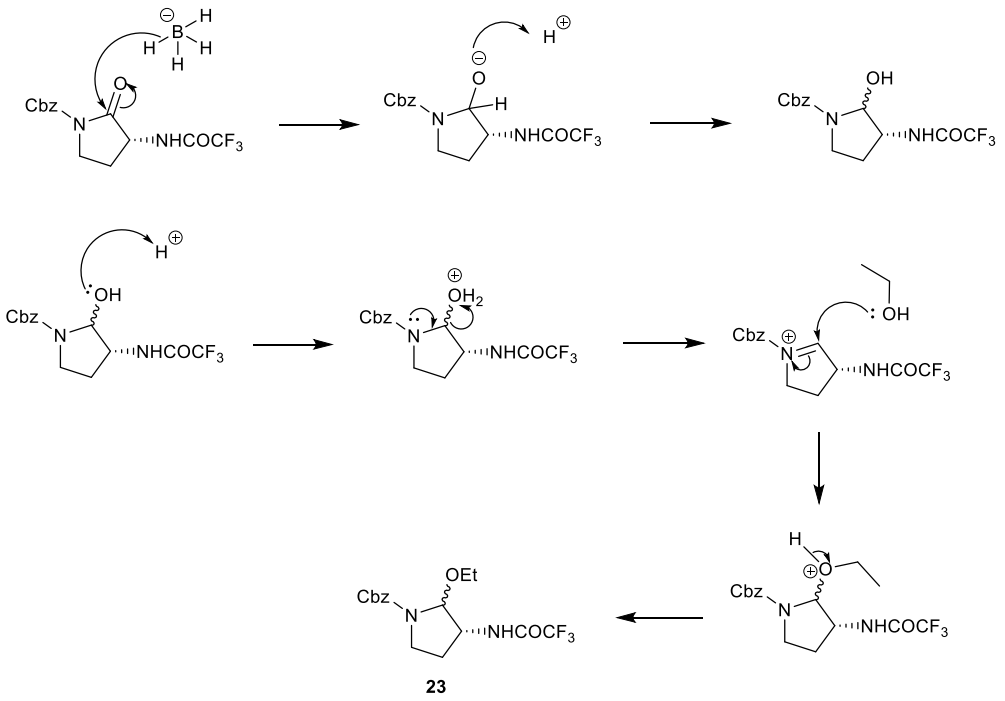

Scheme 4.7. Proposed mechanism for the formation of **67** from **66**.

Reductive etherification of **66** was achieved by reduction of the carbonyl with lithium borohydride and etherification with ethanol under strongly acidic conditions (Scheme 4.8).

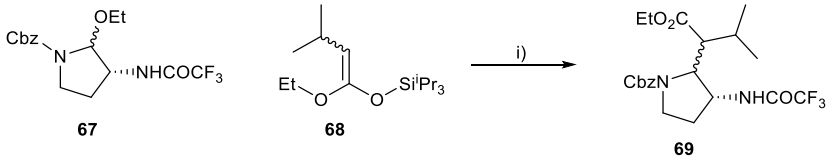

Scheme 4.8. Reaction scheme for the alkylation of **67**. Reaction conditions: i) $BF_3{\cdot}OEt_2$, DCM, -20 °C to rt, 1.5 h, carried forward without purification.

However, the following step involved the addition of another compound with a stereocentre, so separation of the two diastereomers was unnecessary. The synthesis of ketene acetal **68** was required before the reaction could be executed (Scheme 4.9).

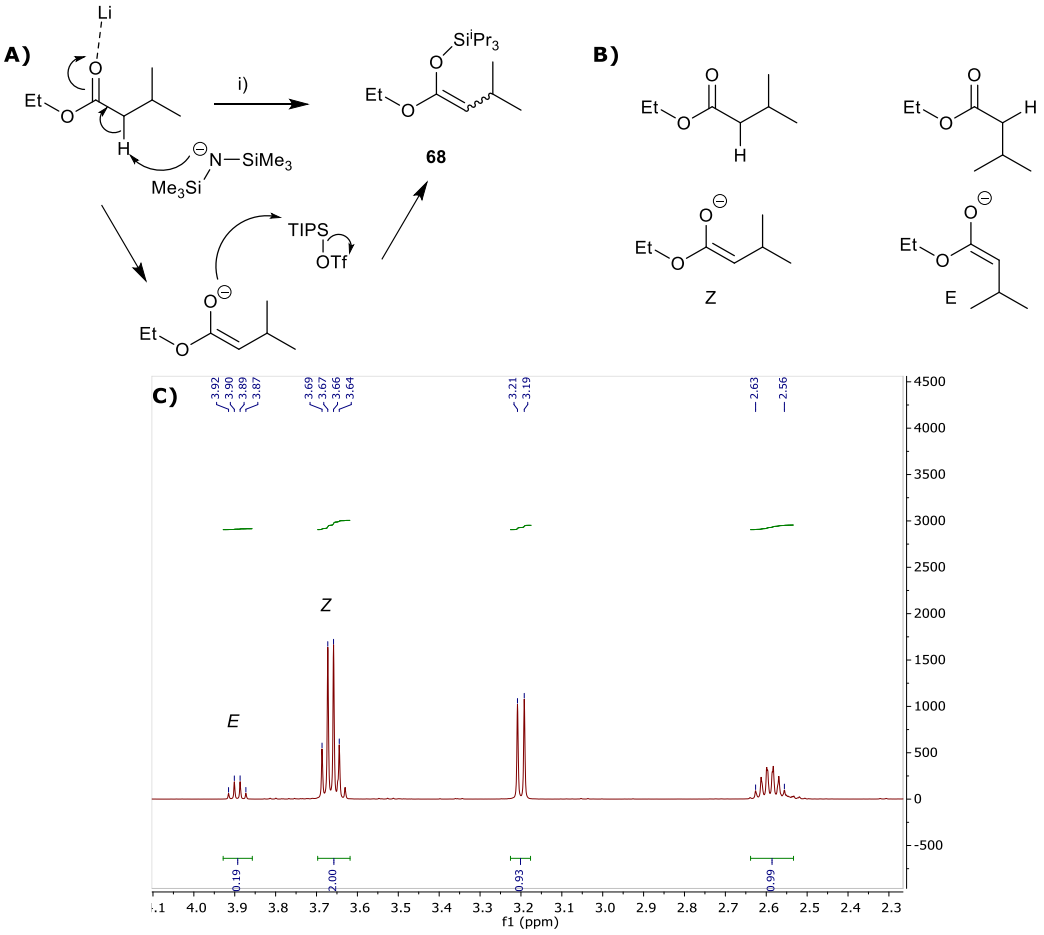

Scheme 4.9. A) Proposed mechanism of synthesis for the generation of ketene acetal **68**; Reaction conditions: i) LiHMDS, THF/DMPU, 1 h, -78 °C, then TIPS-OTf, 2 h, 10%. B) two conformers of ethyl isovalerate that can be deprotonated to form either *Z* or *E* isomer; C) ^{1}H NMR spectrum showing the ratio of *Z* and *E* isomers.

The reaction involved the deprotonation of ethyl isovalerate by lithium bis(trimethylsilyl)amide (LiHMDS), resulting in the formation of an enolate (Scheme 4.9). The enolate was then reacted with triisopropylsilyl triflate, the triflate acting as a good leaving group. Due to the rotation present in ethyl isolvalerate, deprotonation of the alpha proton can generate two products: *E* and *Z* (Scheme 4.9). The ratio of the two compounds was determined to be 91:9 *Z*/*E* through ^{1}H NMR, by the CH_2 of the ethyl group (Scheme 4.9, C). The crude product was purified using vacuum distillation to separate the starting

material from the product. This proved challenging due to their similar properties and boiling points, and the acetal proved too labile to use other methods of purification. After the majority of the starting material was removed, the ketene acetal was then reacted with ethyl ether **67** in a large excess (5 equivalents) (Scheme 4.10).

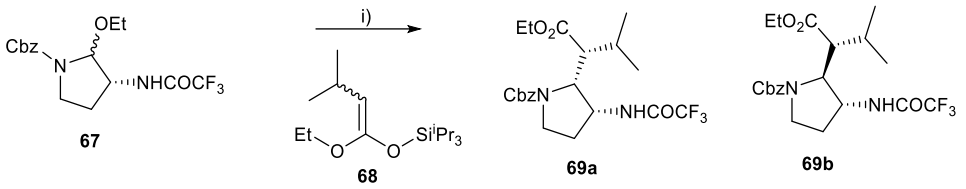

Scheme 4.10. Reaction of **67** to **69**. Reaction conditions: i) $BF_3{\cdot}OEt_2$, DCM, -20 °C to rt, 1.5 h, carried forward without purification.

The successive step was to alkylate ethyl ether **67** with the ketene acetal **68** in the presence of the Lewis acid boron trifluoride etherate (Scheme 4.11). The boron trifluoride complexes with the ethyl ether and the pyrrolidine forms an iminium species. This can then react with the ketene acetal, giving a mixture of isomers.

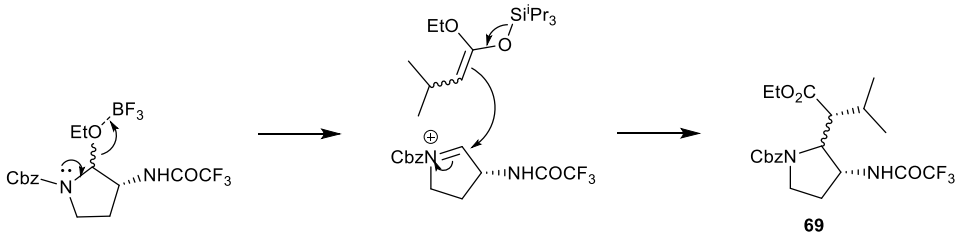

Scheme 4.11. Proposed mechanism of the formation of **69**.

After generating **69**, removal of the trifluoroamido protecting group was required before the second cyclisation step can occur (Scheme 4.12). This was achieved by refluxing compound **69** with K_2CO_3 in a mixture of ethanol and water for 4 hours, monitoring the presence of starting material by HPLC. The amine **70** was dried *in vacuo* to ensure there was no residual water present before the next step.

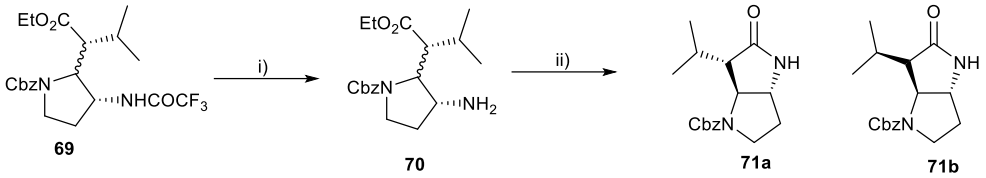

69 70 71a 71b

Scheme 4.12. Deprotection of the amine and lactamisation of **70** to generate **71**; Reaction conditions: i) K_2CO_3, EtOH/H_2O, reflux, 4 h, carried forward without purification; ii) THF: TMEDA 1:1, *tert*-BuMgCl, 0 °C, 2 h, 30% of **71a**, after purification.

The lactamisation of compound **70** was achieved using a mixture of anhydrous TMEDA and THF to dissolve the amine, before the addition of *tert*-butyl magnesium chloride at 0 °C. The Grignard agent ^{t}BuMgCl was used as a base here, and there is the possibility that one of the protons from the amine group is removed, generating a strong nucleophile, enabling it to attack the ester.

The requirement of the TMEDA was elucidated by MacDonald, with the hypothesis that it chelated the by-product MgO, which was found to react with the cyclised product **71a**, lowering the yield and affecting the diastereomer ratio. Upon completion of the reaction, the diastereomers were separated by column chromatography, and the isolation of the intended isomer elucidated through the combination of ^{1}H NMR and X-ray crystallography (Figure 4.4).

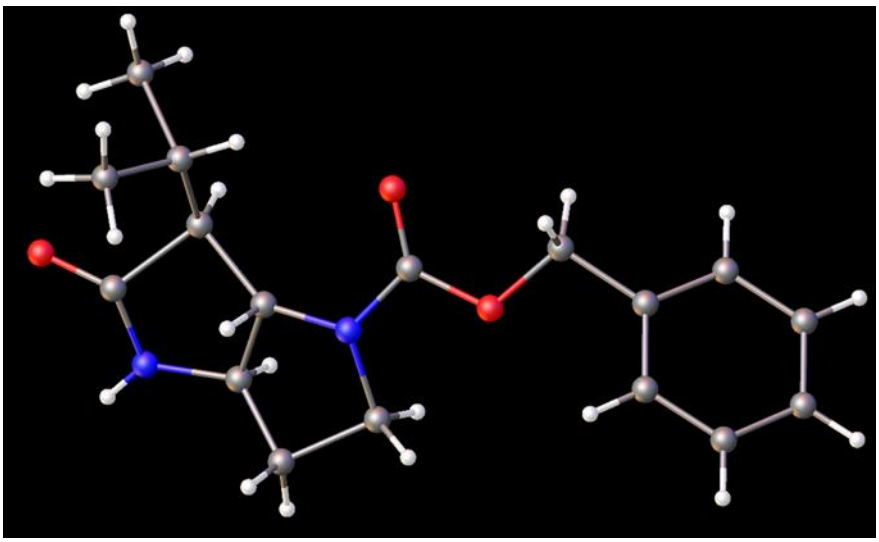

Figure 4.4. X-ray crystallography image of **71a**, confirming the correct diastereomer was isolated.

After successfully cyclising and purifying the bicyclic lactam, the next step was to sulfonate the amide (Scheme 4.13).

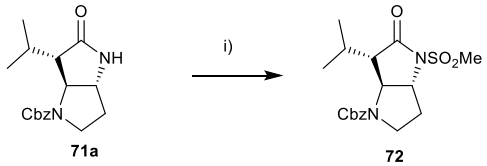

Scheme 4.13. The generation of the sulphonamide **72**. Reaction conditions: THF, LiHMDS, -78 °C, 1 h, then $MeSO_2Cl$, 1 h, 50%.

This reaction was achieved by deprotonation of the amide using LiHMDS under anhydrous conditions and reacting it with methanesulfonyl chloride, whereby the sulfonyl group is attacked by the deprotonated amide with subsequent elimination of the chloride. The reaction was difficult to force to completion but purified by flash chromatography, with the remaining starting material recovered and reused.

The final step before conjugation of the warhead to the hydrophilic tail involved removal of the remaining protecting group, the carboxybenzyl group (Scheme 4.14). This was achieved in high yields by hydrogenation in the

presence of the catalyst palladium hydroxide on carbon. The reaction required 2 hours for a quantitative conversion and required no further purification.

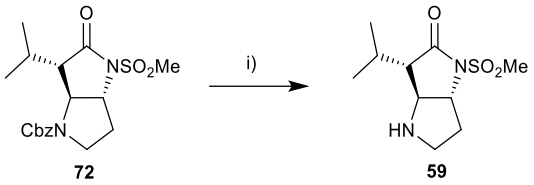

72 59

Scheme 4.14. Removal of the Cbz protecting group to generate amine **59**. Reaction conditions: i) $Pd(OH)_2/C$, H_2, 3 h, quant.

4.4 Preparation of the hydrophilic component of GSK inhibitor

In addition to the warhead which directly binds to the enzyme active site, the GSK inhibitor also comprises of a 'tail': a longer hydrophilic moiety which has secondary interactions with the tunnel leading to the active site. The original design required a slight modification to contain a suitable functional group for conjugation to the dye (Figure 4.6).

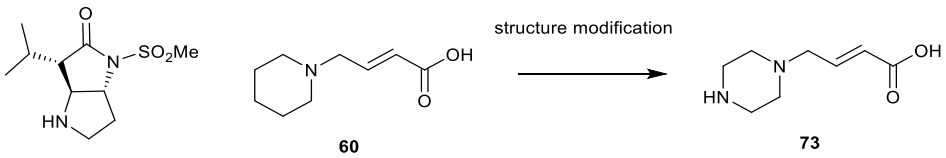

60 73

Figure 4.5. The structure modification of the original tail **60** to **73**, to incorporate an amine group suitable for the addition of a fluorophore.

The addition of the piperazine rather than a piperidine to **73** would give rise to a secondary amine that could react with a carboxyl functionalised fluorophore. The synthetic pathway to **73** was like that of **60**, except that it required an additional protecting group on the secondary amine and an additional deprotection step (Scheme 4.15).

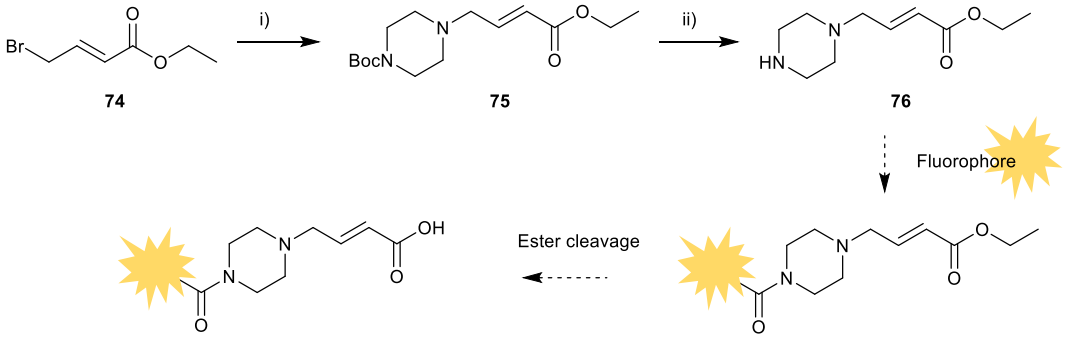

Scheme 4.15. Synthesis of the piperazine modified tail in solution. Reaction conditions: i) *N*-Boc piperazine, K_2CO_3, MeCN 63%; ii) 4 M HCl/dioxane & EtOH, reflux, 3 h, quant.

The ester ethyl-4-bromocrotonate underwent an S_N2 reaction with mono *N*-Boc protected piperazine to form the intermediate **75** in a 63% yield. The Boc group was selectively cleaved through acidic hydrolysis in the solvent system ethanol and dioxane. The subsequent step was to react **76** with a fluorophore and its activated carboxylic acid group. Although the synthetic route was straightforward, the handling of **76** proved challenging. Several reactions were attempted to complete the final conjugation to the dye, but all were met with little to no reaction (Table 4.1). The activating agents were altered, in addition to the quantity of the base, and the dye as it was assumed the accessibility of the carboxyl group interfered with the reaction. All the alterations gave no noticeable effect to increasing reaction yield.

Table 4.1. Reaction conditions investigated for the addition of a fluorophore to **76**. * = Visible on HPLC chromatogram.

Reaction conditions	Fluorophore	Product
DIPEA	**25**	No
TEA	BODIPY-NHS	No
HSPyU, DIPEA	Cy5 **27**	<5%*
Oxyma, DIC	Cy5 **27**	No
PyBrOP, DIPEA	Cy5** **34**	No

To circumvent the use of **76**, the problem was approached in a different manner (Scheme 4.16). The need for a terminal carboxylic acid meant it was possible to use solid phase synthesis as a method of solving the handling issues associated with the hydrophilicity of the compound. An additional benefit of using this technique would be lack of protecting groups, as the Boc group on the piperazine would no longer be necessary. The use of solid phase synthesis is also advantageous for modifying the tail structure, as it would be possible to modify the reaction by simply adding a different fluorophore or an extended spacer.

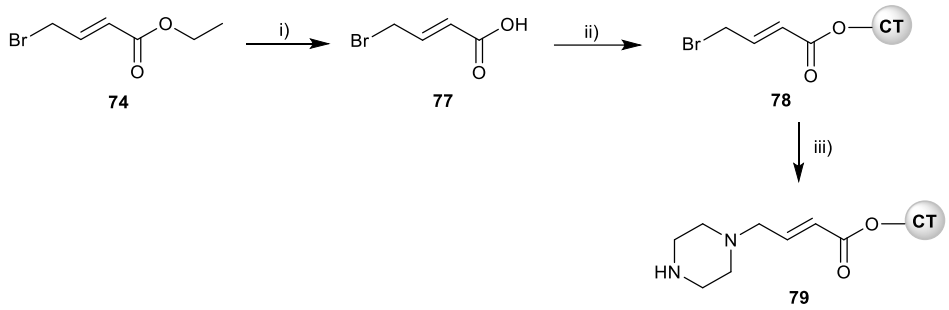

Scheme 4.16. The solid-phase approach to synthesis of tail **79**. Reaction conditions: i) $Ca(OH)_2$, $EtOH/H_2O$ (1:1), 18 h, 35%; ii) 2-chlorotrityl polystyrene resin, $SOCl_2$, DCM, 1 h, then **77** (625 mM), DMF, 2 h; iii) piperazine, DMF, DIPEA, 2 h, carried forward without purification. CT = 2-chlorotrityl polystyrene resin.

To generate the tail, the carboxylic acid of **74** was first unmasked using calcium hydroxide in a mixture of water and ethanol (Scheme 4.14). This was a poor yielding reaction, but it produced enough material for the subsequent reaction. The polystyrene 2-chlorotrityl resin was first activated using thionyl chloride under anhydrous conditions. The acid was dissolved in the minimum amount of DMF required and added to the resin at a concentration of 625 mM, to give as a high a loading onto the resin as possible. The resin then was swelled with DCM and a solution of piperazine in DMF was added. The reaction was monitored using the chloranil test instead of the traditional

Kaiser test as it had to highlight the presence of a secondary amine on the resin, instead of a primary.[114] Confirmation of reaction was achieved by a test cleavage of the compound from the resin and HPLC analysis (Figure. 4.6).

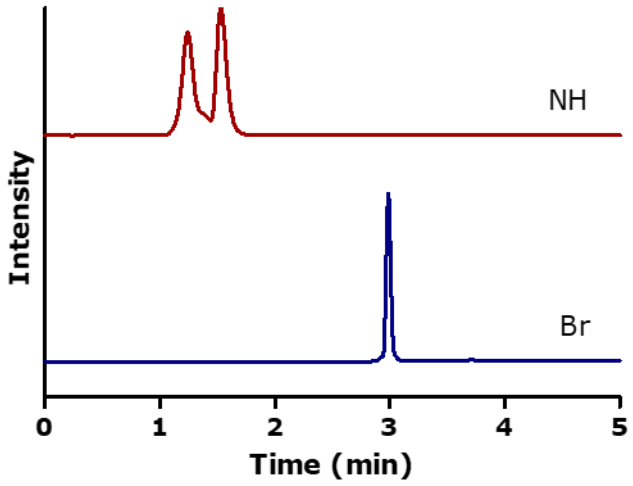

Figure 4.6. HPLC traces monitoring the formation of the hydrophilic tail on resin. Bottom trace is a test cleave of the bromo crotonate **78** (blue, t_R = 2.98 min) and top chromatogram is the piperazine modified crotonate, **79** (red, t_R = 1.51 min). All traces were analysed in the ELSD channel.

4.4.1 Addition of the fluorophore to the tail

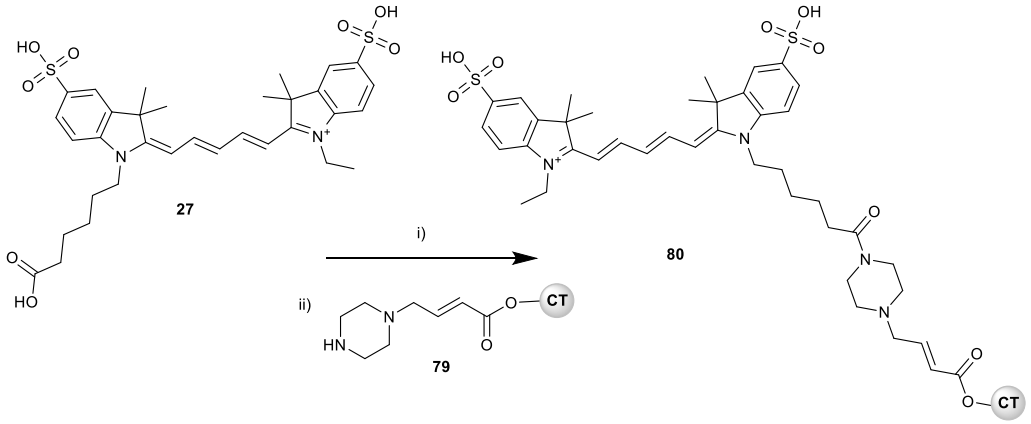

Scheme 4.17. Solid-phase synthesis of the tail **80**. Reaction conditions: i) HSPyU, DIPEA, DMF, 3 h; ii) **79**, DIPEA, 18 h, 8% after purification (assuming >90% loading onto resin). Cleavage from the linker was achieved with 20% HFIP in DCM.

To complete the synthesis of the tail, Cy5 dye **27** was activated using HSPyU and DIPEA, with active ester formation confirmed through HPLC analysis (Scheme 4.17). The activation of the carboxyl group was quantitative, but subsequent conjugation of the activated dye to the piperazine was poor yielding, regardless of the ratio/concentration of starting materials used.

The test cleavages showed both starting material and product, but longer reaction times did not lead to full conversion. The crude product was removed from the resin using the cleavage cocktail of 20% HFIP in DCM. Product **80** was then isolated using reverse phase semi-preparative HPLC (Figure 4.7).

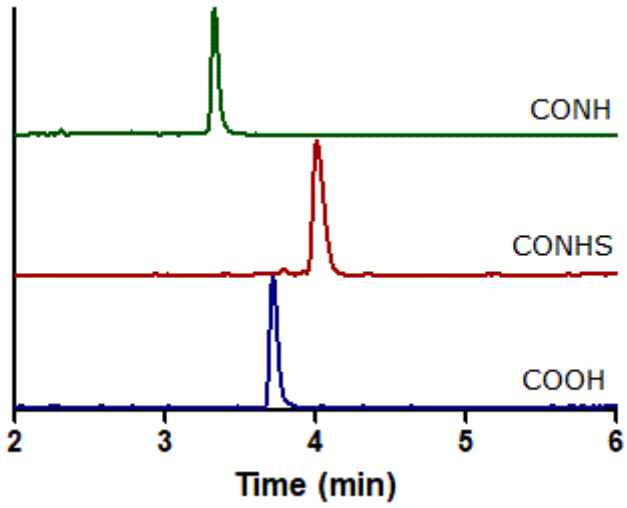

Figure 4.7. HPLC traces monitoring the activation of the carboxylic acid on Cy5 dye **27** (blue trace, t_R = 3.71 min) to an active ester (red trace, t_R = 4.01 min), and after the reaction with the piperazinyl moiety to form the amide **80** (green trace, t_R = 3.16 min). Data was normalised to 1, and the reaction monitored on the ELSD channel.

4.4.2 Generation of the far-red elastase specific optical probe

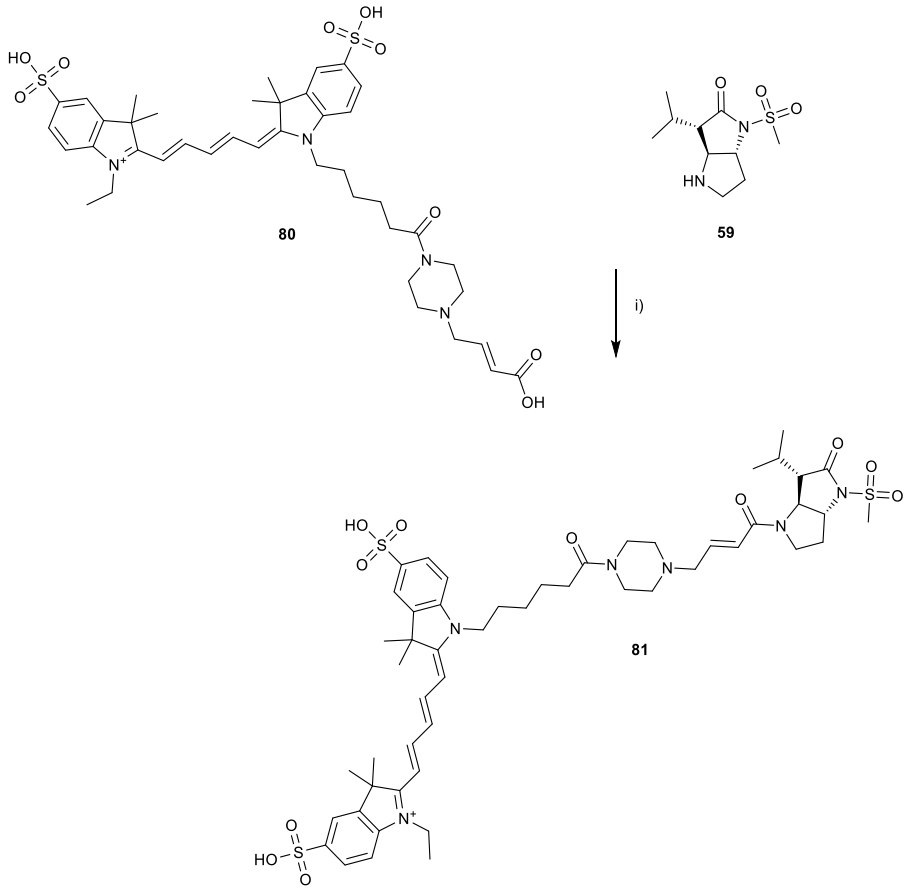

Scheme 4.18. The final reaction for the generation of optical probe **81**. Reaction conditions: i) EDC.HCl, HOBt, MeCN, DMF, 18 h, 10% after purification.

Conjugation of the tail to the warhead was achieved using EDC (*N*-(3-dimethylaminopropyl)-*N*′-ethylcarbodiimide) and HOBt (hydroxy benzotriazole) as coupling reagents (Scheme 4.18). Thus, activation of the carboxylic acid via an *O*-acylurea intermediate was followed by subsequent attack by HOBt to generate the HOBt ester which reacted with the amine to generate the desired amide (Scheme 4.19).

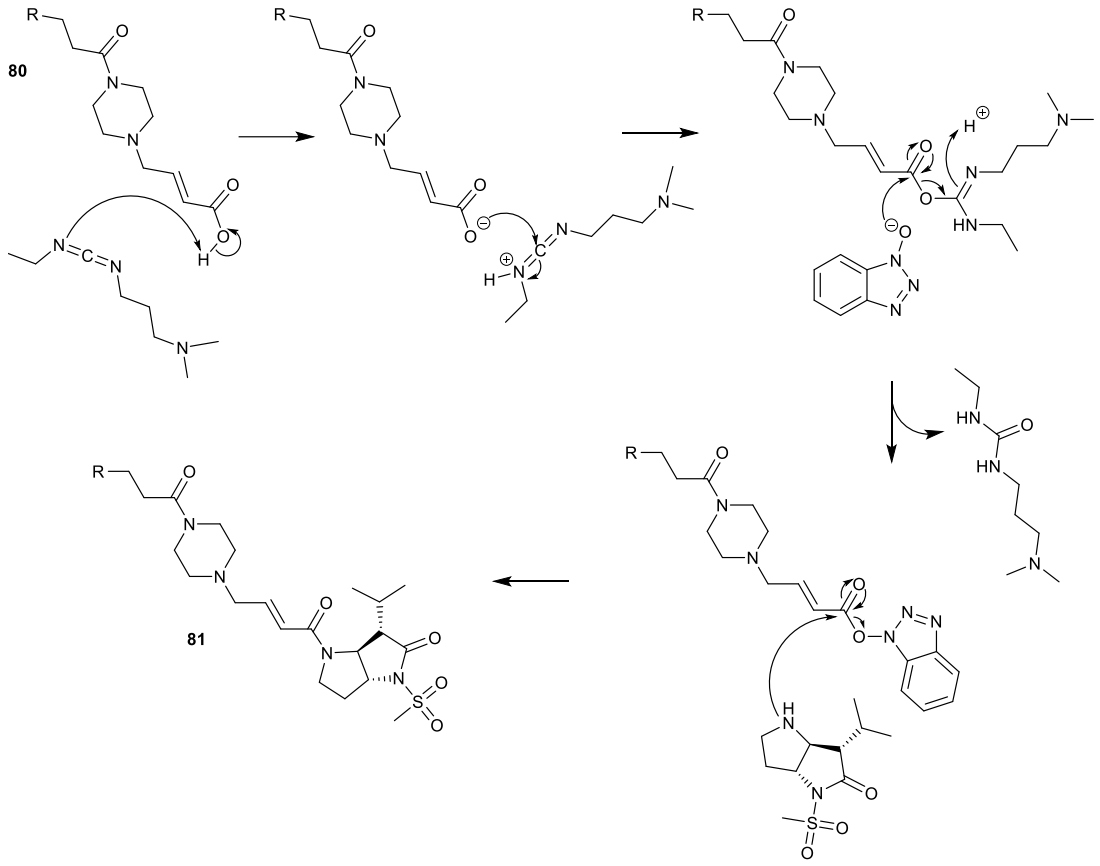

Scheme 4.19. Proposed mechanism of carboxylic acid activation using HOBt and EDC.HCl, before amidation.

The hydrophilicity of the final compound meant it required purification using reverse phase semi-preparative HPLC, with probe formation confirmed through mass spectrometry. The overall yield of the reaction was poor, with a final mass of 1.2 mg and 10% yield, however this was sufficient for further biological evaluation. Probe **81** was analysed to determine its excitation and emission spectra (Figure 4.9).

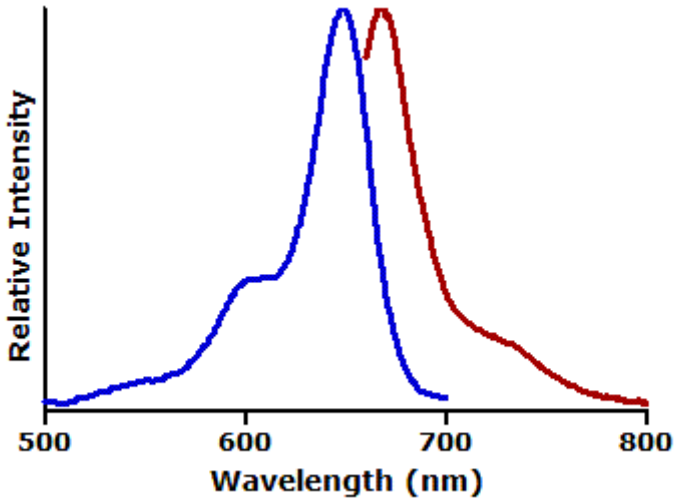

Figure 4.9. Absorption (blue, λ_{Ex} = 648 nm) and emission (red, λ_{Em} = 666 nm) spectra of **81** in PBS, normalised to 1 (emission spectrum observed after excitation at 630 nm).

4.5 Biological evaluation of far-red optical probe 81

The optical probe **81**, after purification, was then investigated for its suitability in a biological setting. This involved determining the toxicity towards mammalian erythrocytes, the K_i when incubated with HNE and *in vitro* live cell imaging of neutrophils.

4.5.1 K_i determination for the optical probes

The inhibitor **58** was investigated by McDonald and was determined to have a K_i of 0.31 nM.[113] The far-red probe **81** was investigated in a similar manner to determine how the K_i had changed through the addition of the dye. This was achieved by using the substrate for the enzyme MeOSuc-Ala-Ala-Pro-Val-pNA. A serial dilution of the probe from 500 nM to 7.8 nM and then added to the enzyme and cleavage of the peptide was monitored by absorbance. For

each inhibitor concentration, the progress curve was transformed into k_{obs} and plotted against the concentration (Figure 4.10).

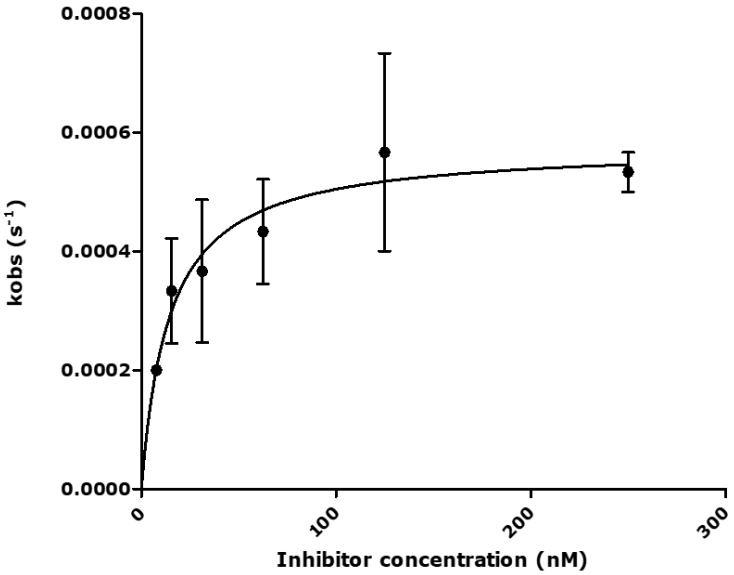

Figure 4.10. Graph of k_{obs} against concentration of optical probe **81**, for the determination of K_i (extrapolated as the Km of the line of best fit), n=3.

The K_i, the Km of the line of best fit, which was found to be 37 nM, a hundred-fold higher than that of its parent molecule **58**, but it had still retained efficiency. The error bars present in Figure 4.10 highlights the variety in results k_{obs} varied throughout the concentrations, and so more experiments should be done to achieve a more reliable value.

4.5.2 Toxicity of optical probes

With the aim of using the optical probe *in vivo*, toxicity of the compound had to be taken into consideration. Probe **81** was incubated with human erythrocytes, as a haemolysis assay gave a more realistic idea of toxicity in the area of interest over other, more frequently used assays. The assay involved an hour incubation of the probes with isolated erythrocytes at 37 °C. The assay involved removing any whole cells left through centrifugation and absorbance

of the supernatant was analysed to identify how much porphyrin was released through lysis of the cells, in comparison to a calibration curve.

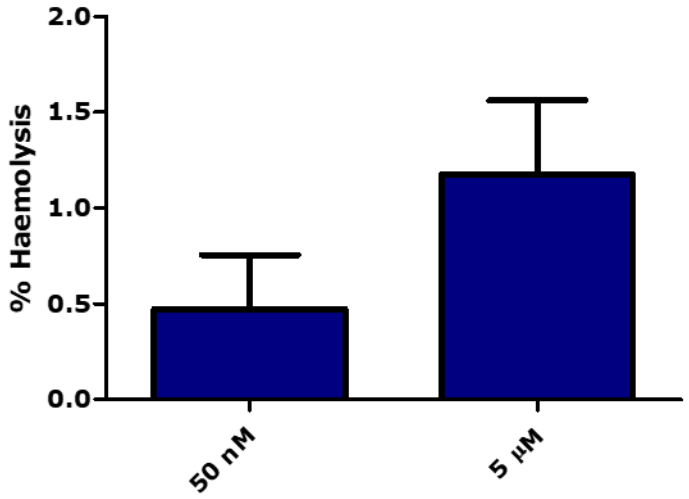

Figure 4.11. Haemolysis assay of the optical probe **81** at two different concentrations, with the data compared to control haemolysis, n=3.

The data interpretation highlights that even at ten-fold concentration required for imaging has an average toxicity of 1.2%, and a toxicity of 0.5% at a ten-fold less concentration required for confocal imaging. This demonstrated minimal toxicity of **81**, particularly at the concentrations required for imaging, which is beneficial for the end use of *in vivo* imaging.

4.5.3 Scanning confocal microscopy of optical probe **81**

Due to the nature of the compound, the imaging agent had to confirm that it was possible to use it as an optical imaging agent. Neutrophils were isolated from whole human blood and activated using a calcium ionophore (1 μM) for two minutes before adding probe **81** and Neutrophil Activated Probe, or NAP (Figure 1.19, **20**). NAP is a peptide based optical probe that was developed previously in the research group, which is a tri-branched peptide containing self-quenched fluorescein. Upon addition to HNE, the enzyme cleaves the

peptide chain, releasing the fluorescein from the self-quenching mechanism. Figure 4.12 shows the overlap of both HNE targeting probes, confirming qualitatively that **81** can label HNE expression from neutrophils.

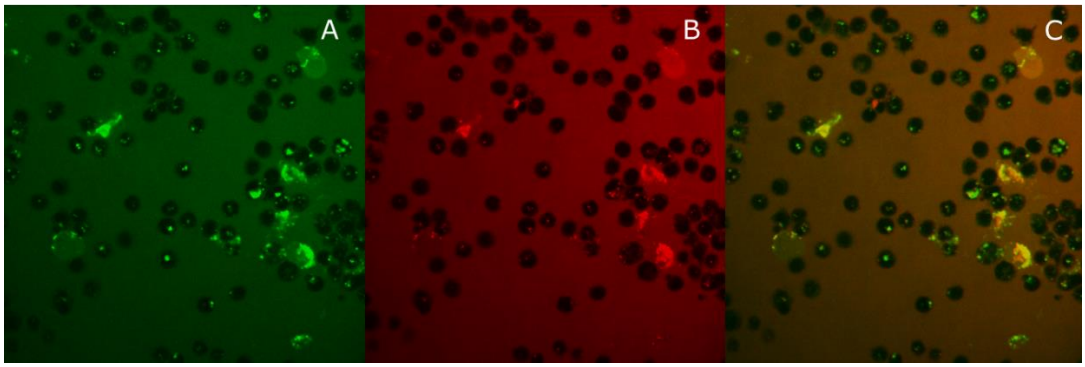

Figure 4.12. Live confocal imaging of human neutrophils activated by calcium ionophore (1 μM, 5 min) with the optical probe **81** and HNE specific in-house probe, NAP **20** (green). Image (A) was NAP (2 μM, 10 min incubation), (B) was stained with **81** (2 μM, 10 min incubation), and (C) is a merged overlay of both A and B.[‡]

4.6 Conclusions

HNE inhibitors with high water solubility are ideal to microdose in the lung (through a bronchoscope) to identify potential inflammatory sites, or to aid in rapid diagnosis of pulmonary diseases. The GSK drug for COPD, **58**, has proven to be a highly designed compound for the active site of the enzyme HNE. This has been successfully manipulated to include a secondary amine and to it, a far-red dye has been added. This created a highly specific, always-on, optical probe to detect HNE at physiological levels.

The Ki was determined to be only slightly affected by the addition of the with a small reduction in efficacy, as **58** had a Ki of 0.31 nM and the Ki of the far-

[‡] Images taken by Thane Campbell

red optical probe **81** was determined to be 37 nM. The far-red probe was shown to be non-toxic towards erythrocytes, as well as neutrophils. It was possible to image neutrophils *in vitro* using confocal microscopy.

Chapter 5 Experimental

5.1 General remarks

Chemicals were purchased from Sigma Aldrich, Honeywell, Merck, Acros, VWR International, TCI Chemicals, or Fischer Scientific and used without further purification. All experiments that required an oxygen free environment were carried out using Schlenk techniques unless otherwise stated. Solvent removal was carried out at a reduced pressure on a Büchi rotary evaporator, or overnight in a Heraeus vacuum oven at 40 °C.

All melting points were obtained using a SMP10 melting point apparatus from Bibby Scientific Ltd. Infrared spectra were obtained using a Bruker FT-IR Tensor 27. All ^{1}H and ^{13}C NMR spectra reported were carried out at 297 K (unless otherwise stated) in deuterated solvents (D_2O, $CDCl_3$, DMSO or MeOD) and recorded using a Bruker AVA 500 or a Bruker AVA 600 (500 and 126 MHz; 600 and 150 MHz), and all coupling constants are reported in Hz. The ^{1}H spectra are characterised as singlet (s), broad singlet (br s), doublet (d), doublet of doublet (dd), triplet (t), quartet (q) or multiplet (m). Analytical TLC was carried out using Merck aluminium backed silica gel plates (F_{254}), reverse phase TLC using Macherey Nagel RP-18 ALUGRAM (UV_{254}) sheets, both visualised using a Mineralight UV lamp with illumination at wavelengths of 254 and 365 nm. Chromatography purification was carried out using silica gel (60–120 mesh). Reverse phase chromatography was on a Biotage Isolera using SNAP Ultra C18 columns (12 g, 30 g). Microwave assisted reactions were executed using a Biotage Initiator, irradiating at 2.5 GHz, with temperature control.

Low resolution mass spectrometry data was obtained using an Agilent 6130 Quadrupole LC-MS system, and high-resolution mass spectrometry determined on a Bruker 3.0T Apex Spectrometer.

Reverse-phase preparative HPLC was achieved using an Agilent 1260 Series ChemStation and on an Eclipse XDB C-18 column (5 μm, 9.4 × 250 mm), or Kinetex 5 μm XB-C18 100A (150 × 21.2 mm). The solvents used were MeCN + 0.1% FA and H_2O + 0.1% formic acid, initially 5% MeCN and increased by 1% per minute for 20 mins. The procedure had a flow rate of 2 mL/min and UV detection at 254 nm. Analytical HPLC was achieved using an Agilent 1100 Series ChemStation and on an Eclipse C-18 column (5 μm, 9.4 × 150 mm). Solvents used for Method A were MeCN + 0.1% formic acid and H_2O + 0.1% formic acid, with an initial gradient of 5% MeCN, increasing by 15% per minute for 6 min, maintained at 95% MeCN for 3 min. The procedure had a flow rate of 1 mL/min and the traces stated are from an ELSD unless otherwise stated. Absorbance and fluorescence spectra were obtained using either a Fluoromax spectrophotometer, or a Synergy Biotek plate reader and analysed using the Gen5 software.

Enzymatic assays were carried out on a Synergy Biotek plate reader. Gel electrophoresis was carried out on a buffered gel system using a Bio-Rad PowerPac 300 power supply and analysed on a Bio-Rad Gel Doc XR+ system. Flow cytometry was achieved using a 5L LSR Fortessa and the data analysed using FlowJo software (version 7.2.4). Live cell imaging used a Leica SP8 confocal microscope or an Andor spinning disc microscope, using the laser lines: 405 nm, 488 nm and 630 nm.

5.2 Synthesis of molecules

5- and 6-Carboxyfluorescein diacetate *N*-hydroxysuccinimide ester (25 and 26)

5(6)-Carboxyfluorescein (15.0 g, 40 mmol) was added to acetic anhydride (180 mL, 1.9 mol) and pyridine (18 mL) and was heated to reflux (120 °C) for 1 h. The conversion was confirmed by HPLC analysis (t_R = 4.85 min, ELSD). The solvent was removed *in vacuo* and the crude product was redissolved in EtOAc (150 mL) before being washed with $KHSO_4$ (1 M, 2 × 100 mL) and brine (100 mL). The organic layer was collected and dried with $MgSO_4$ and the solvent removed *in vacuo*, with the crude product 5(6)-carboxyfluorescein diacetate used without further purification in the subsequent reaction.

5(6)-Carboxyfluorescein diacetate (40 mmol) and *N*-hydroxsuccinimide (5.50 g, 47.9 mmol) was added to DCM (100 mL) and left to stir until dissolved. To the solution DIC (7.4 mL, 47.9 mmol) was slowly added and the reaction was left to stir for 0.5 h. After confirmation of reaction by TLC, it was washed with H_2O (100 mL), brine (100 mL) and dried using $MgSO_4$. DCM was removed *in vacuo*. The crude product was purified using a silica column with isocratic solvent system of EtOAc/toluene (2:8) to afford 5-carboxyfluorescein diacetate *N*-hydroxysuccinimde ester **25** (36%) and 6-carboxyfluorescein diacetate *N*-hydroxysuccinimde ester **26** (24%) as colourless solids.[87]

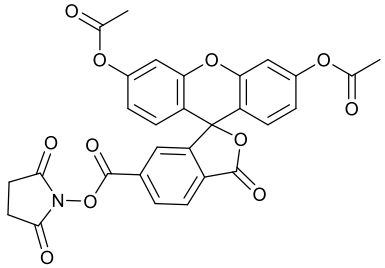

5-Carboxyfluorescein diacetate *N*-hydroxysuccinimide ester (25)

Colourless solid, yield: 8.67 g (36%); **^{1}H NMR** δ (500 MHz, $CDCl_3$) 8.40 (dd, 1H, *J* = 8.1, 1.3 Hz, Ar*H*), 8.18 (dd, 1H, *J* = 8.0, 0.6 Hz, Ar*H*), 7.93 (dd, 1H, *J* = 1.3, 0.6 Hz, Ar*H*), 7.14 (d, 2H, *J* = 2.3 Hz, Ar*H*), 6.86 (dd, 2H, *J* = 2.3, 8.7 Hz, Ar*H*), 6.79 (d, 2H, *J* = 8.7 Hz, Ar*H*), 2.88 (br s, 4H, 2 × CH_2), 2.31 (s, 6H, 2 × CH_3); **^{13}C NMR** δ (126 MHz, $CDCl_3$) 168.78 (C=O × 2), 168.77 (C=O × 2), 167.54 (C=O), 160.63 (C=O), 153.10 (C), 152.56 (2 × C), 151.71 (2 × C), 132.26 (CH),

131.74 (C), 131.47 (C), 128.98 (2 × CH), 126.46 (CH), 126.03 (CH), 118.23 (2 × CH), 115.37 (2 × C), 110.81 (2 × CH), 82.45 (C), 25.77 (2 × CH_2), 21.27 (2 × CH_3); **Rf**: 0.53 (EtOAc:Toluene 50:50); **HPLC** (Method 1/ACN) $\mathbf{t_R}$ = 5.22 min, purity 100% (ELSD); **ESI-MS** (MeCN): ***m/z*** = 465.1 $[M+Na]^+$. Data in accordance with the literature.[87]

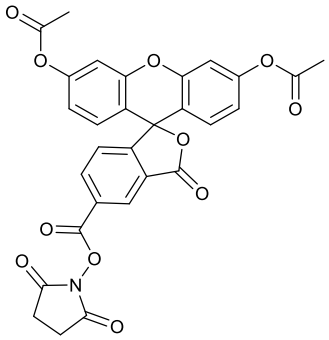

6-Carboxyfluorescein diacetate *N*-hydroxysuccinimide ester (26)

Colourless solid, yield: 4.67 g (24%); **^{1}H NMR** δ (500 MHz, $CDCl_3$) 8.81 (dd, 1H, *J* = 1.5, 0.7 Hz, Ar*H*), 8.41 (dd, 1H, *J* = 8.1, 1.6 Hz, Ar*H*), 7.36 (dd, 1H, *J* = 8.1, 0.7 Hz, Ar*H*), 7.13 (d, 2H, *J* = 2.2 Hz, Ar*H*), 6.85 (dd, 2H, *J* = 8.7, 2.3 Hz, Ar*H*), 6.80 (d, 2H, *J* = 8.7 Hz, Ar*H*), 2.93 (br s, 4H, 2 × CH_2), 2.31 (s, 6H, 2 × CH_3); **^{13}C NMR** δ (126 MHz, $CDCl_3$) 168.93 (C=O × 2), 168.84 (C=O × 2), 167.35 (C=O), 160.60 (C=O), 158.24 (C), 152.53 (2 × C), 151.58 (2 × C), 136.98 (CH), 128.95 (2 × CH), 128.12 (CH), 127.74 (C), 127.25 (C), 125.18 (CH), 118.20 (2 × CH), 115.31 (2 × C), 110.81 (2 × CH), 82.15 (C), 25.81 (2 × CH_2), 21.23 (2 × CH_3); **HPLC** (Method 1/ACN) $\mathbf{t_R}$ = 5.38 min, purity 100% (ELSD); **Rf**: 0.37 (EtOAc:Toluene 50:50); **ESI-MS** (MeCN): ***m/z*** = 465.3 $[M+Na]^+$. This is in accordance with the literature.[87]

2,3-Trimethyl-3*H*-indole-5-potassium sulfonate (28)

4-Hydrazinobenzenesulfonic acid (6.00 g, 0.032 mol) and 3-methyl-2-butanone (10.2 mL, 0.096 mol) were dissolved in acetic acid (30 mL) and the stirred solution refluxed for 3 hours. The solvent was removed under vacuum. The

residue was then dissolved in methanol (30 mL) and stirred in a saturated solution of KOH in 2-propanol (200 mL). The potassium salt was collected from the resulting solution by filtration.

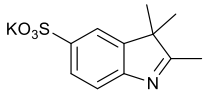

Pale orange solid, yield: 7.761 g, (78%). **IR** υ_{max} / cm^{-1}: 1574 (C=C str), 1265 (C-N_{ar} str), 1193 (S=O str); **^{1}H NMR** δ (500 MHz, MeOD) 8.12 (1H, d, *J* = 1.3 Hz, Ar*H*), 8.04 (1H, dd, *J* = 8.4, 1.6 Hz, Ar*H*), 7.89 (1H, d, *J* = 8.4 Hz, Ar*H*), 4.11 (3H, s, CH_3), 1.65 (6H, s, 2 × CH_3); **^{13}C NMR** δ (126 MHz, MeOD) 199.47 (C), 148.47 (C), 144.42 (C), 143.11 (C), 128.32 (CH), 122.08 (CH), 116.16 (CH), 56.00 (C), 35.47 (CH_3), 22.33 (2 × CH_3); **ESI-MS** (MeCN): *m/z* = 278.1 $[M-H]^+$. Data in accordance with the literature.[98]

1-Ethyl-2,3,3-trimethyl-5-sulfo-*3H*-indolinium (29)

Iodoethane (12 mL, 0.15 mol) and the sulfonated indole **28** (2.00 g, 0.18 mol) were added together, flushed with N_2 and were left to reflux for 48 h with the reaction monitored by HPLC. Upon completion, the reaction precipitate was filtered, washed with Et_2O (2 × 150 mL), and dried in a vacuum oven overnight to give the product as a purple solid (2.51 g, 98%).

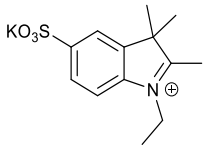

Pale solid, yield: 2.51 g (98%). **IR** υ_{max} / cm^{-1}: 1224 (C-N_{ar} str), 1185 (S=O str); **^{1}H NMR** δ (500 MHz, MeOD) 8.17 (1H, d, *J* = 1.2 Hz, Ar*H*), 8.09 (1H, dd, *J* = 8.4, 1.6 Hz, Ar*H*), 7.98 (1H, d, *J* = 8.4 Hz, Ar*H*), 4.62 (2H, q, *J* = 8.4 Hz, CH_2), 3.97 (1H, m, C*H*), 1.67 (6H, s, 2 × CH_3), 1.62 (3H, t, *J* = 7.4 Hz, CH_3); 1.19 (3H, s, CH_3); **^{13}C NMR** δ (126 MHz, MeOD) 199.32 (C), 148.58 (C), 143.58 (C), 143.11 (C), 128.47 (CH), 122.37 (CH), 116.41 (CH), 56.17 (C), 44.98 (CH_2), 25.25 (CH_3), 22.51

(2 × CH_3), 13.10 (CH_3); **ESI-MS** (MeCN): *m/z* = 306.1 $[M-H]^-$. Data in accordance with the literature.[99]

1-(5-Carboxypentyl)-2,3,3-trimethyl-5-sulfo-*3H*-indolium (30)

6-Bromohexanoic acid (1.0 g, 5.12 mmol) and the sulfonated indole **28** (1.2 g, 5 mmol) were added together and diluted in a mixture of MeCN and DMF (9:1, 20 mL) and heated in the microwave for 3 h to 120 °C, with the reaction monitored by HPLC. Upon completion, the reaction precipitate was filtered, washed with Et_2O (2 × 150 mL), and dried in a vacuum oven overnight to produce the product as a dark red solid (1.06 g, 60%).

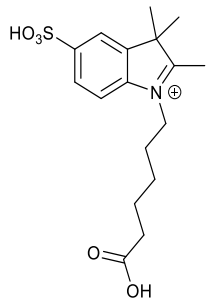

Dark red solid, yield: 1.06 g, (60%). **IR** υ_{max}/cm^{-1}: 2924 (O-H br, str), 1710 (C=O str), 1592 (C=C), 1161 (S=O str); **^{1}H NMR** δ (500 MHz, MeOD) 8.17 (d, *J* = 1.3 Hz, 1H, Ar*H*), 8.10 (1H, dd, *J* = 8.4, 1.6 Hz, Ar*H*), 7.96 (1H, d, *J* = 8.5 Hz, Ar*H*), 4.59 (2H, m, CH_2), 2.38 (2H, t, *J* = 7.2 Hz, CH_2), 2.02 (2H, m, 2H, CH_2), 1.74 (2H, m, CH_2), 1.67 (6H, s, 2 × CH_3), 1.58 (2H, m, CH_2), 1.54 (3H, s, CH_3); **^{13}C NMR** δ (126 MHz, MeOD) 198.31(C), 175.70 (C), 147.23 (C), 142.07 (C), 127.12 (CH), 120.98 (CH), 115.17 (CH), 54.82 (C), 47.88 (CH_2), 32.94 (CH_2), 27.05 (CH_2), 25.64 (CH_2), 23.98 (CH_2), 21.38 (CH_3), 21.24 (2 × CH_3); **ESI-MS** (MeCN): *m/z* = 354.1 $[M-H]^-$. Data in accordance with the literature.[98]

2-[5-[1-(5-Carboxypentyl)-1,3-dihydro-3,3-dimethyl-5-sulfo-2*H*-indol-2-ylidene]-1,3-pentadien-1-yl]-1-ethyl-3,3-dimethyl-5-sulfo-3*H*-Indolium (27)

29 (0.50 g, 1.87 mmol) and malonaldehyde dianilide hydrochloride (0.546 g, 2.11 mmol) were added together, diluted with a mixture of AcOH and acetic anhydride (1:1, 20 mL) and left to reflux for 4 h. The solvent was removed *in vacuo*, and the crude product was washed repeatedly with a mixture of Et_2O/EtOAc (1:1, 250 mL) until the filtrate turned colourless. The crude product was collected and dried in a vacuum oven at 40 °C for 18 h.

The dark brown product (0.491 g, 1.2 mmol) was added to **30** (0.416 g, 1.18 mmol) and a mixture of AcOH and acetic anhydride added (3:1, 8 mL). After the reactants had dissolved, NaOAc (0.377 g, 4.6 mmol) was added and the reaction was left to reflux for 4 h, with the reaction monitored by HPLC. The crude reaction mixture was added slowly to stirring Et_2O (150 mL), the dark blue precipitate collected by filtration and washed several times with Et_2O (3 x 100 mL). The crude product was dried and purified using reverse phase chromatography to yield **27** as a dark blue solid (0.49 g, 26%).

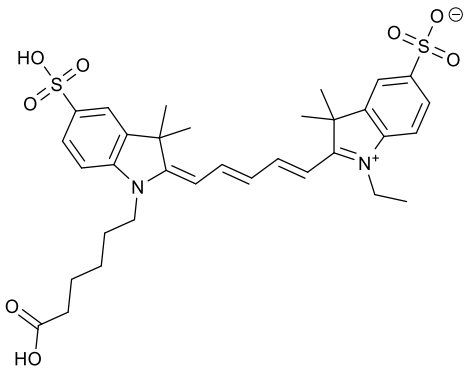

Dark blue solid, yield: 0.485 g, (26%); **IR** υ_{max}/cm^{-1}: 2928 (O-H, str), 1708 (C=O, str), 1326 (C-N_{ar}, str), 1216 (S=O, str); **^{1}H NMR** δ (500 MHz, D_2O) 8.05 (1H, dd, J = 12.9, 6.7 Hz, CH_{ar}), 8.03 (1H, dd, J = 13.1, 6.6 Hz, CH_{ar}), 7.88 (1H, d, J = 1.7 Hz, CH_{ar}), 7.86 (1H, d, J = 1.6 Hz, CH_{ar}), 7.84 (1H, dd, J = 8.4, 1.8 Hz, CH_{ar}), 7.81 (1H, dd, J = 8.7, 2.0 Hz, CH_{ar}), 7.36 (1H, d, J = 8.4 Hz, CH_{ar}), 7.32 (1H, d, J = 8.4 Hz, CH_{ar}), 6.55 (1H, t, J = 12.5 Hz, CH_{ar}), 6.28 (1H, d, J = 14.1 Hz, CH_{ar}), 6.22 (1H, d, J = 13.6 Hz, CH_{ar}), 4.11 (2H, q, J = 7.5 Hz, NCH_2), 4.06 (2H, t, J = 7.1 Hz, NCH_2), 2.38 (2H, t, J = 7.3 Hz, CH_2COOH), 1.86-1.80 (2H, m, CH_2), 1.67

(6H, s, 2 × CH_3), 1.67 (6H, s, 2 × CH_3), 1.67-1.63 (2H, m, CH_2), 1.46-1.40 (2H, m, CH_2), 1.36 (3H, t, *J* = 7.4 Hz, CH_2CH_3); **^{13}C NMR** δ (126 MHz, MeOD) 177.21 (C=O), 175.32 (C), 175.09 (C), 156.39 (CH), 156.21 (CH), 144.92 (C), 144.42 (C), 143.51 (C), 143.39 (C), 142.75 (C), 142.59 (C), 128.09 (CH), 128.06 (CH), 127.65 (CH), 121.42 (CH), 121.37 (CH), 111.62 (CH), 111.40 (CH), 105.17 (CH), 104.95 (CH), 50.65 (C), 50.59 (C), 45.07 (CH_2), 40.25 (CH_2), 34.58 (CH_2), 28.09 (CH_2), 27.83 (2 × CH_3), 27.72 (2 × CH_3), 27.30 (CH_2), 25.66 (CH_2), 12.50 (CH_3); **HPLC** (Method 1/MeCN) $\mathbf{t_R}$ = 3.67 min, purity 100% (ELSD); **ESI-MS** (MeCN): *m/z* = 657.3 $[M-H]^-$. Data in accordance with the literature.[99]

2,3-Dimethyl-5-sulfo-*3H*-indole-3-butanesulfonic acid (38)[98]

Sodium hydride (60% wt., 2.90 g, 72.8 mmol) was flushed with N_2, before DMF (40 mL) was added, the mixture was cooled to 0 °C and left to stir for 10 min. Ethyl 2-methylacetoacetate (9.80 mL, 69.3 mmol) was added slowly, maintaining the temperature, and the mixture was left until effervescence had halted. The reaction mixture was then heated to 60 °C for 3 h. 1,4-butane sultone (7.2 mL, 69.3 mmol) was added slowly, keeping the temperature at 30 °C. The mixture was then heated to 50 °C for 18 h. The solvent was removed *in vacuo*, the crude mixture re-dissolved in H_2O (50 mL) and washed with Et_2O (2 × 100 mL). The aqueous layer was isolated, transferred to a round bottom flask, and to it sodium hydroxide (3.56 g, 89.1 mmol) was added. The reaction was left at 90 °C for 18 h. The mixture was cooled to 30 °C and washed with hexane (2 × 30 mL). The aqueous phase was collected, cooled in an ice bath, and acidified to pH 2 using HCl. The solvent was removed *in vacuo*, and NaCl precipitated out. The residue was dissolved in MeOH (75 mL) and triturated for 10 min, before filtration to remove the salt. The methanolic solution was collected and the solvent was removed *in vacuo* to produce the crude product as a thick pale-yellow residue.

The yellow residue was dissolved in acetic acid (225 mL), flushed under N_2 atmosphere and to the mixture, 4-hydrazinobenzenesulfonic acid (13.0 g, 69.3 mmol) was added. The reaction was heated to 105 °C for 12 h. The solvent was removed *in vacuo* to approx. 30 mL, and to the crude mixture isopropanol (150 mL) was added, and left to stir at 60 °C for 2.5 h. The yellow precipitate was filtered off, washed with isopropanol (2 × 100 mL) and re-dissolved in a minimal amount of H_2O (20 mL). 2 M aq. soln NaOH (approx. 10 mL) was added to the solution until the pH = 8. The solution was lyophilised to give the product as a yellow solid (10.3 g, 41% in 94% purity).

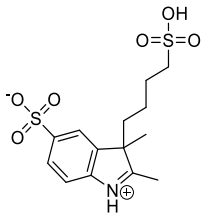

Yellow solid, yield: 10.3 g, (41%). **mp** > 250 °C; **IR** υ_{max} / cm^{-1}: 1384 (S=O, str), 1335 (C-N_{ar}, str); **^{1}H NMR** δ (500 MHz, DMSO) 7.55 (1H, d, *J* = 1.5 Hz, Ar*H*), 7.52 (1H, dd, *J* = 1.7, 7.9 Hz, Ar*H*), 7.31 (1H, d, *J* = 7.9 Hz, Ar*H*), 2.20 (2H, m, CH_2), 2.17 (3H, s, CH_3), 1.85 (1H, m, C(*H*)H), 1.74 (1H, m, C(H)*H*), 1.41 (2H, m, CH_2), 1.21 (3H, s, CH_3), 0.67 (1H, m, C(*H*)H), 0.48 (1H, m, C(H)*H*); **ESI-MS** (MeOH): *m/z* = 360.1[M-H]$^-$. Data in accordance with the literature.[98]

2,3-Dimethyl-5-sulfo-1,3-bis(4-sulfobutyl)-*3H*-indolinium (39)[98]

38 (0.50 g, 1.39 mmol) was loaded into a microvial and flushed with N_2 and *N*,*N*-dimethylacetamide (12 mL) was added. The mixture was heated to 150 °C, and after 10 min of trituration, 1,4-butane sultone (1.4 mL, 13.9 mmol) was added and the mixture was heated to 150 °C for 24 h. The reaction was cooled and filtered under N_2. The solid was refluxed in EtOAc (10 mL) for 2 h and filtered again. The remaining solid was dried in a vacuum oven at 40 °C overnight. The solid was then refluxed in MeOH (10 mL) for 10 min,

isopropanol was added and left to stir at 50 °C for 2 h before being filtered and washed thoroughly with isopropanol. The collected precipitate was left to dry in a vacuum oven overnight at 40 °C, to produce **39** (0.35 g, 51%) as a dark red solid.

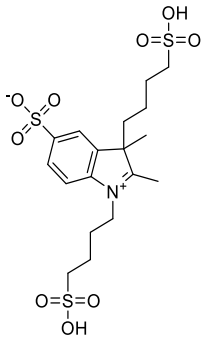

Dark red solid, yield: 0.35 g, (51%). **mp** 200 °C; **IR** υ_{max} / cm^{-1}: 1605 (C=C, str), 1331 (S=O, str); **^{1}H NMR** δ (500 MHz, DMSO) 7.92 (1H, d, *J* = 8.7 Hz, Ar*H*), 7.91 (1H, s, Ar*H*), 7.76 (1H, d, *J* = 8.7 Hz, Ar*H*), 4.42 (2H, t, *J* = 7.6 Hz, CH_2), 2.81 (3H, s, CH_3), 2.25 (2H, m, CH_2), 2.18 (1H, m, C(*H*)H), 2.03 (1H, m, C(H)*H*), 1.87 (2H, m, CH_2), 1.70 (2H, m, CH_2), 1.47 (3H, s, CH_3), 1.37 (2H, m, CH_2), 0.69 (1H, m, C(*H*)H), 0.49 (1H, m, C(H)*H*); **^{13}C NMR** δ (126 MHz, DMSO) 197.27 (C), 149.46 (C), 141.56 (C), 139.87 (C), 126.55 (CH), 120.79 (CH), 115.05 (CH), 58.59 (C), 50.33 (CH_2), 50.09 (CH_2), 47.52 (CH_2), 35.96 (CH_2), 26.19 (CH_2), 24.74 (CH_2), 22.48 (CH_2), 22.18 (CH_2), 21.41 (CH_3), 14.04 (CH_3); **ESI-MS** (MeCN): *m/z* = 497.3 $[M-H]^-$. Data in accordance with the literature.[98]

1-(5-Carboxypentyl)-2-5-[3,3-dimethyl-5-sulfo-1-(4- sulfobutyl)-2,3-dihydro-1*H*-2-indolyliden]-1,3-pentadienyl-3,3- dimethyl-3*H*-5-indoliumsulfonate (34)

Indole **30** (559 mg, 1.6 mmol) was added to malonaldehyde dianilide hydrochloride (563 mg, 2.2 mmol) and a mixture of acetic anhydride and acetic acid (1:1, 20 mL). The reaction was heated to reflux for 2 hours and monitored by HPLC until complete. After cooling the reaction mixture, it was slowly

added to a mixture of Et_2O and EtOAc (2:1, 150 mL). The precipitate formed was collected and washed with EtOAc (250 mL) and dried in a vacuum oven overnight. The intermediate was added to the sulfonate indole **39** (986 mg, 2.0 mmol) in a mixture of acetic acid and acetic anhydride (1:2, 20 mL). Sodium acetate (1.07 g, 13 mmol) was added and the reaction mixture was heated to reflux until the reaction was complete. The crude mixture was cooled, added slowly to stirring Et_2O (200 mL) and the product filtered off, dried and purified using semi-preparative HPLC to yield the product as a dark blue solid (170 mg, 12%).

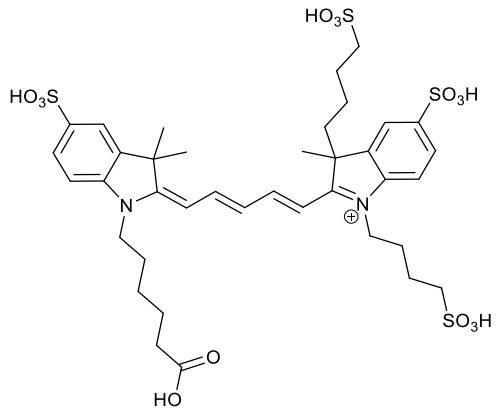

Dark blue solid, yield: 0.170 g, (12%); **^{1}H NMR** δ (500 MHz, MeOD) 8.28 (2H, d, J = 12.8 Hz, CH_{ar}), 7.85 (4H, m, 4 × CH_{ar}), 7.33 (2H, m, 2 × CH_{ar}), 6.69 (1H, t, J = 12.4 Hz CH_{ar}), 6.41 (1H, d, J = 13.5 Hz CH_{ar}), 6.34 (1H, d, J = 13.7 Hz CH_{ar}), 4.12 (4H, m, 2 × NCH_2), 2.91 (2H, br s, CH_2), 2.64 (2H, br s, CH_2), 2.49 (1H, m, C*H*H), 2.31 (2H, t, J = 7.3 Hz CH_2COOH), 2.21 (1H, m, CH*H*), 1.94 (4H, br s, 2 × CH_2), 1.80 (2H, m, CH_2), 1.73 (3H, s, CH_3), 1.72 (3H, s, CH_3), 1.71 (3H, s, CH_3), 1.65 (4H, m, 2 × CH_2), 1.46 (2H, m, CH_2), 1.02 (1H, br s, (C*H*H) 0.69 (1H, br s, (CH*H*); **^{13}C NMR** δ (126 MHz, MeOD) 177.15 (C=O), 175.62 (C), 175.54 (C), 173.54 (C), 173.51 (C), 156.39 (CH), 155.64 (CH), 145.93 (C), 144.95 (C), 142.72 (C), 140.75 (C), 128.28 (2 × CH), 128.06 (CH), 121.34 (CH), 121.30 (CH), 111.76 (CH), 111.59 (CH), 105.93 (CH), 105.60 (CH), 54.94 (C), 52.27 (CH_2), 51.80 (CH_2), 50.66 (C), 45.05 (CH_2), 45.01 (CH_2), 41.99 (CH_2), 34.46 (CH_2), 28.10 (CH_2),

27.88 (CH_3), 27.86 (CH_3), 27.82 (CH_3), 27.27 (CH_2), 27.23 (CH_2), 25.83 (CH_2), 25.64 (CH_2), 24.94 (CH_2), 23.54 (CH_2); **HPLC** (Method 1/ACN) $\mathbf{t_R}$ = 3.62 min, purity 100% (650 nm); **ESI-MS** (MeCN): *m/z* = 888.3 $[M-H]^-$. Data in accordance with the literature.[98]

3,3-Diethyl-1-(*N*-aminobenzylamino)-2,4-azetidinedione (49)

Diethylmalonyl dichloride (0.19 mL, 1.12 mmol) was added to dry dioxane (5 mL) and to the solution *N*-Boc-aminobenzylamine (0.25 g, 1.12 mmol) was added in anhydrous dioxane (5 mL) over an hour. To the mixture NEt_3 (0.7 mL) in dioxane was added slowly and then the reaction was left to stir at rt, for 18 h. The solid formed was filtered off, washed with hexane and the filtrate was dried *in vacuo*. The residue was purified using silica column chromatography (EtOAc:hexane, 0.2:9.8 → 1:1). This produced **49** (0.099 g, 25%) as a colourless solid.

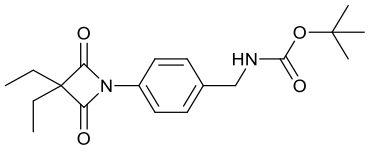

Colourless solid, yield: 0.099 g, (25%); **IR** υ_{max}/cm^{-1}: 3330 (N-H, str), 1713 (C=O, str), 1456 (C=C); **^{1}H NMR** δ (500 MHz, $CDCl_3$) 7.77 (2H, d, *J* = 8.1 Hz, 2 × C*H*), 7.31 (2H, d, *J* = 8.3 Hz, 2 × C*H*), 4.96 (1H, br s, N*H*), 4.28 (2H, d, *J* = 2.3 Hz, NHCH_2), 1.83 (4H, q, *J* = 7.5 Hz, 2 × CH_2), 1.43 (9H, s, 3 × CH_3), 1.04 (6H, t, *J* = 7.5 Hz, 2 × CH_3); **^{13}C NMR** δ (126 MHz, $CDCl_3$) 172.20 (2 × C=O), 155.96 (C=O), 137.86 (C), 132.95 (C), 128.28 (2 × CH), 119.46 (2 × CH), 79.73 (C), 72.21 (C), 44.28 (CH_2), 28.48 (3 × CH_3), 24.03 (2 × CH_2), 9.30 (2 × CH_3); **HPLC** (Method 1/MeCN) $\mathbf{t_R}$ = 5.82 min, purity 100% (ELSD); HRMS (**ESI$^+$**, MeCN) $[M+H]^+$ found 369.17740, $C_{19}H_{26}O_4N_2{}^{23}Na_1$ requires 369.17848.

3,3-Diethyl-1-(*N*-aminobenzylamino)-2,4-azetidinedione (50)

49 (0.099 g, 0.29 mmol) was added to dioxane (3 mL) and to the solution 4M HCl in dioxane (0.7 mL) was added and the reaction was left to stir for 6 h. The reaction mixture was dried *in vacuo* to yield **50** as a white solid (0.071 g, 99%).

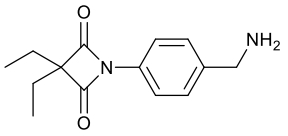

Colourless solid, yield: 0.071 g, (99%); **IR** υ_{max}/cm^{-1}: 1736 (C=O str), 1518 (C=C str); **^{1}H NMR** δ (500 MHz, $CDCl_3$) 7.92 (2H, d, J = 8.1 Hz, 2 × C*H*), 7.61 (2H, d, J = 8.3 Hz, 2 × C*H*), 4.18 (2H, s, NH_2CH_2), 1.90 (4H, q, J = 7.5 Hz, 2 × CH_2), 1.08 (6H, t, J = 7.5 Hz, 2 × CH_3); **^{13}C NMR** δ (126 MHz, $CDCl_3$) 173.22 (2 × C=O), 135.59 (C), 132.95 (C), 131.28 (2 × CH), 120.71 (2 × CH), 73.51 (C), 43.83 (CH_2), 24.74 (2 × CH_2), 9.42 (2 × CH_3); **HPLC** (Method 1/ACN) $\mathbf{t_R}$ = 3.05 min, purity 100% (254 nm); HRMS (**ESI$^+$**, MeCN) $[M+H]^+$ found 247.14400, $C_{14}H_{19}O_2N_2$ requires 247.14410.

3,3-Diethyl-1-(*N*-5-carboxyfluorescein benzylamino)-2,4-azetidinedione (51)

5-Carboxyfluorescein (30 mg, 0.08 mmol) was added to anhydrous DMF (1 mL), PyBrOP (56 mg, 0.12 mmol) and DIPEA (60 µL, 0.32 mmol) and stirred at rt for 15 min. To the reaction mixture **50** (20 mg, 0.08 mmol) was added and left to stir overnight (18 h). The reaction was monitored by HPLC and upon completion, DMF was removed *in vacuo* and the product purified using semi-preparative HPLC to yield **51** (15 mg, 31%) as a yellow solid.

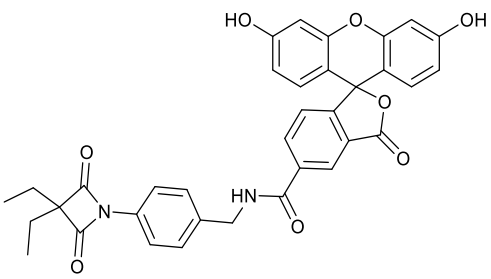

Yellow solid, yield: 0.015 g (31%); **^{1}H NMR** δ (600 MHz, MeOD) 8.49 (1H, m, Ar*H*), 8.27 (1H, dd, *J* = 8.0, 1.6 Hz, Ar*H*), 7.82 (2H, d, *J* = 8.5 Hz, Ar*H*), 7.52 (2H, d, *J* = 8.5 Hz, Ar*H*), 7.34 (1H, d, *J* = 8.0 Hz, Ar*H*), 6.72 (2H, d, *J* = 2.4 Hz, Ar*H*), 6.63 (2H, d, *J* = 8.7 Hz, Ar*H*), 6.57 (2H, dd, *J* = 8.7, 2.4 Hz, Ar*H*), 4.67 (2H, s, CH_2), 1.76 (4H, q, *J* = 7.6 Hz, 2 × CH_2), 1.08 (6H, t, *J* = 7.5 Hz, 2 × CH_3); **^{13}C NMR** δ (126 MHz, MeOD) 173.37 (C=O × 2), 170.55 (C=OO), 168.33 (C=ONH), 161.47 (2 × C), 154.02 (2 × C), 138.89 (2 × C), 137.68 (C), 135.52 (CH), 134.07 (C), 130.15 (2 × CH), 129.89 (C), 129.58 (2 × CH), 125.71 (CH), 124.90 (CH), 120.46 (2 × CH), 113.62 (2 × CH), 110.83 (2 × C), 103.60 (2 × CH), 73.29 (C), 51.39 (C), 44.32 (CH_2), 24.78 (2 × CH_2), 9.44 (2 × CH_3); **HPLC** (Method 1/ACN) $\mathbf{t_R}$ = 5.24 min, purity 100% (ELSD); HRMS (**ESI$^+$**, MeOH) $[M+H]^+$ found 605.19090, $C_{35}H_{29}O_8N_2$ requires 605.19180.

3,3-Diethyl-1-(*N*-Cy5-benzylamino)-2,4-azetidinedione (52)

27 (40 mg, 0.06 mmol) was added to HSPyU (25 mg, 0.06 mmol) and dissolved in dry DMF (2 mL) before DIPEA was added (30 µL, 0.18 mmol). The reaction was left to stir at rt for four hours until no starting material was observed. To the reaction mixture **50** (15 mg, 0.06 mmol) was added and additional DIPEA (30 µL, 0.18 mmol). The reaction was left to stir overnight. The reaction mixture was dried *in vacuo* and the crude product was purified by reverse phase chromatography (H_2O/MeCN 95:5 → 70:30) with the product dried by freeze drier to yield **52** as a dark blue solid (14 mg, 27%).

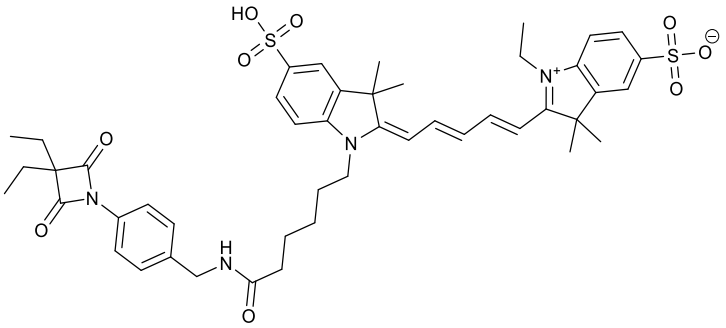

Dark blue solid, yield: 0.014 g, (27%); **IR** υ_{max} / cm^{-1}: 1736 (C=O str), 1183 (S=O str); **^{1}H NMR** δ (500 MHz, MeOD) 8.34 (2H, td, J = 13.1, 4.7, 1 Hz, 2 × CH_{ar} bridge), 7.94 (2H, s, 2CH_{ar}), 7.94-7.90 (2H, m, 2 CH_{ar}), 7.77 (2H, d, J = 8.6 Hz, 2 × CH_{ar}), 7.40 (2H, d, J = 8.7 Hz, 2 × CH_{ar}), 7.39-7.34 (2H, m, 2 × CH_{ar}), 6.70 (1H, m, C$H_{ar\ bridge}$), 6.36 (2H, m, 2 × C$H_{ar\ bridge}$), 4.38 (2H, s, PhCH_2), 4.20 (2H, q, J = 7.1 Hz, NCH_2), 4.14 (2H, t, J = 7.2 Hz, CH_2), 2.30 (2H, t, J = 7.2 Hz, CH_2), 1.83-1.90 (2H, m, CH_2), 1.85 (4H, q, J = 7.6 Hz, 2 × CH_2), 1.77 (12H, s, 4 × CH_3), 1.76 (2H, m, CH_2), 1.49 (2H, m, CH_2), 1.42 (3H, t, J = 7.2 Hz, CH_3), 1.05 (6H, t, J = 7.5 Hz, 2 × CH_3); **^{13}C NMR** δ (126 MHz, MeOD) 175.75 (C=O), 173.36 (2 × C=O), 156.36 (CH), 156.14, 144.90 (C), 144.43(C), 142.76(C), 142.59(C), 139.10(C), 133.94(C), 129.58 (2 × CH), 128.10 (2 × CH), 127.63 (CH), 121.44 (2 × CH), 120.42 (2 × CH), 111.63 (CH), 111.45 (CH), 105.18 (CH), 104.98 (CH), 73.27 (C), 50.66 (C), 50.58 (C), 45.00 (CH_2), 43.66 (CH_2), 40.28 (CH_2), 36.57 (CH_2), 28.08 (CH_2), 27.86 (2 × CH_3), 27.72 (2 × CH_3), 27.31 (CH_2), 26.42 (CH_2), 24.75 (2 × CH_2), 12.52 (CH_3), 9.45 (2 × CH_3); **HPLC** (Method 1/ACN) $\mathbf{t_R}$ = 4.90 min, purity 100% (ELSD); HRMS (**ESI$^+$**, MeCN) $[M+H]^+$ found 885.3520, $C_{47}H_{57}O_9N_4S_2^+$ requires 885.3561.

3,3-Diethyl-1-(*N*-Boc-ethylamino)-2,4-azetidinedione (53)

Diethylmalonyl dichloride (0.87 mL, 5.07 mmol) was added to dry dioxane (5 mL) and cooled to -10 °C. To the solution *N*-Boc-ethylenediamine (0.80 mL, 5.07 mmol) was added in anhydrous dioxane (5 mL) over an hour. To the mixture NEt_3 (4.7 mL) in dioxane was added slowly and then the reaction was left to stir at rt, for 18 h. The solid formed was filtered off, washed with hexane and the filtrate was dried *in vacuo*. The residue was purified using silica column chromatography (EtOAc: hexane, 1:4 → 100% EtOAc). This produced **53** (0.342 g, 22%) as a colourless oil.

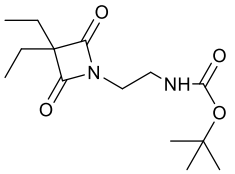

Colourless oil, yield: 0.342 g, (14%); **IR** υ_{max} / cm^{-1}: 3330 (N-H str), 1729 (C=O str); **^{1}H NMR** δ (500 MHz, $CDCl_3$) 4.94 (1H, br s, N*H*), 3.45 (2H, m, CH_2), 3.38 (2H, m, CH_2), 0.99 (4H, q, J = 7.5 Hz, 2 × CH_2), 1.43 (9H, s, 3 × CH_3), 0.99 (6H, t, J = 7.5 Hz, 2 × CH_3); **^{13}C NMR** δ (126 MHz, $CDCl_3$) 174.76 (2 × C=O), 164.45 (C=O), 71.07 (C), 60.13 (C), 39.51 (CH_2), 39.04 (CH_2), 28.48 (3 × CH_3), 23.55 (2 × CH_2), 9.34 (2 × CH_3); **HPLC** (Method 1/MeCN) **t_R** = 4.06 min, purity 100% (ELSD); HRMS (**ESI$^+$,** MeCN) $[M+Na]^+$ found 307.16330, $C_{14}H_{24}O_4N_2Na$ requires 307.16283.

3,3-Diethyl-1-ethylamino-2,4-azetidinedione (54)

53 (0.342 g, 1.12 mmol) was added to anhydrous dioxane (4 mL) and to the solution, HCl in dioxane (4 M, 4 mL) was added. The reaction was left to stir for 4 h, after which a precipitate was observed. The mixture was filtered, and the precipitate was isolated and dried to produce **54** as a colourless solid (205 mg, 98%).

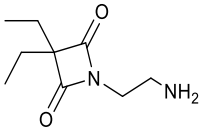

Colourless solid, yield: 205 mg, (98%); **IR** υ_{max} / cm^{-1}: 3359 (N-H str), 1722 (C=O str); **^{1}H NMR** δ (500 MHz, $CDCl_3$) 8.48 (2H, br s, NH_2), 3.87 (2H, t, J = 6.1 Hz, CH_2), 3.42 (2H, t, J = 6.2 Hz, CH_2), 1.80 (4H, q, J = 7.5 Hz, 2 × CH_2), 0.99 (6H, t, J = 7.5 Hz, 2 × CH_3); **^{13}C NMR** δ (126 MHz, $CDCl_3$) 174.58 (2 × C=O), 70.64 (C), 38.51 (CH_2), 36.97 (CH_2), 23.17 (2 × CH_2), 9.23 (2 × CH_3); **HPLC** (Method 1/MeCN) **t_R** = 3.78 min, purity 100% (ELSD); HRMS (**ESI$^+$,** MeCN) $[M+Na]^+$ found 185.12850, $C_9H_{17}O_2N_2$ requires 185.12845.

3,3-Diethyl-1-(*N*-5-carboxylfluorescein-ethylamino)-2,4-azetidinedione (55)

25 (21 mg, 0.044 mmol) was added to anhydrous DMF (1 mL) and DIPEA (11 µL, 0.132 mmol) and **54** (8 mg, 0.044 mmol) and left to stir overnight. The reaction was monitored by HPLC and upon completion, DMF was removed *in vacuo* and the product purified using semi-preparative HPLC to yield **55** (12 mg, 21%) as a yellow solid.

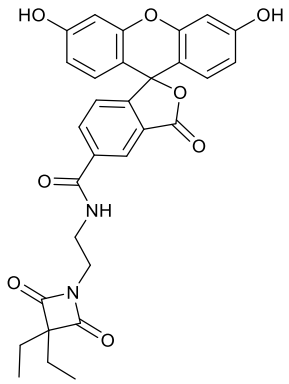

Yellow solid, yield: 0.012 g (21%); $\mathbf{R_f}$ = 0.33 (DCM:MeOH:AcOH, 100:10:1); **IR** υ_{max} / cm^{-1}: 1728 (C=O str), 1605 (C=O str); **^{1}H NMR** δ (500 MHz, MeOD) 8.42 (1H, m, Ar*H*), 8.19 (1H, dd, *J* = 8.1, 1.7 Hz, Ar*H*), 7.32 (1H, dd, *J* = 8.1, 0.7 Hz, Ar*H*), 6.71 (2H, d, *J* = 2.3 Hz, Ar*H*), 6.61 (2H, d, *J* = 8.7, Ar*H*), 6.56 (2H, dd, *J* = 8.7, 2.5 Hz, Ar*H*), 3.69 (2H, m, CH_2), 3.66 (2H, m, CH_2), 1.76 (4H, q, *J* = 7.6 Hz, 2 × CH_2), 0.99 (6H, t, *J* = 7.5 Hz, 2 × CH_3); **^{13}C NMR** δ (126 MHz, MeOD) 176.00 (C=O × 2), 170.52 (C=OO), 168.76 (C=ONH), 161.56 (2 × C), 156.66 (2 × C), 154.06 (2 × C), 137.70 (C), 135.45 (CH), 130.12 (2 × CH), 128.75 (C), 125.74 (CH), 124.90 (CH), 113.74 (2 × CH), 110.86 (2 × C), 103.62 (2 × CH), 71.75 (C), 54.79 (C), 39.55 (CH_2), 39.10 (CH_2), 9.44 (2 × CH_3); **HPLC** (Method 1/ACN) $\mathbf{t_R}$ = 4.54 min, purity 100% (ELSD); HRMS (**ESI$^+$,** MeOH) $[M+H]^+$ found 543.17690, $C_{30}H_{27}O_2N_8$ requires 543.17619.

3,3-Diethyl-1-(*N*-Cy5-ethylamino)-2,4-azetidinedione (56)

27 (54 mg, 0.08 mmol) was added to HSPyU (36 mg, 0.08 mmol) and dissolved in dry DMF (2 mL) before DIPEA was added (40 μL, 0.24 mmol). The reaction was left to stir for four hours until no starting material was observed. To the reaction mixture **54** (15 mg, 0.08 mmol) was added and additional DIPEA (40 μL, 0.24 mmol). The reaction was left to stir at rt overnight. The reaction mixture was dried *in vacuo* and the crude product was purified by reverse phase chromatography with the product dried by freeze drier to yield **56** as a dark blue solid (31 mg, 45%).

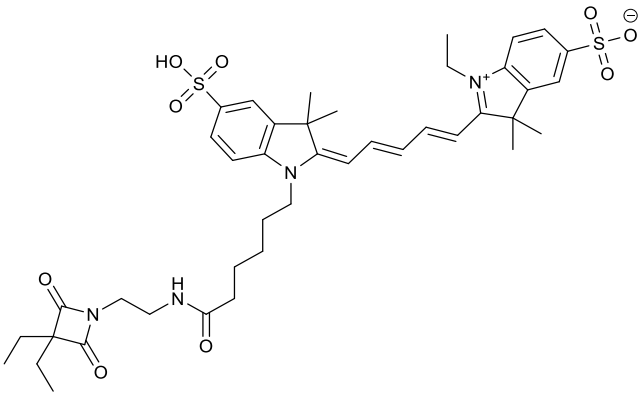

Dark blue solid, yield: 0.031 g (45%); **IR** υ_{max} / cm^{-1}: 1728 (C=O str), 1605 (C=O str); **^{1}H NMR** δ (600 MHz, MeOD) 8.35 (2H, t, *J* = 13.8 Hz, Ar_{bridge}), 7.92 (4H, m, Ar*H*), 7.38 (2H, t, *J* = 8.5 Hz, Ar*H*), 6.71 (1H, t, *J* = 12.4 Hz, Ar_{bridge}), 6.61 (2H, d, *J* = 13.7 Hz, Ar_{bridge}), 4.21 (2H, q, *J* = 7.2 Hz, NCH_2), 4.16 (2H, t, *J* = 7.4 Hz, NCH_2), 3.50 (2H, m, CH_2), 3.41 (2H, m, CH_2), 2.22 (2H, t, *J* = 7.3 Hz, COCH_2), 1.85 (2H, m, CH_2), 1.78 (6H, s, 2 × CH_3), 1.78 (6H, s, 2 × CH_3), 1.77 (4H, q, *J* = 7.5 Hz, 2 × CH_2), 1.72 (2H, m, CH_2), 1.50 (2H, m, CH_2), 1.42 (3H, t, J = 7.3 Hz, CH_2CH_3), 1.00 (6H, t, *J* = 7.5 Hz, 2 × CH_3); **^{13}C NMR** δ (126 MHz, MeOD) 176.23 (C), 175.95 (C=O × 2), 175.31 (C), 175.04 (C), 156.34 (CH), 156.23 (CH), 144.92 (C), 144.43 (C), 143.47 (C), 143.41 (C), 142.74 (C), 142.61(C), 128.10 (CH), 128.06 (CH), 127.65 (CH), 121.41 (CH), 121.36 (CH), 111.66 (CH), 111.40 (CH), 105.21 (CH), 104.92 (CH), 71.68 (C), 50.64 (C), 50.59 (C), 45.01 (CH_2), 40.25 (CH_2), 39.26 (CH_2), 38.72 (CH_2), 36.67 (CH_2), 28.12 (CH_2), 27.84 (2 × CH_3), 27.72 (2 × CH_3), 27.30 (CH_2), 26.30 (CH_2), 23.99 (2 × CH_2), 12.52 (CH_3), 9.50 (2 × CH_3); **HPLC**

(Method 1/ACN) $\mathbf{t_R}$ = 4.02 min, purity 100% (ELSD); HRMS (**ESI$^+$,** MeCN) $[M+H]^+$ found 823.33810, $C_{42}H_{55}O_9N_4S_2^+$ requires 823.34050.

(1*R*-Carbamoyl-3-methylsulfanyl-propyl)carbamic acid *tert*-butyl ester (62)[115]

(*R*)-Methionine (2.50 g, 16.8 mmol), 1,4-dioxane (10 mL) and 1.25 M NaOH (13 mL) were added to a round bottom flask and cooled to 0–6 °C. A solution of di-*tert*-butyl-dicarbonate (3.84 g, 17.6 mmol) in 1,4-dioxane (3 mL) was slowly added over 15 min, and the reaction was slowly warmed to room temperature and stirred for 3.5 h. 1,4-Dioxane was removed *in vacuo* and the residue was diluted using 1 M $KHSO_4$ (17 mL), and washed with EtOAc (3 × 100 mL). The organic extracts were collected and washed with water (150 mL) and brine (100 mL) before being dried using $MgSO_4$. The solvent was removed *in vacuo* to produce a pale-yellow oil, which was diluted in DMF (7 mL). To the solution was added ammonium bicarbonate (1.46 g, 18.47 mmol), pyridine (0.63 mL) and di-*tert*-butyl-dicarbonate (4.02 g, 18.5 mmol) dissolved in DMF (2 mL). Effervescence was exhibited and the mixture was left to stir at room temperature for 18 h. Water was added (100 mL) and extracted using EtOAc (3 × 50 mL), and the organic extracts were washed again with brine (2 × 100 mL) and dilute H_2SO_4 solution (100 mL) before being dried using $MgSO_4$ and the solvent removed *in vacuo*. The crude white solid was triturated in Et_2O (50 mL) for 20 min, before filtration and purification using silica column chromatography (EtOAc: cyclohexane, 1:1). This produced **62** (2.09 g, 50%) as a colourless solid.

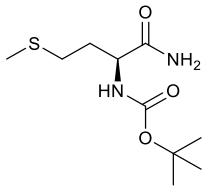

Colourless solid, yield: 2.09 g, (50%). **mp** 120-22 °C, lit 118-9 °C; **IR** υ_{max} / cm^{-1}: 3393 (N-H str), 3346 (N-H str), 1679 (C=O str), 1640 (C=O str); **^{1}H NMR** δ (500 MHz, $CDCl_3$) 6.39 (1H, br s, *NH*), 5.85 (1H, br s, *NH*), 5.31 (1H, m, *NH*), 4.31 (1H, m, C*H*), 2.57 (2H, t, *J* = 7.4 Hz, CH_2SCH_3), 2.10 (3H, s, SCH_3), 1.92 (2H, m, CH_2), 1.43 (9H, s, CH_3); **^{13}C NMR** δ (126 MHz, $CDCl_3$) 174.25 (C), 155.82 (C), 80.40 (C), 53.16 (CH), 31.77 (CH_2), 30.35 (CH_2), 28.45 (3 × CH_3), 15.46 (CH_3). The spectroscopic data is in agreement with the literature.[115]

(2*R*-*tert*-Butoxycarbonylamino-4-methylsulfanyl-butyryl)-carbamic acid benzyl ester (63)[115]

62 (4.40 g, 17.7 mmol) was dissolved in anhydrous THF (30 mL) and cooled to -70 °C. *n*-Butyllithium (14.2 mL, 35.4 mmol, 2.5 M in hexane) was added slowly over 10 min such that the temperature remained below -65 °C. To the reaction mixture was added benzyl chloroformate (2.5 mL, 17.7 mmol) and was left to stir at -65 °C for 1.5 h. To quench the reaction, aq. NH_4Cl solution (15 mL) was added and left to warm to room temperature. The mixture was extracted with EtOAc (3 × 50 mL) which were then washed with brine (3 × 100 mL), dried using $MgSO_4$ and the solvent removed *in vacuo* to produce a pale-yellow oil. The crude product was then purified using silica column chromatography (EtOAc: cyclohexane, 1:1). This produced **63** (6.19 g, 96%) as a pale-yellow oil.

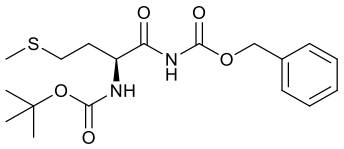

Pale yellow oil, yield: 6.19 g, (96%). **IR** υ_{max} / cm^{-1}: 3280 (N-H str), 2976 (C-H_{ar} str), 2918 (C-H_{alk} str), 1771 (C=O str), 1686 (C=O str); **^{1}H NMR** δ (500 MHz, $CDCl_3$) 8.66 (1H, br s, N*H*), 7.34 (5H, m, Ar*H*), 5.31 (1H, br s, N*H*), 5.17 (2H, s, PhCH_2O), 4.71 (1H, m, C*H*), 2.56 (2H, t, *J* = 7.4 Hz, CH_3SCH_2), 2.12 (1H, m, CH(*H*)), 2.06 (3H, s, CH_3SCH_2), 1.86-1.79 (1H, m, C*H*(H)), 1.40 (9H, s, 3 × CH_3);

^{13}C NMR δ (126 MHz, $CDCl_3$) 172.05 (C), 155.96 (C), 150.88 (C), 134.97 (C), 128.71 (3 × CH), 128.61 (2 × CH), 80.68 (C), 60.03 (CH_2), 53.96 (CH), 31.59 (CH_2), 30.30 (CH_2), 28.33 (3 × CH_3), 15.47 (CH_3). The spectroscopic data is in agreement with the literature.[115]

(4-Benzyloxycarbonylamino-3*R*-*tert*-butoxycarbonylamino-4-oxo-butyl)-dimethyl-sulfonium iodide (64)[115]

63 (3.67 g, 10.1 mmol) was dissolved in acetone (5.7 mL) and iodomethane (3.11 mL, 50.3 mmol) was added. The reaction was left in the dark to stir for 3 days. The solvent was removed *in vacuo* and the product was recrystallized using acetone and Et_2O (1:20) to produce **64** as a pale yellow solid (2.86 g, 78%).

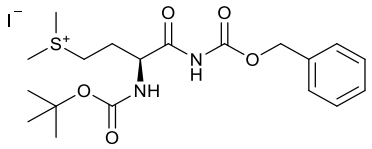

Pale yellow solid, yield: 2.86 g, (78%). **mp** 129-131 °C, **IR** υ_{max} / cm^{-1}: 3383 (N-H str), 3085 (C-H_{ar} str), 2952 (C-H_{ar} str), 1775 (C=O str), 1699 (C=O str); **^{1}H NMR** δ (500 MHz, $CDCl_3$) 9.25 (1H, br s, N*H*), 7.38-7.31 (5H, m, *H*Ar), 6.15 (1H, br s, N*H*), 5.16 (2H, s, PhC*H*$_2$O), 4.79 (1H, br s, CH_2C*H*NH), 3.97 (1H, m, CH_2C*H*(H)), 3.55 (1H, m, CH_2CH(*H*)), 3.24 (3H, s, SC*H*$_3$), 3.19 (3H, s, SC*H*$_3$), 2.56 (1H, m, Me_2SCH(*H*)), 2.22 (1H, m, Me_2SC*H*(H)), 1.40 (9H, s, 3 × C*H*$_3$); **^{13}C NMR** δ (126 MHz, $CDCl_3$) 170.77 (C), 156.49 (C), 151.25 (C), 135.02 (C), 128.82 (2 × CH), 128.75 (CH), 128.43 (2 × CH), 81.13 (C), 68.15 (CH_2), 53.12 (CH), 41.43 (CH_2), 28.46 (3 × CH_3), 27.60 (CH_2), 26.41 (CH_3), 26.14 (CH_3).

(*R*)-3-*tert*-Butoxycarbonylamino-2-oxo-pyrrolidine-1-carboxylic acid benzyl ester (65)[115]

Amberlite IRA-410 chloride (1.00 g, 1.25 wt. eq.) was washed with NaOH solution (10 M, 3 × 10 mL), followed by a washing of H_2O (2 × 10 mL), MeCN (2 × 10 mL) and Et_2O (2 × 10 mL). The resin was added to **64** (0.75 g, 1.98 mmol) in acetonitrile (1.5 mL). After the addition of crushed and activated 4 Å molecular sieves (0.1 wt. eq., 0.075 g), the mixture was left to stir at 40 °C for 4.5 h, during which further resin was added (0.25 g). The reaction was quenched by filtering the mixture, washing with EtOAc (3 × 25 mL). The solvent was removed *in vacuo* and recrystallized using cyclohexane: EtOAc (3.3:1) to produce **65** as a white solid (0.40 g, 64%).

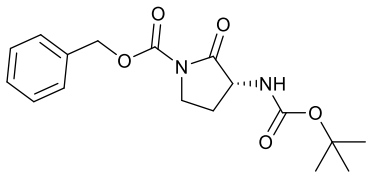

Pale yellow solid, yield: 0.40 g, (64%). **mp** 142 °C, lit[115] 139-41 °C; **IR** υ_{max} / cm^{-1}: 3346 (N-H, str), 2975 (C-$H_{ar,}$ str), 1774 (C=O, str), 1698 (C=O, str); **^{1}H NMR** δ (500 MHz, $CDCl_3$) 7.43-7.33 (5H, m, Ar*H*), 5.29 (2H, s, PhCH_2O), 5.08 (1H, br s, N*H*), 4.27 (1H, br s, NHC*H*CH_2), 3.90 (1H, dd, *J* = 10.5, 9.4 Hz, CH_2C*H*(H)N), 3.60 (1H, ddd, *J* = 11.5, 11.1, 6.4 Hz, CH_2CH(*H*)N), 2.62 (1H, m, CH_2C*H*(H)CH), 1.89 (1H, m, CH_2CH(*H*)CH), 1.45 (9H, s, 3 × CH_3); **^{13}C NMR** δ (126 MHz, $CDCl_3$) 171.79 (C), 155.70 (C), 151.32 (C), 135.17 (C), 128.77 (2 × CH), 128.66 (CH), 128.37 (2 × CH), 80.55 (C), 68.51 (CH_2), 53.73 (CH), 42.98 (CH_2), 28.44 (3 × CH_3), 27.13 (CH_2). The spectroscopic data is in agreement with the literature.[115]

2-Oxo-3*R*-(2,2,2-trifluoro-acetylamino)pyrrolidine-1-carboxylic acid benzyl ester (66)[115]

65 (0.41 g, 1.77 mmol) was dissolved in 1,4-dioxane (2 mL) and to the reaction 2 M HCl in 1,4-dioxane (1.87 mL) was added and left to stir for 3.5 h. The reaction mixture was concentrated *in vacuo* and the solid produced was added

to DCM (2.5 mL), MeOH (1 mL), methyl trifluoroacetate (0.89 mL, 8.83 mmol) and *N*-methyl morpholine (0.29 mL, 2.65 mmol) and was left to stir at rt for 18 h. The reaction was quenched with DCM (10 mL), aq. 2 M HCl solution (10 mL), and aq. 1 M NH_4Cl solution (5 mL). The organic solvent was collected and washed with additional aq. 2 M HCl solution (15 mL), brine (2 x 25 mL) and dried using $MgSO_4$. The solvent was removed *in vacuo* and the solid was triturated in Et_2O: cyclohexane 1:1 (20 mL) for 20 min. The solid was filtered off and dried in a 40 °C vacuum oven for 18 h to produce **66** as a pale pink solid (0.27 g, 51%).

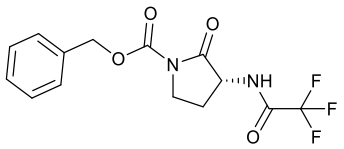

Pale pink solid, 0.27 g, (51%); **mp** 157 °C, lit[115] 152-4 °C; **IR** υ_{max} / cm^{-1}: 3284 (N-H, str), 1772 (C=O, str), 1714 (C=O, str), 1688 (C=O, str); **^{1}H NMR** δ (500 MHz, $CDCl_3$) 7.42-7.33 (5H, m, Ar*H*), 7.11 (1H, s, N*H*), 5.28 (2H, s, CH_2O), 4.54 (1H, ddd, *J* = 12, 8.3, 6.0 Hz, NHC*H*CH_2), 3.92 (1H, t, *J* = 10.7 Hz, CH_2C*H(*H*)*N) 3.66 (1H, td, *J* = 11.1, 6.4 Hz, CH_2CH*(H)*N), 2.73 (1H, m, CH_2C*H*(H)CH), 1.94 (1H, m, CH_2CH(*H*)CH); **^{13}C NMR** δ (126 MHz, $CDCl_3$) 170.32 (C), 158.21 (C-F), 157.91 (C-F), 157.61 (C-F), 157.30 (C-F), 150.92 (C), 134.29 (C), 128.90 (CH), 128.86 (2 × CH), 128.49 (2 × CH), 119.04 (C-F), 116.75 (C-F), 114.46 (C-F), 112.18 (C-F), 68.90 (CH_2), 52.86 (CH), 43.25 (CH_2), 26.09 (CH_2); ESI-MS (MeCN): ***m/z*** = 331.1 $[M+H]^+$. The spectroscopic data is in agreement with the literature.[115]

2-Ethoxy-3*R*-(2,2,2-trifluoro-acetylamino)pyrrolidine-1-carboxylic acid benzyl ester (67)[115]

66 (3.5 g, 11 mmol) was added to anhydrous THF (30 mL) and after cooling to -40 °C, $LiBH_4$ in THF (2M, 5.6 mL) was added slowly, and the reaction was left stirring at -40 °C until HPLC showed completion. The crude mixture was

diluted with EtOH (10 mL) and to the solution, a mixture of H_2SO_4 and EtOH (3:10, 5.2 mL) was added slowly. The reaction was left to warm to room temperature over 2 h and upon completion, it was quenched with an aqueous $NaHCO_3$ solution (1M, 30 mL). The ethanol was removed *in vacuo* and the aqueous mixture was extracted with EtOAc (3 × 100 mL). The organic layer was washed with brine (100 mL), dried using $MgSO_4$ and concentrated *in vacuo*, to give the two ethers as an oil.

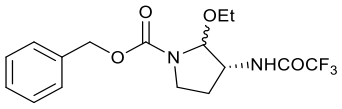

Colourless oil, 3.80 g, (97%); **^{1}H NMR** δ (500 MHz, $CDCl_3$) 7.37-7.32 (5H, m, Ar*H*), 6.90-6.75 (1H, m, N*H*), 5.17-5.10 (3H, m), 4.30 (1H, m), 3.72-3.39 (4H, m), 2.45-2.34 (1H, m), 1.94 (1H, m), 1.19-1.09 (3H, m); $\mathbf{t_R}$: 4.49 and 5.06 min (GE10 MeCN, 254 nm); ESI-MS (MeCN): ***m/z*** = 360.1 $[M+H]^+$. The spectroscopic data is in agreement with the literature.[115]

_Z_-(1-Ethoxy-3-methyl-but-1-enyloxy)-triisopropyl-silane (68)[115]

DMPU and THF (2:3, 35 mL) were mixed and cooled to -40 °C, before the addition of LiHMDS (1M in THF, 16 mL). The solution was cooled down to -78 °C and ethyl isovalerate (3.05 mL, 0.020 mol) was added slowly, maintaining the internal temperature. After 1 h, tri-isopropyl triflate (5.43 mL, 0.202 mol) was added slowly and the reaction was left to warm overnight. The reaction was quenched at 5 °C with aqueous 1M $NaHCO_3$ solution (30 mL) and washed with hexane (4 × 25 mL), which was collected and washed with H_2O (5 × 40 mL). The organic layer was collected, dried with $MgSO_4$ and dried *in vacuo* to yield **68** as a crude product. **68** was then purified using vacuum distillation (65-80 °C, 1-0.1 mbar) to yield **68** as a colourless liquid (0.58 g, 10%)

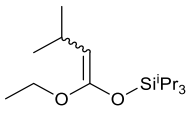

Colourless liquid, 0.58 g, (10%); **^{1}H NMR** δ (500 MHz, $CDCl_3$) 3.89 (0.2H, q, J = 7.05 Hz, CH_2CH$_3$), 3.66 (2H, q, J = 7.05 Hz, CH_2CH$_3$), 3.20 (1H, d, J = 8.25 Hz, iPrC*H*), 2.59 (1H, m, C=C*H*), 1.26 (3H, t, J = 7.0 Hz, CH$_2$CH_3), 1.18 (3H, m, 3 × iPrC*H*) 1.07 (18H, m, 3 × CH(CH_3)$_2$), 0.96 (6H, d, J = 6.8 Hz, CH(CH_3)$_2$); **^{13}C NMR** δ (126 MHz, $CDCl_3$) 154.69 (C), 82.79 (CH), 62.68 (CH_2), 24.91 (2 × CH_3), 24.50 (CH), 18.08 (6 × CH_3), 14.64 (CH_3), 13.00 (3 × CH). The spectroscopic data is in agreement with the literature.[115]

(2*S*,3*R*)-3-Amino-2-(Rel-1*S*-ethoxycarbonyl-2-methylpropyl) pyrrolidine-1-carboxylic acid benzyl ester (71)

67 (0.559 g, 1.55 mmol) was added to dry DCM (10 mL) and cooled to 5 °C before adding **68** (1.33 g, 4.65 mmol) and BF_3.OEt_2 (1.15 mL, 9.3 mmol) slowly to the solution, with the reaction monitored by HPLC (peaks at 5.37 min and 5.71 min, ELSD). Upon completion, the reaction mixture was purified crudely to yield the ester **69**. After this, **69** (599 mg, 1.35 mmol) was added to a mixture of EtOH and H_2O (1:1, 10 mL) and K_2CO_3 (0.931 g, 1.35 mmol). The mixture was heated to reflux, and the reaction monitored by TLC and HPLC (peaks at 3.36 min and 3.45 min, ELSD), and after the reaction was complete the EtOH was removed *in vacuo* and diluted with water (20 mL). The aqueous layer was washed with Et_2O (3 × 40 mL), the organic layers collected and washed with 1M HCl (3 × 100 mL). The acidic aqueous layers were collected and neutralised to pH 7/8 with Na_2CO_3, before the product was extracted with DCM (3 × 100 mL). The DCM washes were collected and dried with $MgSO_4$, and the solvent removed *in vacuo*.

The amine **70** (103 mg, 0.30 mmol) was added to THF (1 mL) and TMEDA (1 mL), cooled to 0 °C and ^{t}BuMgCl (0.9 mL, 0.89 mmol) was added slowly and

the reaction was left to warm to room temperature for 2 h. The reaction was quenched with saturated aqueous ammonium chloride (10 mL) and extracted with EtOAc (3 × 10 mL). The organic washings were collected, dried with $MgSO_4$ and the solvent removed *in vacuo*. The crude mixture was purified using flash chromatography (2:8 cyclohexane: EtOAc → 100% EtOAc), to yield the **71a** as a white solid (15.1 mg, 16%).

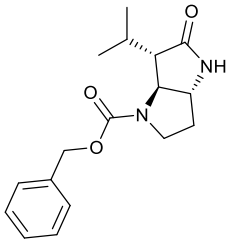

Pale brown solid, yield: 0.015 g, (16%); **IR** υ_{max} / cm^{-1}: 3295 (N-H, str), 3068 (C=C, str), 2920 (C-C, str); **^{1}H NMR** δ (600 MHz, $CDCl_3$) 7.38-7.31 (5H, m, Ar*H*), 5.96 (1H, br s, N*H*), 5.13 (1H, d, *J* = 12.1 Hz, CO_2CHH), 5.09 (1H, d, *J* = 12.1 Hz, CO_2CHH), 3.81 (1H, m, CbzNC*H*H), 3.76 (1H, m, CbzNCH*H*), 3.21-3.16 (2H, m, 2 × NC*H*), 2.68-2.54 (2H, m, ^{i}PrC*H*, CH_3CHCH_3), 2.18 (1H, m, CH_2CH(H)), 1.76 (1H, m, CH_2CH(H)), 1.14 (3H, br s, CH_3) 0.95 (3H, br s, CH_3); **^{13}C NMR** δ (150 MHz, $CDCl_3$) 180.91 (C=O), 155.25 (C=O), 136.28 (C), 128.68 (2 × CH), 128.57 (2 × CH), 128.40 (CH), 67.35 (CH_2), 65.68 (CH), 58.35 (CH), 54.80 (CH), 49.78 (CH_2), 27.50 (CH_2), 26.12 (CH), 21.32 (CH), 16.71 (CH); $\mathbf{t_R}$: 4.79 min (GE10 MeCN, 254 nm); HRMS (**ESI$^+$**, MeCN) $[MH]^+$ found 302.16329, $C_{17}H_{22}O_3N_2$ requires 302.16249. The spectroscopic data is in agreement with the literature.[115]

(3aR,6S,6aS)-6-Isopropyl-4methanesulfonyl-5-oxo-hexahydro-pyrrolo [3,2-b] pyrrole-1-carboxylic acid benzyl ester (72)

To **71a** (60 mg, 0.20 mmol) dissolved in dry THF (1 mL) and cooled down to -78 °C, LiHMDS (0.28 mL) was added and the reaction was left to stir at -78 °C

for 1 hr, before methanesulfonyl chloride (38 µL, 0.50 mmol) was added slowly, with the reaction temperature being monitored. After the reaction was complete, the reaction was quenched with aqueous $NaHCO_3$ (5 mL) and slowly warmed to room temperature. The product extracted with DCM (2 × 10 mL), and the combined extracts were then washed with brine (2 × 10 mL), dried with $MgSO_4$ and the solvent removed *in vacuo*. The crude product was purified using silica column chromatography (EtOAc: hexane, 1:4). This produced **72** (0.40 g, 20%) as a pale-yellow oil.

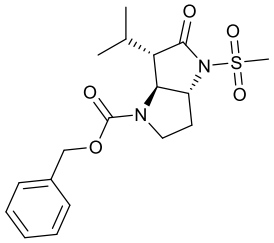

Colourless solid, yield: 0.035 g, (50%); **IR** υ_{max}/cm^{-1}: 3295 (N-H, str), 3068 (C=C, str), 2920 (C-C, str); **^{1}H NMR** δ (500 MHz, $CDCl_3$) 7.39-7.32 (5H, m, Ar*H*), 5.13 (1H, d, *J* = 12.1 Hz, CO_2CHH), 5.09 (1H, d, *J* = 12.1 Hz, CO_2CHH), 3.84 (1H, m, CbzNC*H*H), 3.78 (1H, m, CbzNCH*H*), 3.47 (1H, m, $(SO_2Me)NCH$), 3.27 (1H, m, NC*H*), 3.24 (3H, br s, $(NSO_2)CH_3$), 2.78-2.64 (2H, m, ^{i}PrC*H*, CH_3CHCH_3), 2.55 (1H, m, $CH_2CH(H)$), 2.02 (1H, m, $CH_2CH(H)$), 1.15 (3H, br s, CH_3) 0.95 (3H, br s, CH_3); **^{13}C NMR** δ (126 MHz, $CDCl_3$) 176.26 (C=O), 155.12 (C=O), 136.03 (C), 128.76 (4 × CH), 128.56 (CH), 67.63 (CH_2), 63.34 (CH), 61.74 (CH), 55.98 (CH), 49.42 (CH_2), 40.99 (CH_3), 28.25 (CH_2), 26.54 (CH), 21.04 (CH_3), 16.36 (CH_3); (Method 1/MeCN) $\mathbf{t_R}$: 5.20 min (254 nm); HRMS (**ESI$^+$,** MeCN) $[MH]^+$ found 381.14880, $C_{18}H_{25}O_5N_2{}^{32}S_1$ requires 381.14787. The spectroscopic data is in agreement with the literature.[115]

(3S,6AS,6AR)-6-Isopropyl-4-methanesulfonyl-5-oxo-hexahydro-pyrrolo [3,2-*B*] pyrrol-2-one (59)

72 (0.035 g, 0.091 mmol) was dissolved in EtOAc: dioxane (1:1, 3 mL) and was flushed with N_2, before the addition of $Pd(OH)_2/C$ (8 mg, 0.011 mmol). The mixture was left to stir under H_2 for 3 h, monitoring the reaction until completion. The reaction mixture was filtered through celite, keeping the filter cake damp, and washed through with EtOAc (2 × 15 mL). The solvent was removed *in vacuo* to produce **59** as a pale-yellow oil (0.014 g, 63%)

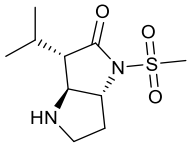

Pale yellow oil, yield: 0.014 g, (63%); **^{1}H NMR** δ (400 MHz, $CDCl_3$): 3.54 (1H, td, *J* = 10.9, 2.1 Hz, HNCH*H*), 3.39 (2H, m, HNC*H*H, C*H*N(SO_2Me)), 3.23 (3H, s, (NSO_2)CH_3), 2.99 (1H, br s, N*H*), 2.94 (1H, dd, *J* = 12.3, 9.5 Hz, C*H*NHCH_2), 2.41 (2H, m, ^{i}PrC*H*, $NHCH_2$C*H*(H)), 2.23 (1H, m, CH_3C*H*CH_3), 1.93 (1H, m, $NHCH_2$CH(*H*)), 1.10 (3H, d, *J* = 6.9 Hz, CH_3) 0.96 (3H, d, *J* = 6.9 Hz, CH_3); **^{13}C NMR** δ (101 MHz, $CDCl_3$) 177.48 (C=O), 64.60 (CH), 63.64 (CH), 56.90 (CH), 48.30 (CH_2), 40.89 (CH_3), 28.26 (CH_2), 26.73 (CH), 21.14 (CH_3), 19.03 (CH_3); $\mathbf{t_R}$: 5.20 min (GE10 MeCN, 254 nm); HRMS (**ESI$^+$,** MeCN) $[MH]^+$ found 247.1126, $C_{10}H_{19}O_3N_2{}^{32}S_1$ requires 247.1111. The spectroscopic data is in agreement with the literature.[115]

(*E*)-Piperazidyl-1-ylbut-2-enoic acid (73)

(*E*)-4-Boc-piperazidyl-1-ylbut-2-enoic acid ethyl ester (1.438 g, 7.25 mmol) was added to dioxane (10 mL) and to it was added 4M HCl in dioxane (10 mL) and water (2 mL) and was left to reflux for 3 hours. The solvent was removed *in vacuo* and the crude product was diluted with water (2 mL) and to it MeOH was added, to give a white precipitate. The precipitate was filtered off and dried *in vacuo*, to give the product (0.23 g, 30%).

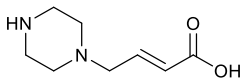

Colourless solid, yield: 0.23 g, (30%); **IR** υ_{max} / cm^{-1}: 2912 (N-H, str), 2250 (O-H, str), 1705 (C=O, str), 1652 (C=C, str); **^{1}H NMR** δ (600 MHz, D_2O) 6.90 (1H, dt, *J* = 15.6, 7.3 Hz, C*H*), 6.37 (1H, d, *J* = 15.6 Hz, C*H*), 4.11 (2H, dd, *J* = 7.3, 1.1 Hz, NCH_2), 3.66 (8H, m, 4 × CH_2); **^{13}C NMR** δ (151 MHz, D_2O) 168.61 (C=O), 133.74 (CH), 131.03 (CH), 56.82 (CH_2), 48.38 (2 × CH_2), 40.90 (2 × CH_2); HRMS (**ESI$^+$,** MeCN) $[MH]^+$ found 171.1131, $C_8H_{15}N_2O_2$ requires 171.1128.

(*E*)-4-Boc-piperazidyl-1-ylbut-2-enoic acid ethyl ester (75)

Ethyl-4-bromocrotonate (1 mL, 7.25 mmol) was added to *N*-Boc piperazine (1.46 g, 7.87 mmol) and diluted with acetonitrile (15 mL). To the mixture potassium carbonate (1.08 g, 7.87 mmol) was added slowly to maintain low temperature inside the flask. The reaction was left to stir for 18 h before removing the solvent *in vacuo* and the residue re-dissolved in H_2O and EtOAc (1:1, 40 mL). The aqueous layer was washed with EtOAc (2 × 10 mL), the organic extracts were collected, dried with $MgSO_4$ and the solvent removed *in vacuo*. The pale-yellow residue was purified using column chromatography (DCM → 10% MeOH) to yield **75** as a pale-yellow oil (1.37 g, 63%).

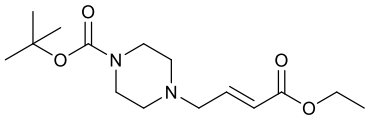

Pale yellow oil, yield: 1.37 g, (63%); **R_f**: 0.59 (DCM: MeOH 90:10); **^{1}H NMR** δ (500 MHz, $CDCl_3$) 6.91 (1H, dt, *J* = 15.7, 6.1 Hz, C*H*), 5.97 (1H, dt, *J* = 15.7, 1.5 Hz, C*H*), 4.18 (2H, q, *J* = 7.1 Hz, C=OCH_2), 3.43 (4H, m, 2 × CH_2), 3.12 (2H, dd, *J* = 6.2, 1.6 Hz, NCH_2), 2.39 (4H, m, 2 × CH_2), 1.44 (9H, s, 3 × CH_3) 1.28 (3H, t, *J* = 7.1 Hz, CH_3); **^{13}C NMR** δ (151 MHz, $CDCl_3$) 166.21 (C=O), 154.81 (C=O), 144.69 (CH), 123.72 (CH), 79.81 (C), 60.54 (CH_2), 59.38 (CH_2), 53.16 (2 × CH_2), 43.65 (br, 2 × CH_2), 28.54 (3 × CH_3), 14.36 (CH_3); **t_R**: 3.01 min (GE10 MeCN, 254

nm); HRMS (**ESI$^+$,** MeCN) $[MH]^+$ found 299.19620, $C_{15}H_{27}N_2O_4$ requires 299.19653.

(*E*)-Piperazidyl-1-ylbut-2-ene ethyl ester (76)

(*E*)-4-Boc-piperazidyl-1-ylbut-2-enoic acid ethyl ester (**75**) (1.37 g, 4.59 mmol) was added to dioxane (10 mL) and to it was added 4N HCl in dioxane (10 mL) and EtOH (5 mL) and was left to reflux for 4 hours. The solvent was removed *in vacuo* to give the product as a pale yellow solid (1.117 g, 108%).

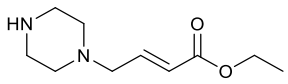

Colourless solid, yield: 1.117 g, (108%); **R_f**: 0.24 (DCM: MeOH 90:10); **^{1}H NMR** δ (500 MHz, MeOD) 7.01 (1H, dt, *J* = 15.6, 7.2 Hz, C*H*), 6.42 (1H, dt, *J* = 15.6, 1.3 Hz, C*H*), 4.26 (2H, q, *J* = 7.1, Hz, CH_2), 4.16 (2H, dd, *J* = 7.3, 1.4 Hz, NCH_2), 3.69 (8H, m, 4 × CH_2), 1.33 (3H, t, *J* = 7.1 Hz, NCH_2); **^{13}C NMR** δ (151 MHz, MeOD) 166.05 (C=O), 134.42 (CH), 132.09 (CH), 62.20 (CH_2), 57.77 (CH_2), 49.54 (2 × CH_2), 42.05 (2 × CH_2), 14.45 (CH_3); HRMS (**ESI$^+$,** MeCN) $[MH]^+$ found 199.1438, $C_{10}H_{19}N_2O_2$ requires 199.1441.

4-Bromo-butenoic acid (77)

Ethyl-4-bromocrotonate (2 mL, 14.6 mmol) was added to a mixture of H_2O and EtOH (1:1, 50 mL) and K_2CO_3 (2.15 g, 15.6 mmol) and the reaction was left to react for 6 h. Ethanol was removed *in vacuo* and the aqueous mixture was washed with EtOAc (2 × 150 mL), before being acidified to pH 1 with HCl. The aqueous layer was then washed with EtOAc (3 × 60 mL), the organic washings collected and dried with $MgSO_4$ and solvent removed *in vacuo* to produce **77** as a pale yellow solid (0.473 g, 20%).

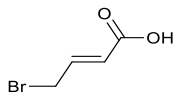

Pale yellow oil, yield: 0.473 g, (20%); **IR** υ_{max} / cm^{-1}: 3062 (O-H br, str), 1684 (C=O, str), 1632 (C=C, str), 688 (CH_2-Br, str); **^{1}H NMR** δ (500 MHz, D_2O) 7.10 (1H, dt, *J* = 15.3, 7.4 Hz, CH), 6.13 (1H, d, *J* = 15.4 Hz, C*H*), 4.17 (2H, dd, *J* = 7.4 Hz, CH_2); **^{13}C NMR** δ (500 MHz, D_2O) 169.79 (C=O), 144.15 (CH), 123.59 (CH), 29.45 (CH_2); **HPLC** (Method 1/ACN) $\mathbf{t_R}$ = 2.98 min, purity 100% (ELSD); ESI-MS (MeCN): ***m/z*** = 165.1 $[M+H]^+$.

Resin bound (*E*)-piperizin-1-yl-but-2-enoic acid (79)

Chlorotrityl resin (1.00 g, 1 mmol) was swollen with dry DCM (3 × 15 mL) in an N_2 atmosphere and to it thionyl chloride (0.18 mL, 2.5 mmol) was added in DCM (15 mL) and left to react for 1 h. The mixture was rinsed off, and the resin washed with DMF (15 mL) and DCM (15 mL). 4-Bromo-butenoic acid (0.454 g, 2.75 mmol) was dissolved in DMF (12 mL) and added to the resin for 2 h. The addition was confirmed by cleaving a sample (<0.01 mmol) with 20% HFIP in DCM (1 mL) and analysing the crude product on HPLC. The resin was washed with DMF (2 × 15 mL) and DCM (2 × 15 mL). To the resin, a solution of piperazine (0.43 g, 5.00 mmol) in DMF (12 mL) was added and left to stir for 2 h. Reaction completion was determined by the chloroanil test on a sample of resin. The excess piperazine was removed by rigorous washing with DMF (3 × 15 mL) and the resin stored in the fridge after swelling and drying the resin with diethyl ether.

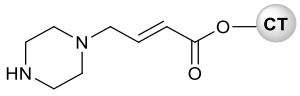

2-[5-[1-(5-Carboxypentyl-1-piperizinyl)-but-2-enoic acid)-1,3-dihydro-3,3-dimethyl-5-sulfo-2*H*-indol-2-ylidene]-1,3-pentadien-1-yl]-1-ethyl-3,3-dimethyl-5-sulfo-3*H*-indolium (80)

27 (0.182 g, 0.28 mmol) was added to HSPyU (0.114 g, 0.28 mmol) and dissolved in dry DMF (10 mL) before DIPEA was added (0.15 mL, 0.83 mmol). The reaction was left to stir for 5 h until no starting material was observed. The resin containing **79** (0.3 g, 0.3 mmol resin) was swelled with DCM (3 × 10 mL), and to it the reaction mixture was added and additional DIPEA (0.15 mL, 0.83 mmol). The reaction was left to stir overnight, and the excess dye was removed. The resin was washed repeatedly, alternating between DMF (10 mL) and DCM (10 mL) until the run off was clear. The resin beads were swollen with DCM (3 × 10 mL) and the product was cleaved from the beads in a solution of 20% HFIP in DCM (v/v) (10 min, 4 × 5 mL). The solution was dried *in vacuo* and the crude product purified by reverse phase chromatography (H_2O/MeCN 95:5 → 70:30) with the product dried by lyophilisation to yield **80** as a dark blue solid (17 mg, 8%).

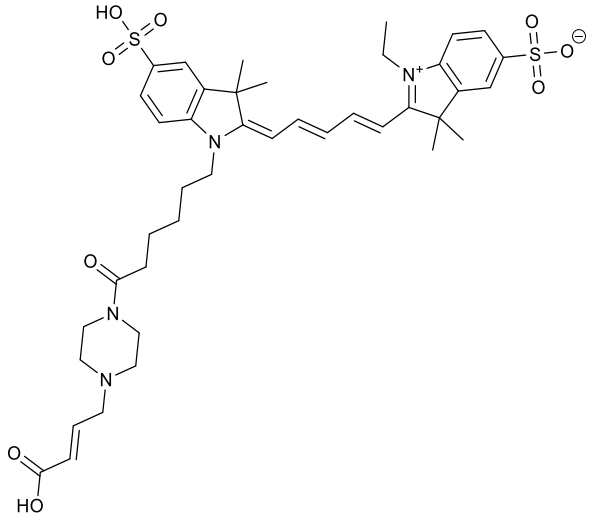

Dark blue solid, yield: 0.017 g, (8%); **^{1}H NMR** δ (500 MHz, DMF-d_7:D_2O, 4:1) 8.48 (2H, t, J = 13.1, Hz, 2 × CH_{ar} bridge), 7.96 (2H, s, 2 × CH_{ar}), 7.91 (2H, d, J =

8.1 Hz, 2 × CH_{ar}), 7.49-7.43 (2H, m, 2 × CH_{ar}), 6.93 (1H, dt, *J* = 15.5, 6.6 Hz, CH_2CH=CH), 6.80 (1H, t, *J* = 12.3 Hz CH_{bridge}), 6.50 (2H, d, *J* = 13.7 Hz, 2 × CH_{ar}), 6.17 (2H, d, *J* = 15.7 Hz, 2 × CH_{ar}), 2.85-2.79 (4H, m, 2 × NCH_2), 2.46 (2H, t, *J* = 7.2 Hz, COCH_2), 1.93-1.87 (2H, m, CH_2), 1.78 (6H, s, 2 × CH_3), 1.78 (6H, s, 2 × CH_3), 1.70-1.65 (2H, m, CH_2), 1.54-1.50 (2H, m, CH_2), 1.42 (3H, t, *J* = 6.6 Hz, CH_3); **^{13}C NMR** δ (500 MHz, DMF-d_7:D_2O, 4:1) 173.65 (C), 173.51 (C), 172.02 (C=O), 167.19 (C=ONR), 154.66 (CH), 154.44 (CH), 144.04 (C), 143.80 (C), 143.08 (C), 142.46 (C), 141.26 (C), 141.11 (C), 141.06 (CH), 126.70 (CH), 126.66 (CH), 126.47 (CH), 126.34 (CH), 120.13 (CH), 120.09 (CH), 110.61 (CH), 110.35 (CH), 103.98 (CH), 103.78 (CH), 57.62 (CH_2), 52.54 (NCH_2), 52.17 (NCH_2), 49.28 (C), 49.18 (C), 44.20 (NCH_2), 43.84 (CH_2), 40.20 (NCH_2), 39.17 (CH_2), 32.08 (CH_2), 26.96 (2 × CH_3), 26.91 (CH_2), 26.80 (2 × CH_3), 25.92 (CH_2), 24.79 (CH_2), 11.86 (CH_3); **HPLC** (Method 1/ACN) $\mathbf{t_R}$ = 3.16 min, purity 100% (ELSD); HRMS (**ESI$^+$**, MeCN) $[M+H]^+$ found 809.3245, $C_{41}H_{53}O_9N_4S_2^+$ requires 809.3248.

(3S,3AS,6AR)-3-Isopropyl-1-methanesulfonyl-4-(2-[5-[1-(5-Carboxypentyl-1-piperizinyl)-but-2-ene)-1,3-dihydro-3,3-dimethyl-5-sulfo-2H-indol-2-ylidene]-1,3-pentadien-1-yl]-1-ethyl-3,3-dimethyl-5-sulfo-3H-indolium)-5-oxo-hexahydro-pyrrolo [3,2-B] pyrrol-2-one (81)

80 (10.0 mg, 0.012 mmol) was added to EDC.HCl (4.6 mg, 0.024 mmol) and HOBt (3.3 mg, 0.024 mmol) dissolved in dry DMF (0.5 mL) before TEA was added (3 µL, 0.024 mmol). The reaction was left to stir at rt for five hours until no starting material was observed. To the reaction mixture **59** (3.0 mg, 0.012 mmol) was added and additional TEA (3 µL, 0.024 mmol). The reaction was left to stir overnight. The reaction mixture was dried *in vacuo* and the crude product was purified by reverse phase chromatography (H_2O/MeCN 95:5 → 70:30) with the product dried by freeze drier to yield **81** as a dark blue solid (1.2 mg, 10%).

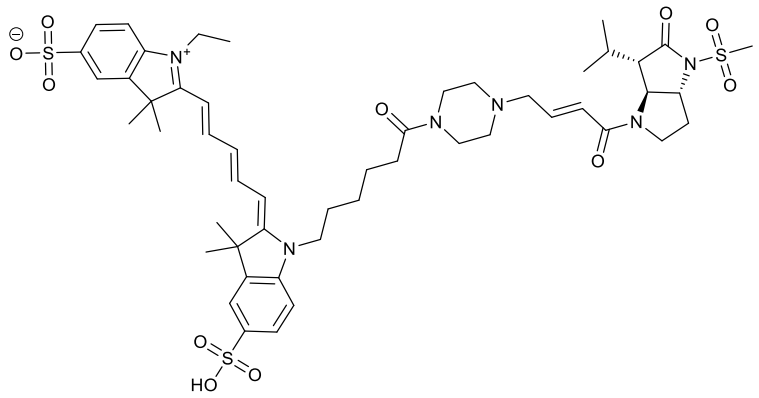

Dark blue solid, yield: 1.2 mg, (10%); **^{1}H NMR** δ (600 MHz, MeOD) 8.38-8.30 (1H, m, CH_{bridge}), 7.94-7.86 (4H, m, CH_{ar}), 7.36 (2H, d, J = 8.2 Hz, 2 × CH_{ar}), 6.84-6.75 (2H, m, 2 × CH_{bridge}), 6.74-6.65 (1H, m, CH=CHCO), 6.44 (1H, d, J = 15.3 Hz, CH=CHCO), 6.36 (2H, m, 2 × CH_{bridge}), 4.20 (2H, q, J = 7.2 Hz, NCH_2), 4.16 (2H, t, J = 7.2 Hz, NCH_2), 3.97 (2H, m, CONCH_2), 3.70-3.63 (1H, m, CHNSO$_2$Me), 3.62-3.58 (2H, m, NCH_2), 3.57-3.53 (2H, m, NCH_2), 3.49-3.39 (1H, m, CHNCH$_2$), 3.26 (3H, s, SO$_2$CH_3), 3.23-3.20 (2H, m, CH_2CH=CH), 3.01 (1H, br s, CH(CH$_3$)$_2$), 2.95 (1H, m, ^{i}PrCH), 2.57-2.50 (1H, m, NCH$_2$CH(H)), 2.50-2.45 (2H, m, NCH_2), 2.45-2.38 (4H, m, CH_2, NCH_2), 2.19-2.09 (1H, m, NCH$_2$CH(H)), 1.86 (2H, p, J = 7.6 Hz, CH_2), 1.77 (2H, m, CH_2), 1.77 (6H, s, 2 × CH_3), 1.77 (6H, s, 2 × CH_3), 1.73-1.65 (2H, m, CH_2), 1.50-1.45 (2H, m, CH_2), 1.41 (3H, d, J = 7.2 Hz, CH$_2$CH_3), 1.28 (3H, d, J = 7.2 Hz, CH(CH$_3$)(CH_3)), 1.02 (3H, d, J = 6.9 Hz, CH(CH_3)(CH$_3$)); **^{13}C NMR** δ (126 MHz, MeOD) 175.11 (C), 173.66 (C), 170.37 (C), 155.80 (CH), 145.60 (C), 144.95 (C), 144.40 (C), 144.12 (C), 143.55 (C), 142.99 (CH), 142.60 (C), 131.40 (C), 130.87 (C), 128.09 (2 × CH), 127.62 (C), 127.51 (C), 125.10 (CH), 121.42 (2 × CH), 111.41 (2 × CH), 104.92 (2 × CH), 66.65 (CH$_2$), 65.26 (CH), 61.76 (CH), 59.95 (CH$_2$), 56.62 (CH), 56.44 (CH), 54.34 (CH$_2$), 53.84 (CH$_2$), 50.67 (C), 50.60 (C), 46.64 (CH$_2$), 45.02 (CH$_2$), 42.63 (CH$_2$), 40.28 (CH$_2$), 39.78 (CH$_3$), 33.40 (CH$_2$), 29.51 (CH$_2$), 28.23 (CH$_2$), 27.87 (2 × CH$_3$), 27.73 (2 × CH$_3$), 27.42 (CH$_2$), 26.04 (CH$_2$), 21.63 (CH$_3$), 16.56 (CH$_3$), 12.52 (CH$_3$); **HPLC** (Method 1/ACN) $\mathbf{t_R}$ = 3.58 min (ELSD); HRMS (**ESI$^+$**, MeCN) [M+Na]$^+$ found 1059.40010, $C_{51}H_{68}O_{11}N_6S_3{}^+Na$ requires 1059.40004.

5.3 Biological methods

5.3.1 HNE IC_{50} determination

The substrate MeOSuc-Ala-Ala-Pro-Val-AMC (Sigma Aldrich, 15 µL, 2.667 mM, 10% DMSO in 0.5 M PBS buffer, final concentration 1 mM) was added to serial dilutions of probe **81** (15 µL, 10 µM to 156.25 nM) and to the mixture within the plate, the enzyme HNE was added (EPC Ltd., 10 µL of 200 nM solution, in 50% PBS 50% gylcerol, pH 5.5, with a final concentration of 50 nM). The fluorescence of the cleaved substrate was monitored over 20 minutes at 460 nm, upon excitation at 360 nm. The positive control contained only substrate and enzyme, and buffer (1:1000 v/v, DMSO in buffer), and the negative control contained no enzyme and only PBS buffer. The progress curves generated were analysed to generate IC_{50} values.

5.3.2 HNE K_i determination

The substrate MeOSuc-Ala-Ala-Pro-Val-pNA (Sigma Aldrich, 20 µL of 10 mM 20% DMSO in 0.1 M HEPES, final concentration 1 mM) was added to serial dilutions of probe **81** (10 µL, 10 µM to 156.25 nM) and diluted with 150 µL of 0.1 M HEPES (pH 7.4). To the mixture HNE was added (EPC Ltd., 20 µL of 300 nM solution, in 50% PBS 50% gylcerol, pH 5.5, to a final concentration of 30 nM). The fluorescence of the cleaved substrate was monitored over 20 min at 460 nm, upon excitation at 360 nm. The positive control contained only substrate and enzyme, and buffer (1:1000 v/v, DMSO in buffer), where the negative control contains no enzyme and only buffer. The progress curves generated were analysed using Grafit to determine the K_i values.

5.3.3 Stability study in buffer

PBS (1 M, pH 7.4, 2.5 mL) was warmed to 37 °C, and probe was added to give a concentration of (25 μL, 10 mM) was added, aliquots of 100 μL were taken at regular time points and analysed via analytical HPLC at 650 nm or at 254 nm.

5.3.4 Stability study in media

Dulbecco's Modified Eagle's Medium (DMEM) media was warmed to 37 °C, and to a volume of 2.475 mL, the probe (25 μL, 10 mM) was added to give a final concentration of 100 μM. Aliquots of 100 μL were taken at regular time points over 10 h, added to acetonitrile (100 μL) (to crash out proteins). The mixture was centrifuged at 7.4 *g* for 4 min, the supernatant collected, filtered and analysed via analytical HPLC at 650 nm or 254 nm.

5.3.5 Confocal microscopy

Neutrophils were purified from a human blood sample using the Percoll preparation.[108] An eight-chamber microscope slide (Ibidi Tech.) was incubated in a fibronectin solution for 30 min at 37 °C. The neutrophils were isolated, and 200000 cells were plated in each well. They were incubated with Dulbecco's PBS (Gibco, containing $CaCl_2$ and $MgCl_2$, pH 7.4) for 0.5 h, before being washed and then incubated with HOECHST 33342 (10 μg/mL) for 15 min. The cells were washed with PBS and the probes were added (500 nM, diluted from 10 mM stock solution in DMSO). The cells were then imaged, without a wash step, the calcium ionophore (5 μM, 2 min) was added, and the neutrophils were imaged again. Leica SP8 Confocal microscope laser settings were: excitation laser lines at 488 nm and 633 nm with emission filters of 414-464 nm for HOECHST 33342, 506-530 nm for fluorescein-based optical probes and 638-718 nm for Cy5-based optical probes.

5.3.6 Flow cytometry

Neutrophils (4 000000 from the Percoll prep[108]) were separated into two populations: one to be activated and the other unactivated. Both populations were incubated in Dulbecco's PBS (Gibco, containing $CaCl_2$ and $MgCl_2$, pH 7.4) for 0.5 h. The unactivated were with PBS buffer and divided with one half treated with the probe. The activated population were incubated with a calcium ionophore (1 μM) for 10 min before being washed and divided with one sample the control and the other had the probe added. Cells were pelleted, washed with PBS, reconstituted and to all samples a neutrophil specific CD66b antibody labelled with phycoerythrin (BD biosciences) added and incubated with the cells for 15 min. The cells were then pelleted again, washed with PBS, and reconstituted in FACS buffer (5% foetal bovine serum in PBS). Immediately before measuring on the flow cytometer, the cells were stained with DAPI to elucidate the viability of the cells.

5.3.7 Haemolysis toxicity assay

For the determination of haemolysis by the compounds, a standard solution of 14% human erythrocytes in PBS (pH 7.4) diluted 1:1 with the compounds in solution. The probes were diluted in DMSO and PBS buffer at two concentrations (100 nM and 10 μM, to give final lysis concentrations of 50 nM and 5 μM). A control of 7% erythrocyte solution in PBS was used to determine baseline lysis. The mixtures were incubated at 37 °C for 1 h and centrifuged at 400 *g* for 5 min. The supernatant was removed and the absorbance at 415 nm was measured, with the data normalised to the probe in PBS to account for background absorbance. The experiment was repeated in triplicate with different samples.

To generate the control percentage of lysis, a serial dilution of 7% erythrocyte solution (100% lysis) to 0.03% erythrocyte solution (0.4% lysis). The solutions were sonicated for 15 sec at 5 mW power, to ensure complete lysis and spun down using a centrifuge at 400 *g* for 5 min. The supernatant was removed and the absorbance at 415 nm was measured, with the data normalised to the probe in PBS to account for background absorbance.

5.3.8 Gel electrophoresis

The samples were mixed with two times concentrated sample buffer (2x Laemmli Sample Buffer, 1:1 v/v) with 50 mM DTT and heated for 5 min at 80 °C. The samples were then were loaded onto 12% (wt./v) polyacrylamide gel and run at a voltage of 120 V for 20 min, followed by 160 V for 40 min using a BIO RAD PowerPac 300 power supply. The gel was imaged in fluorescein and cy5 channels before being stained with Coomassie Blue (0.006% wt./v AcOH in water (1:9)) for 2 h. The stained gel was washed several times with water until the solution ran clear and imaged again using white light.

Chapter 6 References

1 A. Hessenbruch, *Endeavour*, 2002, **26**, 137–141.

2 T. Hussain and Q. T. Nguyen, *Adv. Drug Deliv. Rev.*, 2014, **66**, 90–100.

3 L. Schrievens, N. Lorent, C. Dooms and J. Vansteenkiste, *Oncologist*, 2004, **9**, 633–643.

4 S. Khondee and T. Wang, *J. Healthc. Eng.*, 2013, **4**, 1–22.

5 H. Lusic and M. W. Grinstaff, *Chem. Rev.*, 2013, **113**, 1641–1666.

6 J. I. Bloch, E. T. Chou and J. A. Carrino, *Pain Manag.*, 2007, 106–117.

7 E. M. Gale and P. Caravan, *ACS Chem. Neurosci.*, 2018, **9**, 395–397.

8 M. M. Khalil, J. L. Tremoleda, T. B. Bayomy and W. Gsell, *Int. J. Mol. Imaging*, 2011, **2011**, 1–15.

9 S. Liu, D. S. Edwards and J. A. Barrett, *Bioconjug. Chem.*, 1997, **8**, 621–636.

10 D. D. Nolting, M. L. Nickels, N. Guo and W. Pham, *Am. J. Nucl. Med. Mol. Imaging*, 2012, **2**, 273–306.

11 S. a Hilderbrand and R. Weissleder, *Curr. Opin. Chem. Biol.*, 2010, **14**, 71–79.

12 P. B. Garcia-Allende, M. Koch, J. Glatz, P. Symvoulidis and V. Ntziachristos, *Opt. Mol. Probes, Imaging Drug Deliv.*, 2015, OW1D--1.

13 J. . R. Widengren R., *Bioimaging*, 1996, **4**, 149–157.

14 J. R. Lakowicz, *Principles of Fluorescence Spectroscopy Principles of Fluorescence Spectroscopy*, Springer Science, 2006.

15 H. Kobayashi, M. Ogawa, R. Alford, P. L. Choyke and Y. Urano, *Chem.*

Rev., 2010, **110**, 2620–2640.

16 W. Stummer, U. Pichlmeier, T. Meinel, O. D. Wiestler, F. Zanella and H.-J. Reulen, *Lancet Oncol.*, 2006, **7**, 392–401.

17 J. T. Alander, I. Kaartinen, A. Laakso, T. Pätilä, T. Spillmann, V. V. Tuchin, M. Venermo and P. Välisuo, *Int. J. Biomed. Imaging*, 2012, **2012**, 1–12.

18 M. Hutteman, A. L. Vahrmeijer, J. R. van der Vorst, P. J. K. Kuppen, C. W. G. M. Löwik, C. J. H. van de Velde, B. E. Schaafsma, J. V. Frangioni and J. S. D. Mieog, *J. Surg. Oncol.*, 2011, **104**, 323–332.

19 M. Taniguchi and J. S. Lindsey, *Photochem. Photobiol.*, 2018, **94**, 290–327.

20 T. J. Russin, E. İ. Altinoğlu, J. H. Adair and P. C. Eklund, *J. Phys. Condens. Matter*, 2010, **22**, 334217.

21 T. Robertson, F. Bunel and M. Roberts, *Cells*, 2013, **2**, 591–606.

22 R. Agrawal, S. B. B. Tun, P. K. Balne, H. Y. Zhu, N. Khandelwal and V. A. Barathi, *Ocul. Immunol. Inflamm.*, 2018, **26**, 1–7.

23 A. Baeyer, *Berichte der Dtsch. Chem. Gesellschaft*, 1871, **4**, 555–558.

24 A. R. Akram, S. V Chankeshwara, E. Scholefield, T. Aslam, N. McDonald, A. Megia-Fernandez, A. Marshall, B. Mills, N. Avlonitis, T. H. Craven, A. M. Smyth, D. S. Collie, C. Gray, N. Hirani, A. T. Hill, J. R. Govan, T. Walsh, C. Haslett, M. Bradley and K. Dhaliwal, *Sci. Transl. Med.*, 2018, **10**, eaal0033.

25 C. G. Hadjipanayis, G. Widhalm and W. Stummer, *Neurosurgery*, 2015, **77**, 663–673.

26 A. Mantovani, M. A. Cassatella, C. Costantini and S. Jaillon, *Nat. Rev. Immunol.*, 2011, **11**, 519–531.

27 U. Meyer-Hoffert, *Front. Biosci.*, 2009, **14**, 3409–3418.

28 J. Pillay, I. Den Braber, N. Vrisekoop, L. M. Kwast, R. J. De Boer, J. A. M. Borghans, K. Tesselaar and L. Koenderman, *Blood*, 2010, **116**, 625–627.

29 S. J. Galli, N. Borregaard and T. A. Wynn, *Nat. Immunol.*, 2011, **12**, 1035–1044.

30 E. Kolaczkowska and P. Kubes, *Nat. Rev. Immunol.*, 2013, **13**, 159–175.

31 C. Summers, S. M. Rankin, A. M. Condliffe, N. Singh, A. M. Peters and E. R. Chilvers, *Trends Immunol.*, 2010, **31**, 318–324.

32 OpenStax, *Anatomy & Physiology*, OpenStax CNX, 2016.

33 B. Korkmaz, M. Horwitz, D. Jenne and F. Gauthier, *Pharmacol. Rev.*, 2010, **62**, 726–759.

34 C. T. N. Pham, *Nat Rev Immunol*, 2006, **6**, 541–550.

35 E. Kolaczkowska and P. Kubes, *Nat. Rev. Immunol.*, 2013, **13**, 159–175.

36 V. Delgado-rizo, M. A. Martínez-guzmán, L. Iñiguez-gutierrez and M. Fafutis-morris, *Front. Immunol.*, 2017, **8**, 1–20.

37 V. Papayannopoulos, *Nat. Rev. Immunol.*, 2017, **18**, 134–147.

38 L. E. Edgington, M. Verdoes and M. Bogyo, *Curr. Opin. Chem. Biol.*, 2011, **15**, 798–805.

39 A. Janoff and J. Scherer, *J. Exp. Med.*, 1968, **128**, 1137–1155.

40 B. Korkmaz, T. Moreau and F. Gauthier, *Biochimie*, 2008, **90**, 227–242.

41 S. J. F. Macdonald, M. D. Dowle, L. A. Harrison, G. D. E. Clarke, G. G. A. Inglis, M. R. Johnson, P. Shah, R. A. Smith, A. Amour, G. Fleetwood, D. C. Humphreys, C. R. Molloy, M. Dixon, R. E. Godward, A. J. Wonacott, O. M. P. Singh, S. T. Hodgson and G. W. Hardy, *J. Med. Chem.*, 2002, **45**, 3878–3890.

42 W. L. Lee and G. P. Downey, *Crit. Care Med.*, 2001, **164**, 896–904.

43 Y. Weinrauch, D. Drujan, S. D. Shapiro, J. Weiss and A. Zychlinsky, *Nature*, 2002, **417**, 91–94.

44 B. Korkmaz, M. S. Horwitz, D. E. Jenne and F. Gauthier, *Pharmacol. Rev.*, 2010, **62**, 726–759.

45 U. Bank and S. Ansorge, *J. Leukoc. Biol.*, 2001, **69**, 197–206.

46 T. J. Moraes, C.-W. Chow and G. P. Downey, *Crit. Care Med.*, 2003, **31**, S189–S194.

47 A. Alase, C. W. Wasson, D. McGonagle, M. Stacey, T. Macleod, M. Wittmann and R. Doble, *Sci. Rep.*, 2016, **6**, 4–10.

48 K. Tsushima, L. S. King, N. R. Aggarwal, A. De Gorordo, F. R. D'Alessio and K. Kubo, *Intern. Med.*, 2009, **48**, 621–630.

49 B. Korkmaz and F. Gauthier, in *Handbook of Proteolytic Enzymes*, 2013, vol. 3, pp. 2653–2661.

50 L. L. Warren and G. P. Downey, *Am. J. Respir. Crit. Care Med.*, 2001, **164**, 896–904.

51 K. C. Meyer, *Semin Respir Crit Care Med*, 2007, **28**, 546–560.

52 M. Drent, R. Baughman and K. Meyer, *Diffus. Parenchymal Lung Dis.*, 2007, **36**, 58–67.

53 B. Walker and J. Lynas, *Cell. Mol. Life Sci.*, 2001, **58**, 596–624.

54 H. Ohbayashi, *Expert Opin. Ther. Pat.*, 2005, **15**, 759–771.

55 W. C. Groutas, D. Dou, K. R. Alliston, W. C. Groutas, D. Dou and K. R. Alliston, *Expert Opin. Ther. Pat.*, 2011, **21**, 339–354.

56 Y.-F. Tsai and T.-L. Hwang, *Expert Opin. Ther. Pat.*, 2015, **25**, 1145–1158.

57 M. Poreba, A. Szalek, P. Kasperkiewicz, W. Rut, G. S. Salvesen and M.

Drag, *Chem. Rev.*, 2015, **115**, 12546–12629.

58 J. Lee and M. Bogyo, *ACS Chem. Biol.*, 2010, **5**, 233–243.

59 C. Bremer, V. Ntziachristos and B. Weitkamp, *Invest. Radiol.*, 2005, **40**, 321–327.

60 D. Caglič, A. Globisch, M. Kindermann, N.-H. Lim, V. Jeske, H.-P. Juretschke, E. Bartnik, K. U. Weithmann, H. Nagase, B. Turk and K. U. Wendt, *Bioorg. Med. Chem.*, 2011, **19**, 1055–1061.

61 H. Y. Hu, S. Gehrig, G. Reither, D. Subramanian, M. A. Mall, O. Plettenburg and C. Schultz, *Biotechnol. J.*, 2014, **9**, 266–281.

62 G. Blum, G. Von Degenfeld, M. J. Merchant, H. M. Blau and M. Bogyo, *Nat. Chem. Biol.*, 2007, **3**, 668–677.

63 J. B. Wu, T.-P. Lin, J. D. Gallagher, S. Kushal, L. W. K. Chung, H. E. Zhau, B. Z. Olenyuk and J. C. Shih, *J. Am. Chem. Soc.*, 2015, **137**, 2366–2374.

64 I. R. Corrêa, *Curr. Opin. Chem. Biol.*, 2014, **20**, 36–45.

65 Nakajima, K, Powers, J.C, Ashe, B.M. & Zimmerman and M, *J. Biol. Chem.*, 1979, **254**, 4027-4032.

66 L. E. Edgington, M. Verdoes and M. Bogyo, *Curr. Opin. Chem. Biol.*, 2011, **15**, 798–805.

67 Q. Sun, J. Li, W. N. Liu, Q. J. Dong, W. C. Yang and G. F. Yang, *Anal. Chem.*, 2013, **85**, 11304–11311.

68 M. J. Castillo, K. Nakajima, M. Zimmerman and J. C. Powers, *Anal. Biochem.*, 1979, **99**, 53–64.

69 S. Liu, H. Xiong, R. Li, W. Yang and G. Yang, *Anal. Chem.*, 2019, **91**, 3877–3884.

70 M. Saikiran, D. Sato, S. S. Pandey, S. Hayase and T. Kato, *Bioorg. Med. Chem. Lett.*, 2017, **27**, 4024–4029.

71 S. Gehrig, M. A. Mall and C. Schultz, *Angew. Chemie - Int. Ed.*, 2012, **51**, 6258–6261.

72 P. Kasperkiewicz, M. Poreba, S. J. Snipas, S. J. Lin, D. Kirchhofer, G. S. Salvesen and M. Drag, *PLoS One*, 2015, **10**, e0132818.

73 B. C. Lechtenberg, P. Kasperkiewicz, H. Robinson, M. Drag and S. J. Riedl, *ACS Chem. Biol.*, 2015, **10**, 945–951.

74 M. Drag, M. D'Angelo, G. S. Salvesen, Y. Altman and P. Kasperkiewicz, *J. Am. Chem. Soc.*, 2017, **139**, 10115–10125.

75 P. Kasperkiewicz, M. Poreba, S. J. Snipas, H. Parker, C. C. Winterbourn, G. S. Salvesen and M. Drag, *Proc. Natl. Acad. Sci. U. S. A.*, 2014, **111**, 2518–2523.

76 L. E. Edgington-Mitchell, N. Barlow, L. Aurelio, A. Samha, M. Szabo, B. Graham and N. Bunnett, *Bioorg. Med. Chem. Lett.*, 2017, **27**, 254–260.

77 A.-C. Schulz-Fincke, M. Blaut, A. Braune and M. Gütschow, *ACS Med. Chem. Lett.*, 2018, **9**, 345–350.

78 R. Huisgen, G. Szeimies and L. Möbius, *Chem. Ber.*, 1967, **100**, 2494–2507.

79 N. Avlonitis, M. Debunne, T. Aslam, N. McDonald, C. Haslett, K. Dhaliwal and M. Bradley, *Org. Biomol. Chem.*, 2013, **11**, 4414–4418.

80 T. Craven, T. Walton, A. Akram, N. McDonald, E. Scholefield, T. Walsh, C. Haslett, M. Bradley and K. Dhaliwal, *Lancet*, 2016, **387**, S31.

81 T. H. Craven, N. Avlonitis, N. McDonald, T. Walton, E. Scholefield, A. R. Akram, T. S. Walsh, C. Haslett, M. Bradley and K. Dhaliwal, *Sci. Rep.*, 2018, **8**, 13490.

82 L. Yuan, W. Lin, K. Zheng, L. He and W. Huang, *Chem. Soc. Rev.*, 2013, **42**, 622–661.

83 L. M. Wysocki and L. D. Lavis, *Curr. Opin. Chem. Biol.*, 2011, **15**, 752–759.

84 L. D. Lavis and R. T. Raines, *ACS Chem. Biol.*, 2007, **3**, 142–155.

85 L. D. Lavis and R. T. Raines, *ACS Chem. Biol.*, 2014, **9**, 855–866.

86 L. Thiberville, S. Moreno-Swirc, T. Vercauteren, E. Peltier, C. Cavé and G. Bourg Heckly, *Am. J. Respir. Crit. Care Med.*, 2007, **175**, 22–31.

87 A. Brunet, T. Aslam and M. Bradley, *Bioorg. Med. Chem. Lett.*, 2014, **24**, 3186–3188.

88 Alexafluor 647, https://www.thermofisher.com/order/catalog/product/A20006, (accessed 29 October 2018).

89 WO Pat., 152 389, 2014, 47.

90 M. Schottelius, A. Wurzer, K. Wissmiller, R. Beck, M. Koch, D. Gorpas, J. Notni, T. Buckle, M. N. Van Oosterom, K. Steiger, V. Ntziachristos, M. Schwaiger and F. W. B. Van Leeuwen, *J. Nucl. Med.*, 2019, **60**, 71–79.

91 M. Miampamba, J. Liu, A. Harootunian, A. J. Gale, S. Baird, S. L. Chen, Q. T. Nguyen, R. Y. Tsien and J. E. González, *Theranostics*, 2017, **7**, 3369–3386.

92 G. M. Robinson and R. Robinson, *J. Chem. Soc. Trans.*, 1924, **125**, 827–840.

93 WO Pat., 018 230, 2010, 53.

94 WO Pat., 045 662, 2013, 49.

95 Z. Yu, R. M. Schmaltz, T. C. Bozeman, R. Paul, M. J. Rishel, K. S. Tsosie

and S. M. Hecht, *J. Am. Chem. Soc.*, 2013, **135**, 2883–2886.

96 J. Burggraaf, I. M. C. Kamerling, P. B. Gordon, L. Schrier, M. L. de Kam, A. J. Kales, R. Bendiksen, B. Indrevoll, R. M. Bjerke, S. a Moestue, S. Yazdanfar, A. M. J. Langers, M. Swaerd-Nordmo, G. Torheim, M. V Warren, H. Morreau, P. W. Voorneveld, T. Buckle, F. W. B. van Leeuwen, L.-I. Ødegårdstuen, G. T. Dalsgaard, A. Healey and J. C. H. Hardwick, *Nat. Med.*, 2015, **21**, 955–961.

97 S. A. Esfahani, P. Heidari, S. A. Kim, S. Ogino and U. Mahmood, *Theranostics*, 2016, **6**, 2028–2038.

98 L. I. Markova, I. A. Fedyunyayeva, Y. A. Povrozin, O. M. Semenova, S. U. Khabuseva, E. A. Terpetschnig and L. D. Patsenker, *Dye. Pigment.*, 2013, **96**, 535–546.

99 R. B. Mujumdar, L. A. Ernst, S. R. Mujumdar, C. J. Lewis and A. S. Waggoner, *Bioconjug. Chem.*, 1993, **4**, 105–111.

100 US Patent Office, 8729276B, 2010, 51.

101 S. D. Lucas, E. Costa, R. C. Guedes and R. Moreira, *Med. Res. Rev.*, 2013, **33**, E73–E101.

102 F. von Nussbaum and V. M.-J. Li, *Bioorg. Med. Chem. Lett.*, 2015, **25**, 4370–4381.

103 J. Mulchande, R. Oliveira, M. Carrasco, L. Gouveia, R. C. Guedes, J. Iley and R. Moreira, *J Med Chem*, 2010, **53**, 241–253.

104 J. Mulchande, S. I. Simões, M. M. Gaspar, C. V. Eleutério, R. Oliveira, M. E. M. Cruz, R. Moreira and J. Iley, *J. Enzyme Inhib. Med. Chem.*, 2011, **26**, 169–175.

105 J. Marto, E. Ruivo, S. D. Lucas, L. M. Gonçalves, S. Simões, L. F. Gouveia, R. Felix, R. Moreira, H. M. Ribeiro and A. J. Almeida, *Eur. J.*

Pharm. Biopharm., 2018, **127**, 1–11.

106 L. Glennon-alty, A. P. Hackett, E. A. Chapman and H. L. Wright, *Free Radic. Biol. Med.*, 2018, **125**, 25–35.

107 E. F. P. Ruivo, L. M. Gonçalves, L. A. R. Carvalho, R. C. Guedes, S. Hofbauer, J. A. Brito, M. Archer, R. Moreira and S. D. Lucas, *ChemMedChem*, 2016, **11**, 2037–2042.

108 C. Haslett, L. A. Guthrie, M. M. Kopaniak, R. B. Johnston Jr and P. M. Henson, *Am. J. Pathol.*, 1985, **119**, 101–110.

109 B. G. Zeiher, A. Artigas, J.-L. Vincent, A. Dmitrienko, K. Jackson, B. T. Thompson and G. Bernard, *Crit. Care Med.*, 2004, **32**, 1695–1702.

110 E. Polverino, E. Rosales-mayor, G. E. Dale, K. Dembowsky and A. Torres, *Chest*, 2017, **152**, 249–262.

111 K. Matsuzaki, Y. Hiramtsu, S. Homma, S. Sato, O. Shigeta and Y. Sakakibara, *Ann. Thorac. Surg.*, 2005, **80**, 611–617.

112 K. Kawabata, M. Suzuki, M. Sugitani, K. Imaki, M. Toda and T. Miyamoto, *Biochem. Biophys. Res. Commun.*, 1991, **177**, 814–820.

113 S. J. . Macdonald, M. D. Dowle, L. a Harrison, P. Shah, M. R. Johnson, G. G. . Inglis, G. D. . Clarke, R. a Smith, D. Humphreys, C. R. Molloy, A. Amour, M. Dixon, G. Murkitt, R. E. Godward, T. Padfield, T. Skarzynski, O. M. . Singh, K. A. Kumar, G. Fleetwood, S. T. Hodgson, G. W. Hardy and H. Finch, *Bioorg. Med. Chem. Lett.*, 2001, **11**, 895–898.

114 R. E. Smith and W. R. Davis, *Anal. Chem.*, 1984, **56**, 2345–2349.

115 S. J. F. Macdonald, G. D. E. Clarke, M. D. Dowle, L. a Harrison, S. T. Hodgson, G. G. a Inglis, M. R. Johnson, P. Shah, R. J. Upton and S. B. Walls, *J. Org. Chem.*, 1999, **64**, 5166–5175.